NASA Technical Memorandum 104592

NASA-TM-104592 19940017389

Empirical Wind Model for the Middle and Lower Atmosphere— Part 2: Local Time Variations

A.E. Hedin, E.L. Fleming, A.H. Manson, F.J. Schmidlin, S.K. Avery,
R.R. Clark, S.J. Franke, G.J. Fraser, T. Tsuda, F. Vial, and R.A. Vincent

NOVEMBER 1993

NASA Technical Memorandum 104592

Empirical Wind Model for the Middle and Lower Atmosphere— Part 2: Local Time Variations

A.E. Hedin
Goddard Space Flight Center
Greenbelt, Maryland

E.L. Fleming
Applied Research Corporation
Landover, Maryland

A.H. Manson
University of Saskatchewan
Saskatoon, Saskatchewan, Canada

F.J. Schmidlin
NASA Wallops Flight Facility
Wallops Island, Virginia

S.K. Avery
University of Colorado
Boulder, Coiorado

R.R. Clark
University of New Hampshire
Durham, NH

S.J. Franke
University of Illinois
Urbana, Illinois

G.J. Fraser
University of Canterbury
Christchurch, New Zealand

T. Tsuda
Kyoto University
Kyoto, Japan

F. Vial
Ecole Polytechnique
Palaiseau Cedex, France

R.A. Vincent
University of Adelaide
Adelaide, Australia

National Aeronautics and
Space Administration

Goddard Space Flight Center
Greenbelt, Maryland 20771

1993

Contents

1. Introduction

A previous memorandum [Hedin et al., 1993] describes the local time average portion of the HWM93 (Horizontal Wind Model) based on a diverse set of incoherent scatter radar, MF radar, meteor radar, rocketsonde, rocket grenade, falling sphere, and gradient wind data. The recently published CIRA 1986 (CIRA-86) model containing monthly tabulations of zonal mean wind from 0 to 120 km [Fleming et al., 1990] was a key element which provided the basis for wind profiles throughout the lower atmosphere. The CIRA-86 tabulations, however, did not address tidal components.

The HWM93 model is the successor of the HWM90 analytic empirical model [Hedin et al., 1991] for winds above 100 km based on data from satellites and ground based incoherent scatter radar and Fabry-Perot optical interferometers. The HWM90 model used a limited set of vector spherical harmonics to describe spatial and temporal variations in the exosphere and at selected altitude nodes with cubic spline interpolation between nodes down to 100 km. The formulation of this wind model is analogous to the MSIS-86 [Hedin, 1987] and MSISE-90 [Hedin, 1991] density and temperature models and allows the user to obtain atmospheric parameters at an arbitrary location and time.

It is the goal of the HWM93 model described herein to extend the formulation of the HWM90 model into the mesosphere and to the surface so as to provide a description of the average (climatological) wind system throughout the atmosphere and tidal (local time) variations in the stratosphere and mesosphere. The tidal portion of the model is based on selected historical rocket data, meteor radar and MF radar data, and lower thermosphere incoherent scatter data previously used for HWM90. The new model thus represents a compromise between data sources in the upper stratosphere, mesosphere, and lower thermosphere. Model results and data comparisons are given with emphasis on the mesosphere and lower thermosphere and include also theoretical semidiurnal winds calculated from Forbes and Vial [1989]. The HWM90 model parameters were changed at 100 km to provide a smoother transition into the mesosphere but otherwise remain unchanged in the thermosphere.

2. Data Sources

The data used to generate this model were derived from published tabulations, figures, and original data bases as summarized in Table 1. The number and diversity of data sources is greatest in the mesosphere and lower thermosphere consistent with availability and the emphasis of this paper.

In the mesosphere and lower thermosphere the techniques and sources represented include incoherent scatter radar, MF radar, meteor radar, falling spheres, and rocket grenade soundings. These were supplemented by datasondes in the upper stratosphere and lower mesosphere from the Meteorological Rocket Network (MRN).

Rocketsonde data from the Meteorological Rocket Network were

obtained from the NASA/Wallops database, which is similar to the World Data Center format available from the National Climate Data Center at Asheville, NC. The data cover the time period from 1969 to 1991 and were separated into falling sphere data [Schmidlin, 1985], which make useful measurements to nearly 100 km, and parachute/datasonde measurements which were limited to 75 km. The MRN concentrated on taking data near local noon, but data are available for all parts of the day for most stations. For each station, the data at two kilometer intervals were separated into two hour local time groups. Monthly averages, determined by summing over all available years, were formed separately for the twelve local time groups. These averages, which provide as equitable a local time coverage as possible, were used as the rocketsonde input to the model and data comparisons.

The less frequent rocket grenade data (1960-1972) were not part of the rocketsonde data set and were not averaged. The MF and Meteor radar data were generally provided as monthly averages.

3. Model Formulation

The HWM93 model is an extension of the HWM87 and HWM90 models [Hedin et al., 1988; 1991] summarizing wind measurements in the thermosphere. Latitude and local time variations in the horizontal wind vector are represented by an expansion in vector spherical harmonics [Morse and Feshbach, 1953] with each expansion coefficient represented by a Fourier series in day of year for annual and semiannual variations. The expansion involves two orthogonal vector fields, the divergence B field and the rotational C field. Due to lack of data coverage, tidal components are independent of longitude. Solar activity and magnetic activity variations are not included below 100 km. Hemispheric differences are represented only by the lowest order asymmetric harmonic because of the limited and uneven data coverage between hemispheres. This report will treat only tidal variations, although tidal and non-tidal variations were fit in an iterative fashion to produce as self-consistent an overall model as possible, and tidal variations were limited to above approximately 45 km. No longitude dependence of the tides was considered (apart from local time), given the lack of data coverage.

Below 100 km the wind profiles are represented by a cubic spline, defined by cubic polynomials between specified nodes with first and second derivatives continuous across interior nodes. The nodes were chosen to be at 100, 90, 82.5, 75, 67.5, 60, 52.5, 45, 37.5, 30, 22.5, 15, 7.5, and 0 km providing a convenient division into intervals of approximately one scale height. The wind magnitude and altitude gradient are matched at 100 km with the thermospheric values, and in addition the altitude gradient is specified (fit) at 100 km.

The harmonic expansion at each altitude node is limited to low order terms as summarized in Tables 2a and 2b, thus smoothing the model output in space and time. The classification into symmetrical and asymmetrical is with respect to reflection about the equator with

symmetrical meaning the vector spherical harmonic term provides zonal winds which have the same direction either side of the equator while the meridional wind changes direction. The column value 'm' refers to the local time harmonic content (1 the first harmonic, etc.). The 'n' value is the latitude harmonic order and is always equal to or larger than 'm'. If the n minus m value is even, then the B field term is symmetric and the C field term is asymmetric. The higher the order 'n' the greater the latitude variability that can be represented. Only low order terms were used because of the sparse and uneven latitudinal distribution of measurement stations and the limited time series available covering different time periods for different stations. In Table 2 a dash (-) means this term is not included for this node.

The determination of the harmonic coefficients for the various nodes of the wind profile is accomplished by a least squares fit to selected subsets of the data. The node to node variations of the harmonic coefficients were smoothed by refitting with the sum of the squares of the differences between adjacent node coefficients (multiplied by a constant) added to the usual sums of squares of data minus model differences. The multiplicative (tension) constant was chosen so that the sums of squares of the data residuals increased by no more than one percent.

Root mean square deviations of the data from the model in different altitude regions are given in Tables 3a and 3b. The grenade and incoherent scatter data tend to have the largest average departures because they were not smoothed or based on monthly averages. Natural variability is also high in the upper mesosphere due to breaking gravity waves and lower thermosphere where electrodynamic effects are important. The differences between the model and rocket and incoherent scatter data also reflect possible mismodeling of the zonal average variations (model described in a separate report).

4. Model Examples/Comparisons/Discussion

4.1 Annual Average Diurnal Variations

The annual average diurnal wind amplitudes and phases from the model are illustrated in Fig. 1. Amplitudes are weak in the stratosphere and lower mesosphere (a few meters per second), but reach a peak of tens of meters per second at low- to mid- latitudes in the upper mesosphere and lower thermosphere, where they dominate the semidiurnal tide. At high latitudes, amplitudes peak even more strongly between 110 and 120 km. The accuracy of the detailed latitude patterns near the equator in the mesosphere, particularly the meridional peak near 20N, and in southern latitudes in the lower thermosphere is uncertain because of the lack of data gathering stations.

Further examples of model winds and comparisons with data are shown in Figs. 2 to 5. Here data have been selected for rather broad altitude or latitude intervals and the model wind plotted vs latitude or altitude for the midpoint of the selected intervals. The example model plot will represent the model prediction at the exact altitude or latitude of

individual measurements with a degree of faithfulness that depends on how rapidly the data and model vary with altitude, latitude, etc. The difference between the plotted points and the model line represents the average difference of each measurement, separated by source as specified in Table 1, from the model (calculated exactly for that location) and the error bars represent the one standard deviation scatter of this difference within the plot bin limits. There are two plots for each situation, separating data into two groups: rocket data (stratosphere and mesosphere) and incoherent scatter data (thermosphere); and meteor and MF radars (mesosphere and lower thermosphere). Individual data amplitudes will frequently tend to be larger than model amplitudes because varying or inconsistent phases between data points produces a cancellation effect during generation of the model. The model is based on fourier components and data to model differences were calculated with the fourier components and then the amplitudes and phases reconstructed.

In the upper stratosphere and lower mesosphere tides are determined only by rocketsonde data which are sparse in the southern hemisphere and generally have incomplete local time coverage for individual months. Thus, the model does not include interhemispheric differences or seasonal variations below 75 km. While the scatter of the original measurements can be considerable (particularly at high latitudes) and measurements at different local times are usually from different days, diurnal variations are clearly present with rapid phase changes with height near the equator and little phase change with height below 100 km at higher latitudes. Amplitudes are not very reliable at high latitudes because of the large scatter in the original point measurements. The eastward wind maximizes about six hours later than the northward wind in the northern hemisphere and six hours earlier than the northward wind in the southern hemisphere. These features were previously seen in analysis of earlier data [Reed et al., 1969; Groves, 1980] and are broadly consistent with theory [Forbes, 1982], although theory tends to predict a higher contribution of propagating modes at midlatitudes, and thus more rapid phase changes with altitude, than observed.

Rocket data becomes increasingly scattered in the upper mesosphere so that amplitudes are suspect, but phases generally blend smoothly with MF/Meteor radar data at their lower altitude limit. Model phases agree quite well with MF/Meteor data. The lowest latitude data (Townsville (20S), Christmas Island (2N), and Punta Borinquen (18N)) suggest higher diurnal amplitudes in the upper mesosphere (Figs. 2e and 3e), but these data are from very limited time series and with Kyoto (35N) amplitudes generally being on the small side and Adelaide (35S) on the high side, it is difficult to fit all these stations without increasing the harmonic order considerably and introducing complex latitude and interhemispheric variations which may not be justified. All comparisons must be considered against the background of significant variability in both the diurnal and semidiurnal tides (e.g. Fritts and Isler [1992]) and the fact that the stations are not equivalent in their seasonal coverage or years of measurement.

In the lower thermosphere at high latitudes, the rapid change in diurnal phase above 100 km (Figs. 4f and 5f) with increasing amplitudes

into the thermosphere is reflected in both MF/Meteor data and IS data. However, at mid- to low- latitudes the lack of full daytime coverage by IS plus considerable differences between MF/Meteor radar stations makes the transition of the diurnal tide into the thermosphere poorly defined.

A comparison of rocketsonde and IS radar winds as a function of local time with the HWM93 model (including both the diurnal, semidiurnal, and zonal average components) is shown in Fig. 6 for several altitude and latitude regions. The grenade data generally show the same trends as the rocketsonde data, although with greater scatter. Incoherent scatter radar data is frequently quite variable, particularly at high latitudes.

4.2 Semidiurnal Variations

The annual average semidiurnal wind amplitudes and phases from the model are illustrated in Fig. 7. Amplitudes are weak in the stratosphere and lower mesosphere (a few meters per second). However, amplitudes increase strongly to a peak of 40 to 60 m/s, and are dominant over the diurnal variation, in the lower thermosphere. The accuracy of the detailed latitude patterns near the equator in the mesosphere and in southern latitudes in the lower thermosphere is uncertain because of the lack of data gathering stations. Model and data comparison plots similar to those for diurnal variations are shown in Figs. 8 to 11 (see also Fig. 6 for local time plots). These figures also show the corresponding model prediction from the Forbes and Vial [1989] model (FV89).

In the upper stratosphere and lower mesosphere the same data limitations apply as for diurnal variations and the model does not include interhemispheric differences or seasonal variations below 75 km. Semidiurnal variations are clearly present at low- to mid- latitudes with systematic phase variations with height. Amplitudes are again not very reliable at high latitudes because of the large scatter in the point measurements.

Rocket data becomes increasingly scattered in the upper mesosphere so that amplitudes are suspect, but phases generally blend smoothly with MF/Meteor radar data at their lower altitude limit. Model phases agree quite well with MF/Meteor data, except for the Townsville zonal phase which differs significantly from its northern hemisphere counterparts (Figs. 9d, 9e, and 9f).

Semidiurnal amplitudes increase strongly into the lower thermosphere according to IS data, but not as strongly in meteor radar data (Figs 10e, 10f, 11e, and 11f).

Amplitudes from the Forbes and Vial [1989] model are generally the same order of magnitude as the data and HWM93 model and with similar phase patterns overall.

4.3 Annual-Diurnal Variations

The annual variation of the diurnal amplitudes and phases of the meridional and zonal wind is illustrated for three latitudes in Fig. 12 corresponding to the locations of the Saskatoon, Arecibo, and Christchurch radars. In the upper mesosphere, the meridional amplitude tends to maximize in the summer. The zonal seasonal variation is weaker and less clear. Some stations also had significant semiannual variations but consistency with other stations was not always good.

Data comparison plots are shown in Figs. 13 and 14. The broad seasonal trends in amplitude and phase at high latitudes were captured fairly well except for the meridional phase at Mawson (Fig. 13a). At mid-latitudes the several radar stations were somewhat diverse in measured phases (Figs. 13e and 14e) and helped reduce the model amplitude relative to measured zonal amplitudes (Figs. 14b and 14e). Asymmetries such as the higher amplitudes at Adelaide compared to Kyoto [Vincent et al., 1988] are captured better in the meridional (Figs. 13b and 13e) than the zonal (Figs. 14b and 14e) component. It is apparent that hemispherical asymmetries have a more complicated latitude dependence than assumed here. The strong annual variation in meridional amplitude at Christmas Island (Fig. 13d) without accompanying phase changes or zonal changes could not be captured by the limited harmonic model.

4.4 Annual-Semidiurnal Variations

The annual variation of the semidiurnal amplitudes and phases of the meridional and zonal wind is illustrated for three latitudes in Fig. 15. Semiannual trends in amplitude are more noticeable than annual trends, particularly in the southern hemisphere. However, vertical wavelengths in the mesosphere are shorter in winter than summer as discussed by Manson et al. [1989].

Data comparison plots are shown in Figs. 16 and 17 and include also the Forbes and Vial [1989] model. The annual trends in amplitude and phase at middle to high latitudes were captured fairly well. Phases have a more noticeable annual variation than amplitudes, while amplitudes have a more semiannual character. The FV89 model is generally similar but with a larger seasonal variation in the lower thermosphere. The situation is similar at mid-latitudes, but again the greater diversity of measurement phases lead to somewhat smaller modelled amplitudes. Neither HWM93 nor FV89 does particularly well with the Christchurch and Adelaide meridional phases (Fig. 16b). Christchurch amplitudes are generally higher than the model and data from Adelaide (Figs. 16b and 17b), but data over several years reported by Fraser [1990] indicates that the data used here from 1979 may be unusually high. The trends at Christmas Island (Figs. 16d and 17d) were captured better than for the diurnal tide. The FV89 zonal phase appears to be systematically offset from HWM93 at low latitudes (Fig. 17d).

5. Summary

MF radar and meteor radar, combined with rocket soundings and incoherent scatter radar, have been used to extend the tidal components of the HWM90 spherical harmonic wind model into the mesosphere and upper stratosphere. While month to month details cannot be completely represented, data are fit with an overall rms error of approximately 5 to 10 m/s. Comparison with rocket and radar data indicates that the model represents current knowledge of the climatological average tidal components reasonably well.

References

Avery, S. K., A. C. Riddle, B. B. Balsley, The Poker Flat, Alaska, MST radar as a meteor radar, Radio Sci., 18, 1021-1027, 1983.

Avery, S. K., J. P. Avery, T. A. Valentic, S. E. Palo, M. J. Leary, and R. L. Obert, A new meteor echo detection and collection system: Christmas Island mesospheric wind measurements, Radio Sci., 25, 657-669, 1990.

Bernard, R., Tides in the E-region observed by incoherent scatter over Saint Santin, J. Atmos. Terr. Phys., 36, 1105-1120, 1974.

Bernard, R., J. L. Fellous, M. Massebeuf, and M. Glass, Simultaneous meteor radar observations at Monpazier (France, 44N) and Punta Borinquen (Puerto-Rico, 18N). I-Latitudinal variations of atmospheric tides, J. Atmos. Terr. Phys., 43, 525-533, 1981.

Clark, R. R., Upper atmosphere wind observations of waves and tides with the UNH Meteor Radar System at Durham 43N (1977, 1978 and 1979), J. Atmos. Terr. Phys., 45, 621-627, 1983.

Fleming, E. L., S. Chandra, J. J. Barnett, and M. Corney, Zonal mean temperature, pressure, zonal wind and geopotential height as functions of latitude, Adv. Space Res., 10(12), 11-59, 1990.

Forbes, J. M., Atmospheric tides 1. Model description and results for the solar diurnal component, J. Geophys. Res., 87, 5222-5240, 1982.

Forbes, J. M., and F. Vial, Monthly simulations of the solar semidiurnal tide in the mesosphere and lower thermosphere, J. Atmos. Terr. Phys., 51, 649-661, 1989.

Groves, G. V., Seasonal and diurnal variations of middle atmosphere winds, Phil. Trans. R. Soc. Land.,A296, 19-40, 1980.

Franke, S. J., and D. Thorsen, Mean winds and tides in the upper middle atmosphere at Urbana (40N,88W) during 1991-1992, submitted to J. Geophys. Res, 1993.

Fraser, G. J., Long-term variations in mid-latitude southern hemisphere mesospheric winds, Adv. Apace Res., 10(10), 247-250, 1990.

Fritts, D. C., and J. R. Isler, First observations of mesospheric dynamics with a partial reflection radar in Hawaii (22N, 160W), Geophys. Res. Lett., 19, 409-412, 1992.

Harper, R. M., Tidal winds in the 100- to 200-km region at Arecibo, J. Geophys. Res., 82, 3243-3250, 1977.

Harper, R. M., R. H. Wand, C. J. Zamlutti,and D. T. Farley, E region ion drifts and winds from incoherent scatter measurements at Arecibo, J. Geophys. Res., 81, 25-37, 1976.

Hedin, A. E., MSIS-86 thermospheric model, J. Geophys. Res., 92, 4649-4662, 1987.

Hedin, A. E., Extension of the MSIS thermosphere model into the middle and lower atmosphere, J. Geophys. Res., 96, 1159-1172, 1991.

Hedin, A. E., N. W. Spencer, and T. L. Killeen, Empirical global model of upper thermosphere winds based on Atmosphere and Dynamics Explorer satellite data, J. Geophys. Res., 93, 9959-9989, 1988.

Hedin, A. E., M. A. Biondi, R. G. Burnside, G. Hernandez, R. M. Johnson, T. L. Killeen, C. Mazaudier, J. W. Meriwether, J. E. Salah, R. J. Sica, R. W. Smith, N. W. Spencer, V. B. Wickwar, and T. S. Virdi, Revised global model of thermosphere winds using satellite and

ground-based observations, J. Geophys. Res., 96, 7657-7688, 1991.
Hedin, A. E., E. L. Fleming, A. H. Manson, F. J. Schmidlin, S. K. Avery, and S. J. Franke, Empirical wind model for the middle and lower atmosphere - Part 1: Local time average, NASA Tech. Mem., NASA 104581, 1993.
Johnson, R. M., V. B. Wickwar, R. G. Roble, and J. G. Luhmann, Lower-thermosphere winds at high latitude: Chatanika radar observations, Annales Geophys.,5A, 383-404, 1987.
MacLeod, R., and R. A. Vincent, Observations of winds in the Antarctic summer mesosphere using the spaced antenna technique, J. Atmos. Terr. Phys., 47, 567-574, 1985.
Manson, A. H., and C. E. Meek, Climatologies of mean winds and tides observed by medium frequency radars at Tromso (70N) and Saskatoon (52N) during 1987-1989, Can. J. Phys., 69, 1991.
Manson, A. H., C. E. Meek, H. Teitelbaum, F. Vial, R. Schminder, D. Kurschner, M. J. Smith, G. J. Fraser, and R. R. Clark, Climatologies of semi-diurnal and diurnal tides in the middle atmosphere (70-110 km) at middle latitudes (40 - 55), J. Atmos. Terr. Phys., 51, 579-593, 1989.
Massebeuf, M., R. Bernard, J. L. Fellous, and M. Glass, The mean zonal circulation in the meteor zone above Garchy (France) and Kiruna (Sweden), J. Atmos. Terr. Phys., 41, 647-655, 1979.
Morse, P. M., and H. Feshbach, Methods of Theoretical Physics, McGraw-Hill, New York, 1953.
Reed, R. J., M. J. Oard, and M. Sieminski, A comparison of observed and theoretical diurnal tidal motions between 30 and 60 kilometers, Mon. Weather Rev., 97, 456-459, 1969.
Schmidlin, F. J., Rocket techniques used to measure the neutral atmosphere, Handbook for Map, 19, Ed. R. A. Goldberg, Urbana, IL, 1-28, 1986.
Schmidlin, F. J., M. Carlson, D. Rees, D. Offermann, C. R. Philbrick, H. U. Widdel, Wind structure and variability in the middle atmosphere during the November 1980 Energy Budget Campaign, J. Atmos. Terr. Phys., 47, 183-193, 1985.
Theon, J. S., W. S. Smith, J. F. Casey, and B. R. Kirkwood, The mean observed meteorological structure and circulation of the stratosphere and mesosphere, NASA Tech. Rep., NASA TR R-375, 1972.
Tsuda, T., T. Nakamura, and S. Kato, Mean winds observed by the Kyoto meteor radar in 1983-1985, J. Atmos. Terr. Phys., 49, 461-466, 1987.
Vincent, R. A., and S. M. Ball, Mesospheric winds at low- and mid-latitudes in the southern hemisphere, J. Geophys. Res, 86, 9159-9169, 1981.
Vincent, R. A., T. Tsuda, and S. Kato, A comparative study of mesospheric solar tides observed at Adelaide and Kyoto, J. Geophys. Res.,, 93, 699-708, 1988.
Virdi, T. S., and P. J. S. Williams, Observations of tidal modes in the lower thermosphere using EISCAT, Adv. Space Res., 9(5), 83-86, 1989.
Wand, R. H., Seasonal variations of lower thermospheric winds from the Millstone Hill incoherent scatter radar, J. Geophys. Res., 88, 9227-9241, 1983.

Tables

TABLE 1. Wind Data Summary

Station	Wind Component	Latitude	Longitude	Years	Altitude	Plot Sym	Reference
Incoherent Scatter							
EISCAT	M&Z	69.6N	19.2E	85–87	100–120	B	[Virdi and Williams, 1989][3]
Chatanika	M&Z	65.1N	147.4W	76–82	90–130	1	[Johnson et al., 1987][3]
St. Santin	M	44.6N	2.2E	73–85	90–170	5	[Bernard, 1974][3]
Millstone	M&Z	42.5N	71.5W	76–77	105–135	3	[Wand, 1983][1]
Arecibo	M	18.3N	66.8W	74–77	100–170	6	[Harper et al., 1976][3]
Arecibo	Z			74–75	100–130	6	[Harper, 1977][1]
MF radar, monthly averages							
Tromso	M&Z	70. N	20. E	87–89	67–112	M	[Manson & Meek, 1991][2]
Saskatoon	M&Z	52. N	107. W	85	61–111	F	[Manson et al., 1989][2]
Urbana	M&Z	40. N	88. W	91–92	66–111	T	[Franke & Thorsen, 1993][3]
Townsville	M&Z	20. S	147. E	78–80	70–100	K	[Vincent and Ball, 1981][2]
Adelaide	M&Z	35. S	138. E	84–86	70–100	J	[Vincent et al., 1988][2]
Christchurch	M&Z	44. S	173. E	79	65–102	I	[Fraser, 1990; Manson et al., 1989][2]
Mawson	M&Z	67.6S	62.9E	84–86	76–108	O	[MacLeod and Vincent, 1985][2]
Meteor radar, monthly averages							
Poker Flat	M&Z	65. N	147. W	83–84	75–106	W	[Avery et al., 1983][2]
Garchy	Z	47. N	3. E	79	78–102	+	[Massebeuf et al., 1979; Manson et al., 1989][2]
Monpazier	Z	44. N	1. E	79–80	76–104	L	[Bernard et al., 1981; Manson et al., 1989][2]
Durham	M&Z	43. N	71. W	78–84	77–110	V	[Clark, 1983; Manson et al., 1989][2]
Kyoto	M&Z	35. N	136. E	83–84	82–106	G	[Tsuda et al., 1987][2]
Punta Borinquen	Z	18. N	67. W	77–78	80–100	R	[Bernard et al., 1981][1]
Christmas Is.	M&Z	2. N	158. W	88–91	80–100	S	[Avery et al.,1990][3]
Rocket data							
Grenade	M&Z			60–72	30–100	N	[Theon et al., 1972][1]
Falling sphere	M&Z			69–91	25–100	P	[Schmidlin, 1985][3]
Datasonde	M&Z			69–91	20– 75	C	[Schmidlin, 1986][3]

[1] Wind component is M, Z, or M&Z for meridional, zonal, or both.
[1] Data from published tabulations or plots.
[2] Data from MLT radar database
[3] Data from other original database

Table 2a. Maximum B Field Spherical Harmonic Order (n)

		B field parameter (node altitude)														
Term	m	100	90	82	75	67	60	52	45	37	30	22	15	7	0	grad 100
Symmetrical																
Diurnal	1	5	5	5	5	3	3	3	3	–	–	–	–	–	–	3
Semidiurnal	2	4	4	4	4	4	4	4	4	–	–	–	–	–	–	4
Asymmetrical																
Diurnal	1	2	2	2	2	–	–	–	–	–	–	–	–	–	–	–
Diurnal–annual	1	2	2	2	2	–	–	–	–	–	–	–	–	–	–	–
Semidiurnal	2	3	3	3	–	–	–	–	–	–	–	–	–	–	–	–
Semidiurnal–annual	2	3	3	3	3	–	–	–	–	–	–	–	–	–	–	–
Semidiurnal–semiannual	2	3	3	3	–	–	–	–	–	–	–	–	–	–	–	–

Table 2b. Maximum C Field Spherical Harmonic Order (n)

		C field parameter (node altitude)														
Term	m	100	90	82	75	67	60	52	45	37	30	22	15	7	0	grad 100
Symmetrical																
Diurnal	1	6	6	6	6	4	4	4	4	–	–	–	–	–	–	4
Semidiurnal	2	5	5	5	5	5	5	5	5	–	–	–	–	–	–	5
Asymmetrical																
Diurnal	1	1	1	1	1	–	–	–	–	–	–	–	–	–	–	–
Diurnal–annual	1	1	1	1	1	–	–	–	–	–	–	–	–	–	–	–
Semidiurnal	2	2	2	2	–	–	–	–	–	–	–	–	–	–	–	–
Semidiurnal–annual	2	2	2	2	2	–	–	–	–	–	–	–	–	–	–	–
Semidiurnal–semiannual	2	2	2	2	–	–	–	–	–	–	–	–	–	–	–	–

TABLE 3a. RMS Zonal Wind Differences from HWM93

Data Set	45-60 km		60-90 km		90-120 km	
	rms	pts	rms	pts	rms	pts
Datasonde	7	2152	13	1694		
Falling Sphere	11	701	13	1336	32	135
Grenade	16	474	18	973	55	146
MF radar diurnal			5	918	6	1163
MF radar semidiurnal			5	907	7	1159
Meteor radar diurnal			7	776	7	880
Meteor radar semidiurnal			7	774	8	881
IS radar					47	1329

TABLE 3b. RMS Meridional Wind Differences from HWM92

Data Set	45-60 km		60-90 km		90-120 km	
	rms	pts	rms	pts	rms	pts
Datasonde	4	2152	9	1684		
Falling Sphere	5	701	9	1368	27	138
Grenade	11	474	16	973	50	147
MF radar diurnal			6	894	6	1133
MF radar semidiurnal			6	923	7	1175
Meteor radar diurnal			10	453	10	542
Meteor radar semidiurnal			8	435	11	542
IS radar					34	2064

Here rms is root mean square difference between data and model, pts is number of sample points, MF is medium frequency, and IS is incoherent scatter.

Figures

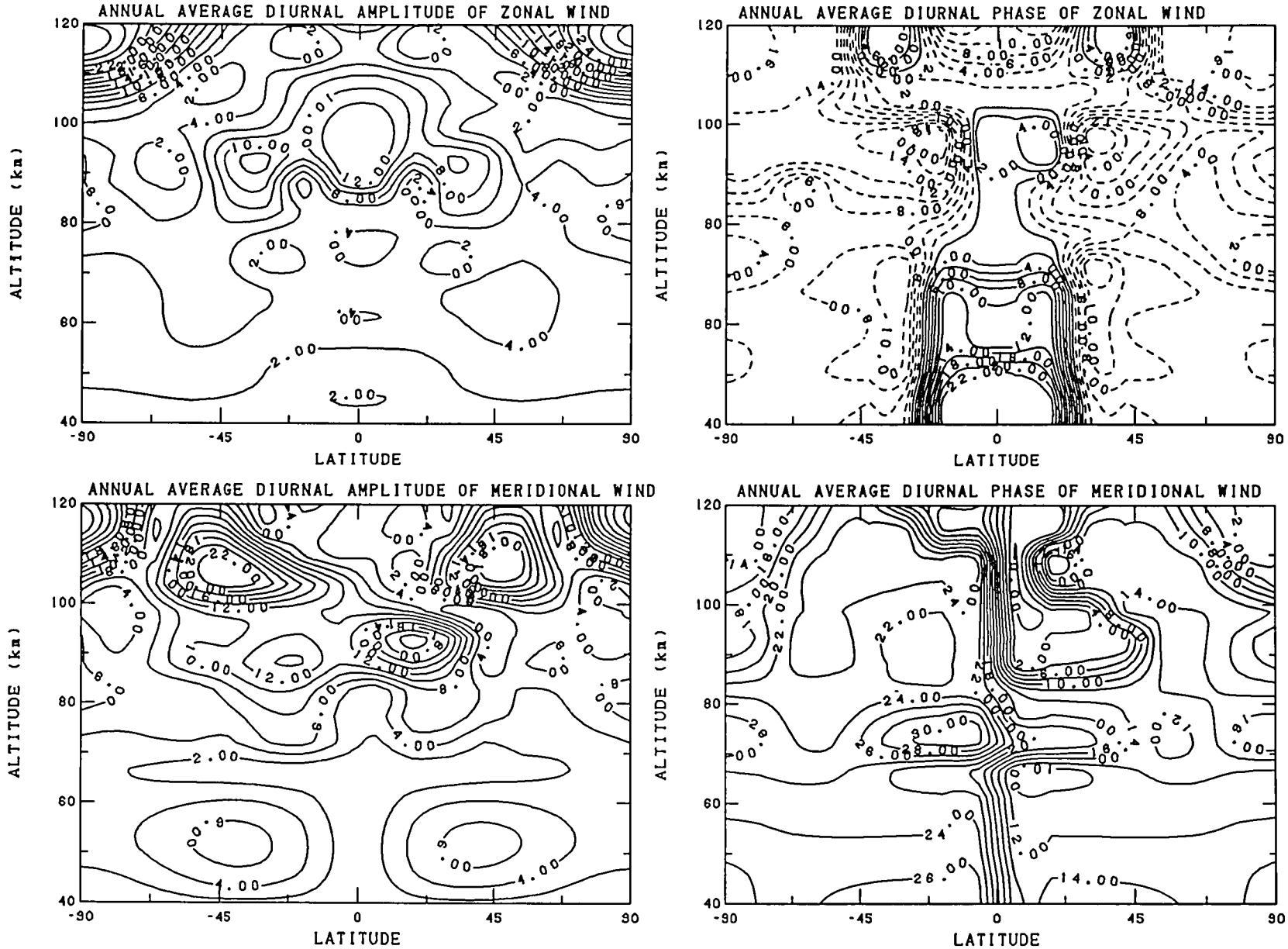

Fig. 1. Contour plots in altitude versus latitude of the seasonal average diurnal wind amplitude and phase (negative phase dashed) for zonal wind (upper panels) and meridional wind (lower panels). Phase indicates local time of maximum eastward or northward wind respectively.

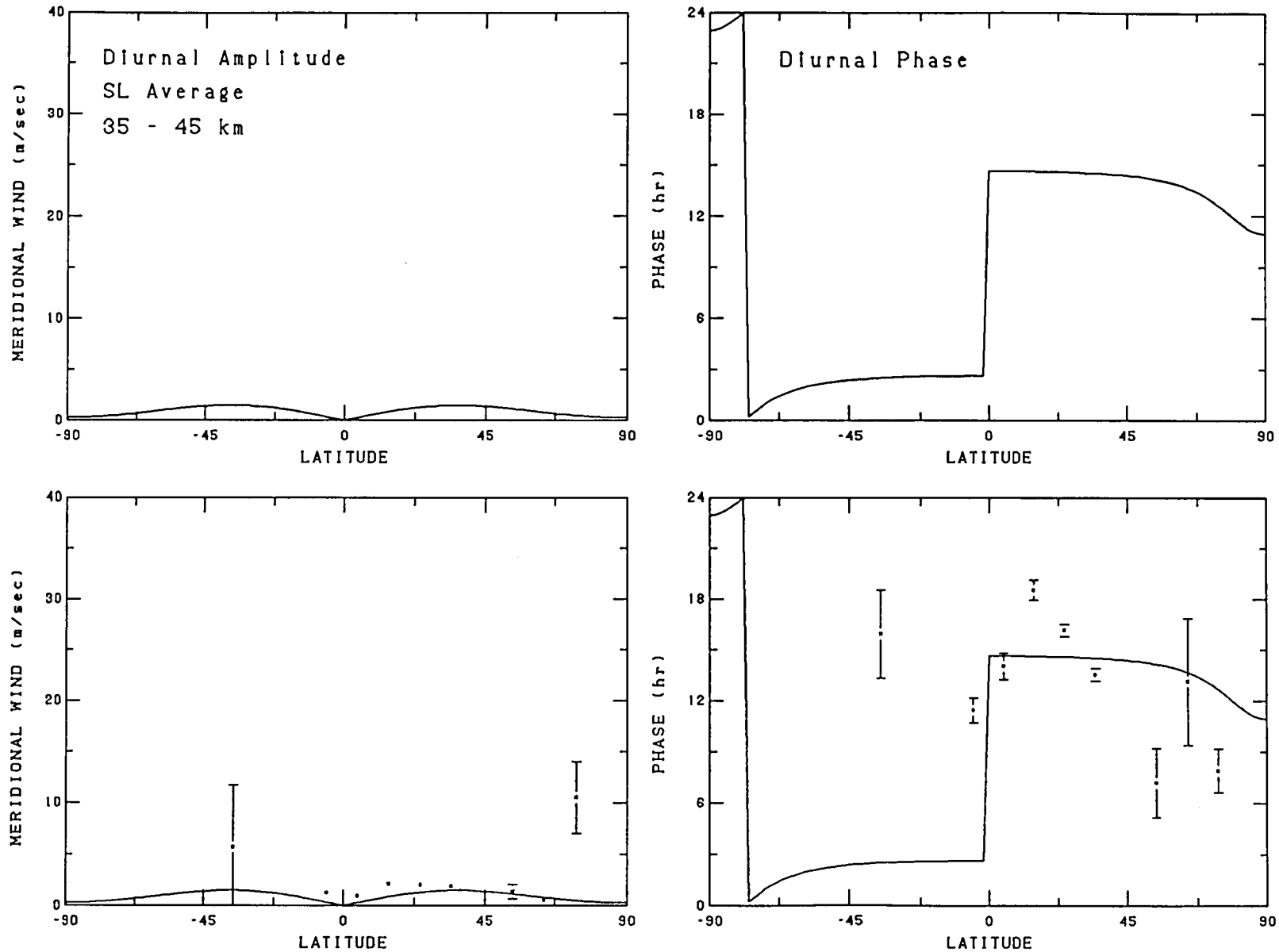

Fig. 2a. Seasonal average diurnal meridional wind amplitude and phase versus latitude for 35 to 45 km. The HWM93 wind (solid line) shown for mid-range conditions. Top row of plots contain MF/Meteor radar data with plot symbols indicated in Table 1. Bottom row contains rocketsonde and IS radar data combined (*).

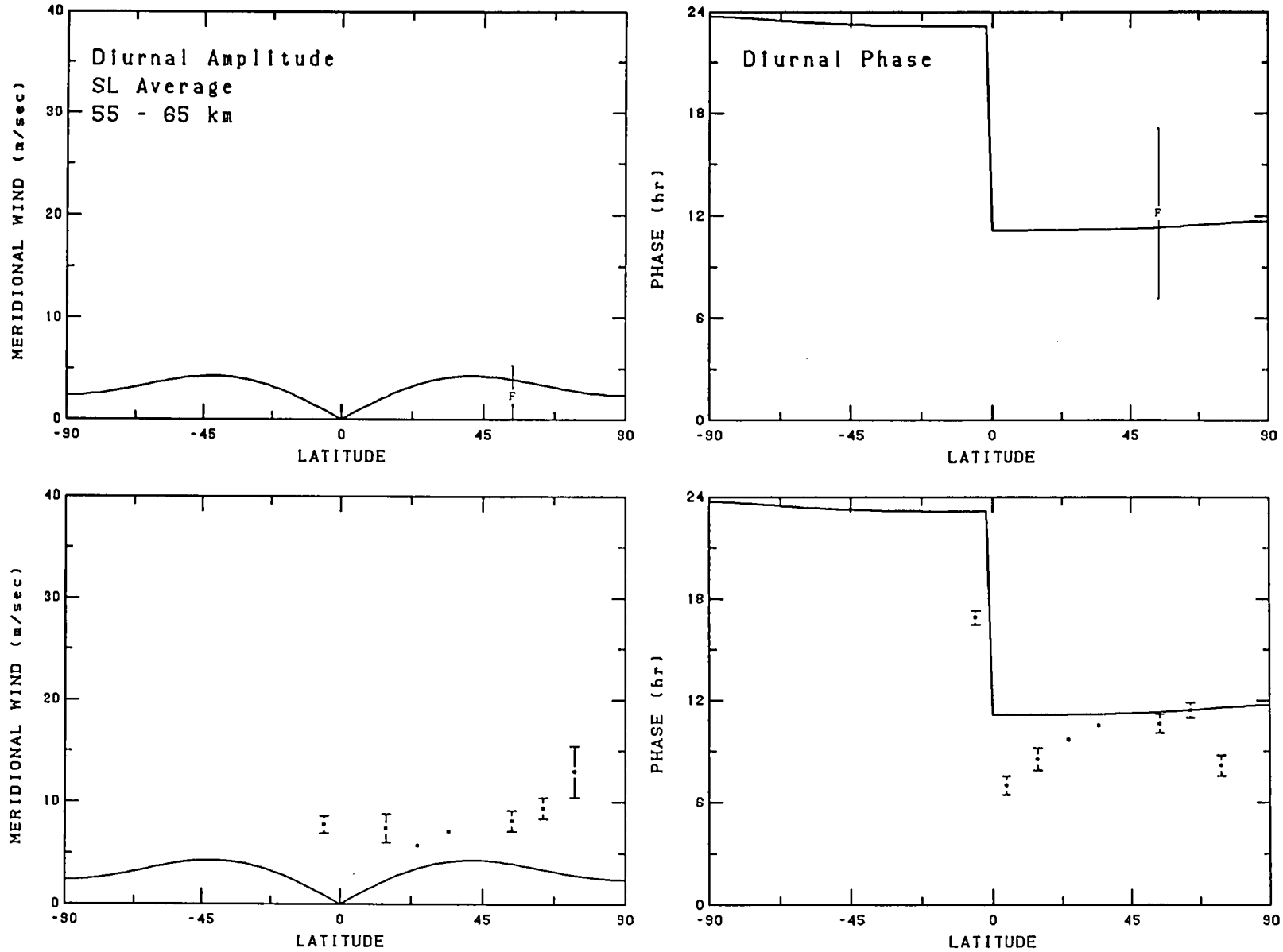

Fig. 2b. Seasonal average diurnal meridional wind amplitude and phase versus latitude for 55 to 65 km. The HWM93 wind (solid line) shown for mid-range conditions. Top row of plots contain MF/Meteor radar data with plot symbols indicated in Table 1. Bottom row contains rocketsonde and IS radar data combined (*).

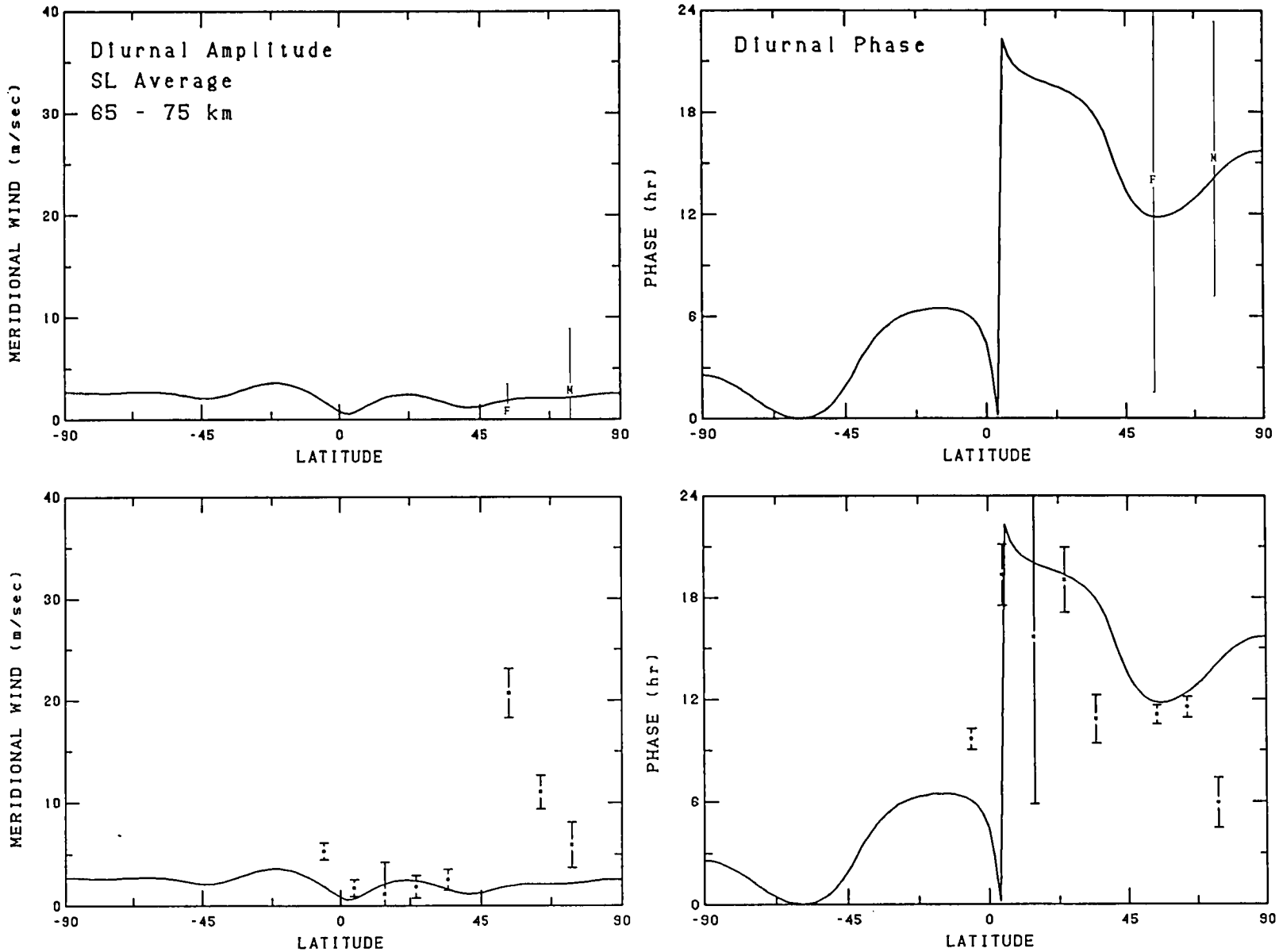

Fig. 2c. Seasonal average diurnal meridional wind amplitude and phase versus latitude for 65 to 75 km. The HWM93 wind (solid line) shown for mid-range conditions. Top row of plots contain MF/Meteor radar data with plot symbols indicated in Table 1. Bottom row contains rocketsonde and IS radar data combined (*).

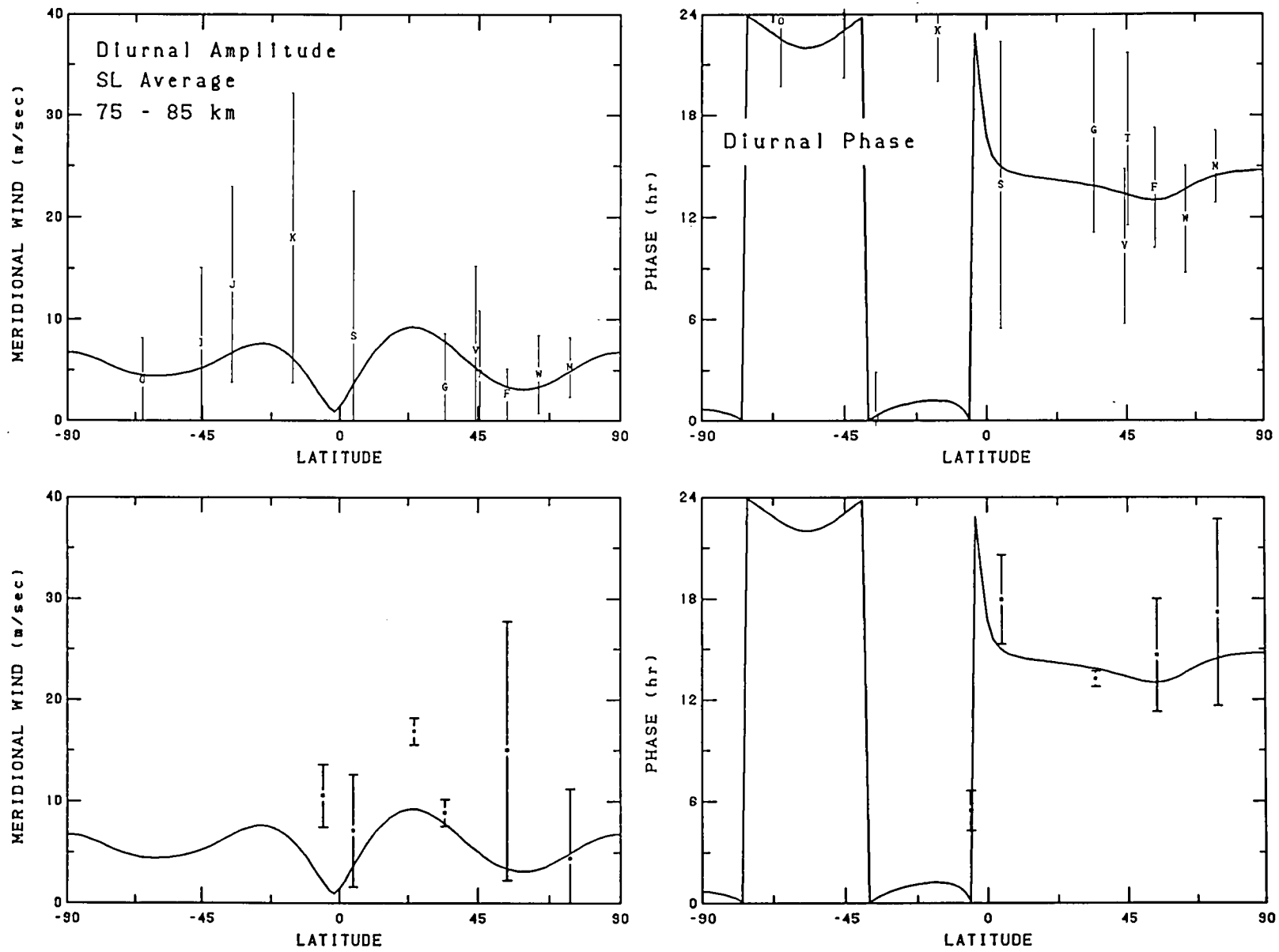

Fig. 2d. Seasonal average diurnal meridional wind amplitude and phase versus latitude for 75 to 85 km. The HWM93 wind (solid line) shown for mid-range conditions. Top row of plots contain MF/Meteor radar data with plot symbols indicated in Table 1. Bottom row contains rocketsonde and IS radar data combined (*).

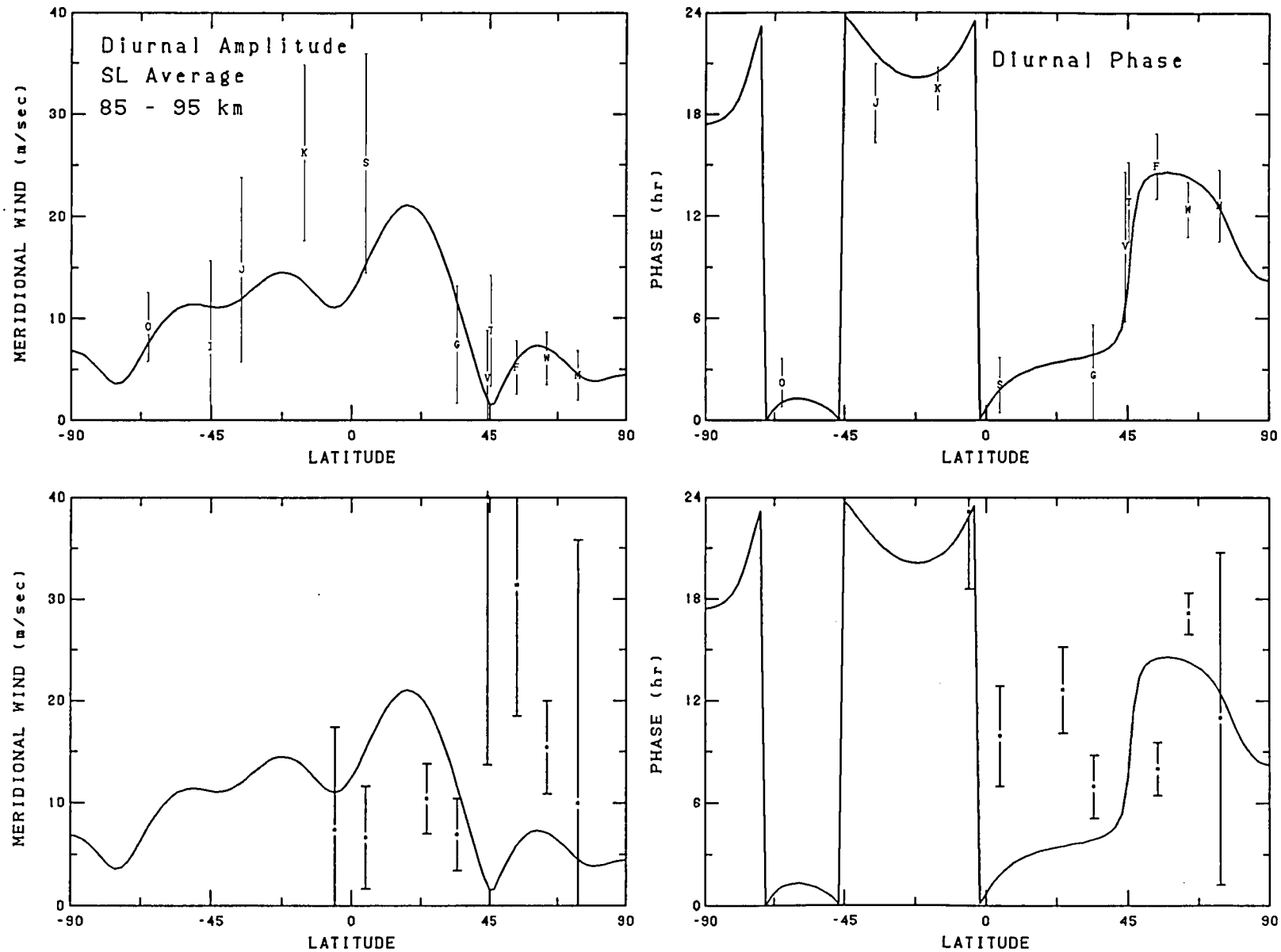

Fig. 2e. Seasonal average diurnal meridional wind amplitude and phase versus latitude for 85 to 95 km. The HWM93 wind (solid line) shown for mid-range conditions. Top row of plots contain MF/Meteor radar data with plot symbols indicated in Table 1. Bottom row contains rocketsonde and IS radar data combined (*).

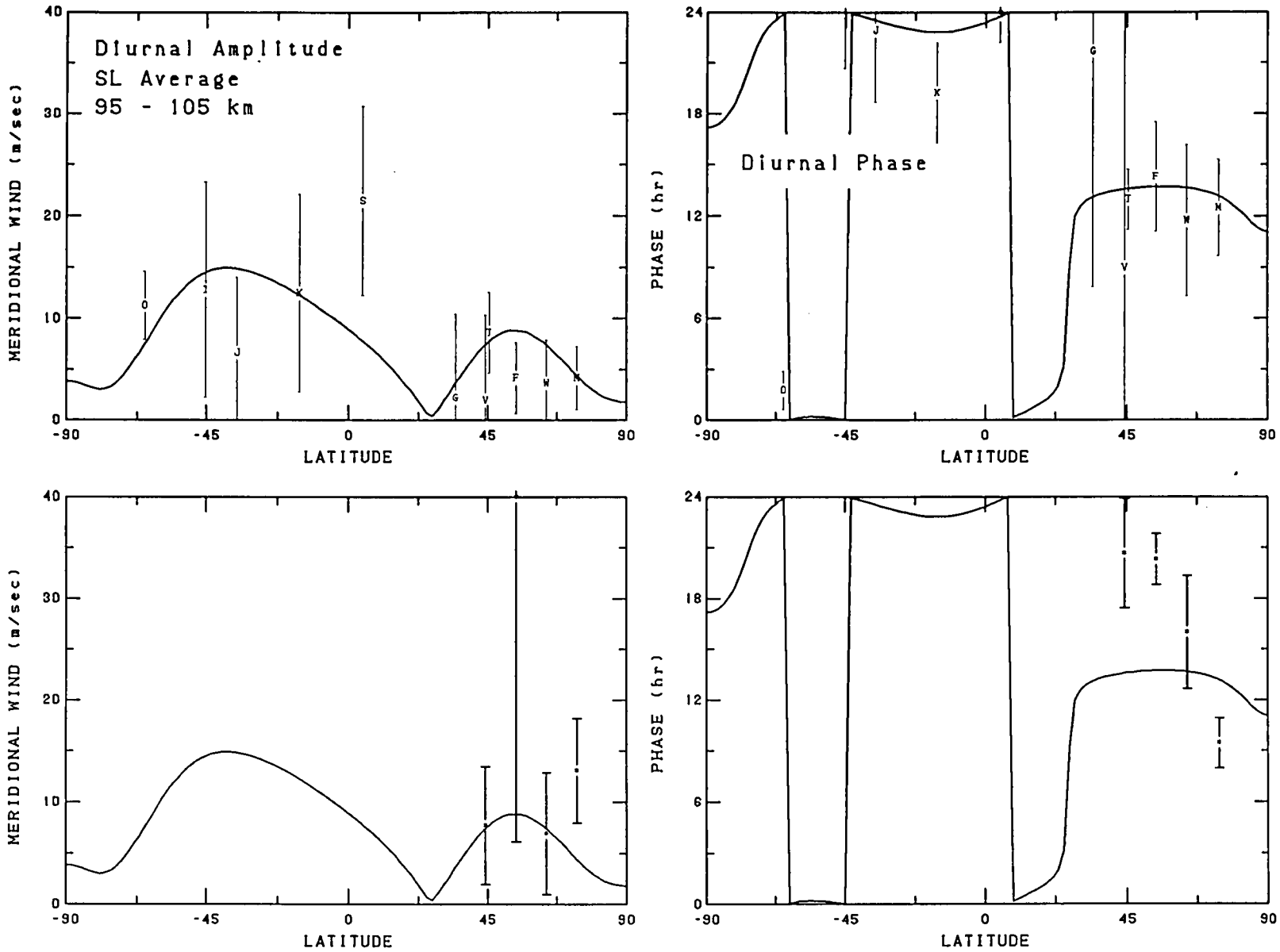

Fig. 2f. Seasonal average diurnal meridional wind amplitude and phase versus latitude for 95 to 105 km. The HWM93 wind (solid line) shown for mid-range conditions. Top row of plots contain MF/Meteor radar data with plot symbols indicated in Table 1. Bottom row contains rocketsonde and IS radar data combined (*).

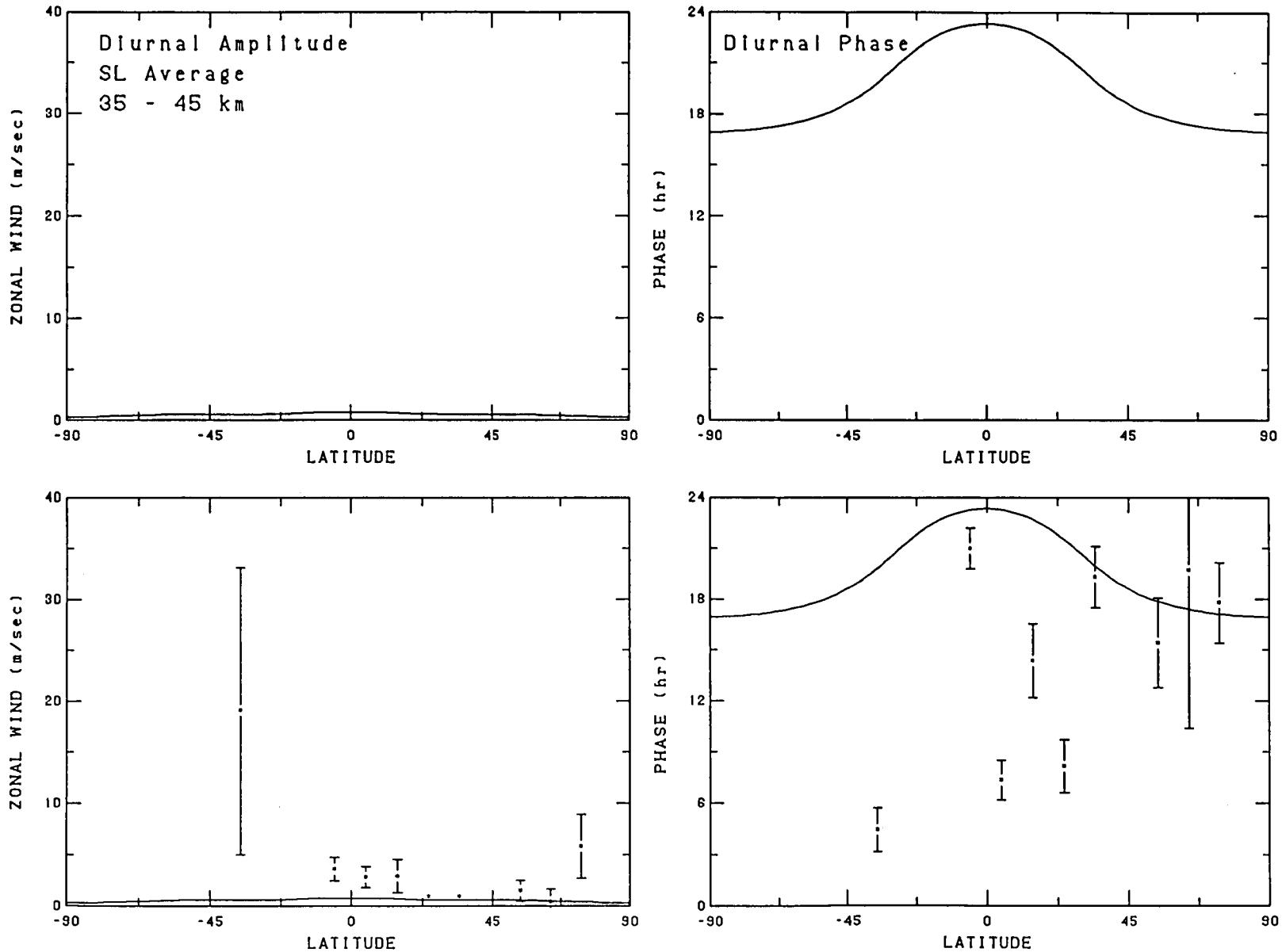

Fig. 3a. Seasonal average diurnal zonal wind amplitude and phase versus latitude for 35 to 45 km. The HWM93 wind (solid line) shown for mid-range conditions. Top row of plots contain MF/Meteor radar data with plot symbols indicated in Table 1. Bottom row contains rocketsonde and IS radar data combined (*).

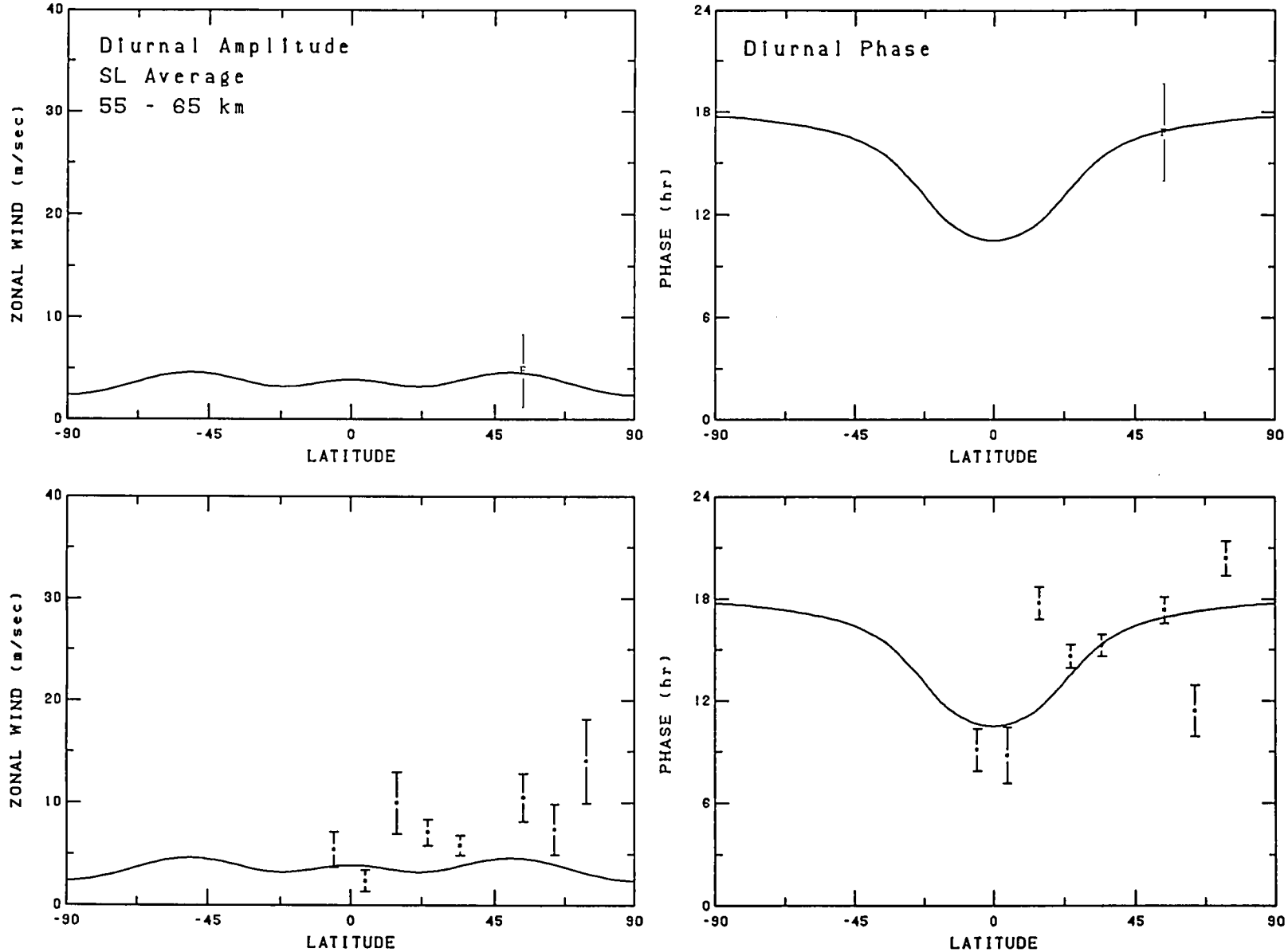

Fig. 3b. Seasonal average diurnal zonal wind amplitude and phase versus latitude for 55 to 65 km. The HWM93 wind (solid line) shown for mid-range conditions. Top row of plots contain MF/Meteor radar data with plot symbols indicated in Table 1. Bottom row contains rocketsonde and IS radar data combined (*).

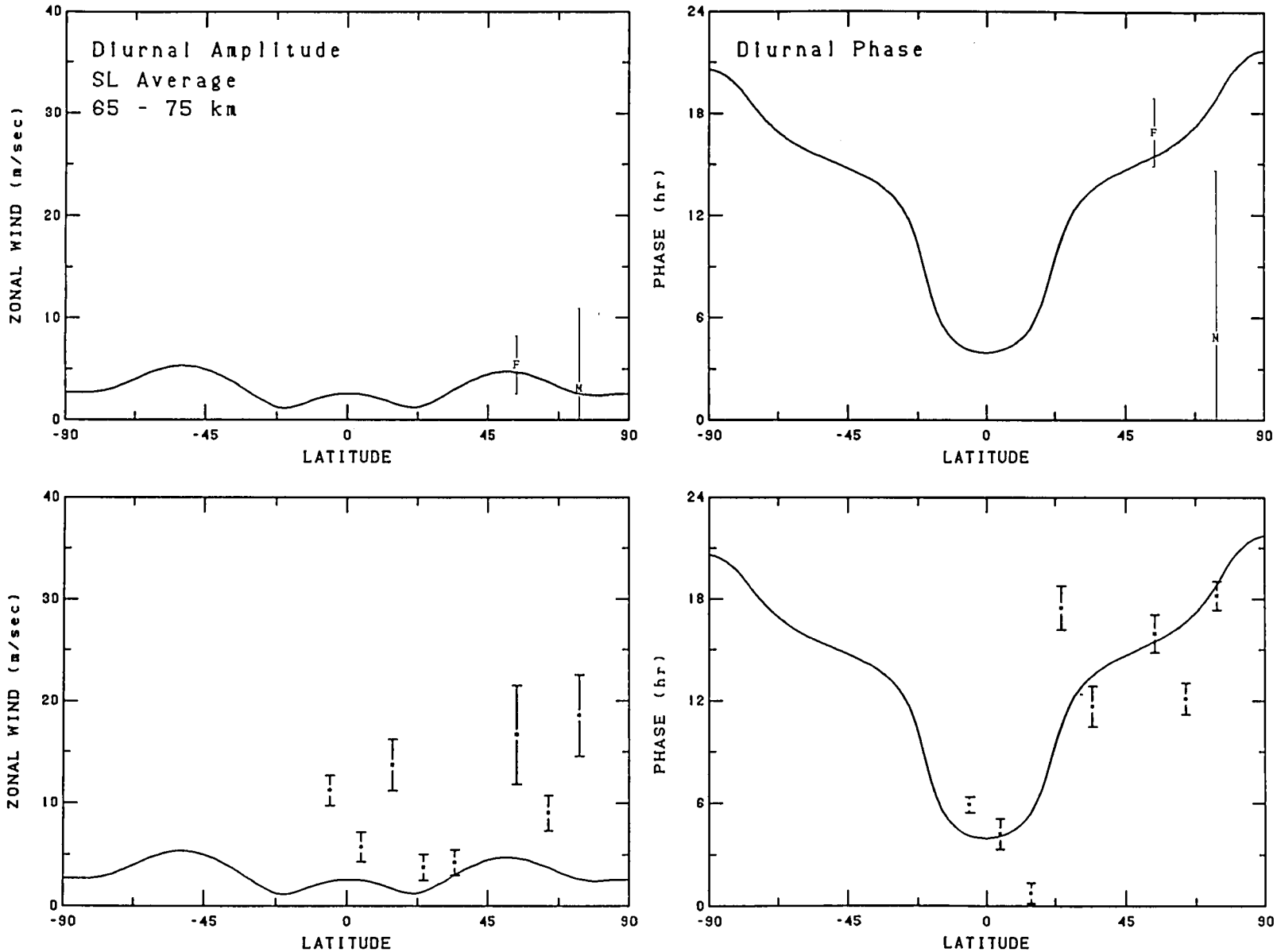

Fig. 3c. Seasonal average diurnal zonal wind amplitude and phase versus latitude for 65 to 75 km. The HWM93 wind (solid line) shown for mid-range conditions. Top row of plots contain MF/Meteor radar data with plot symbols indicated in Table 1. Bottom row contains rocketsonde and IS radar data combined (*).

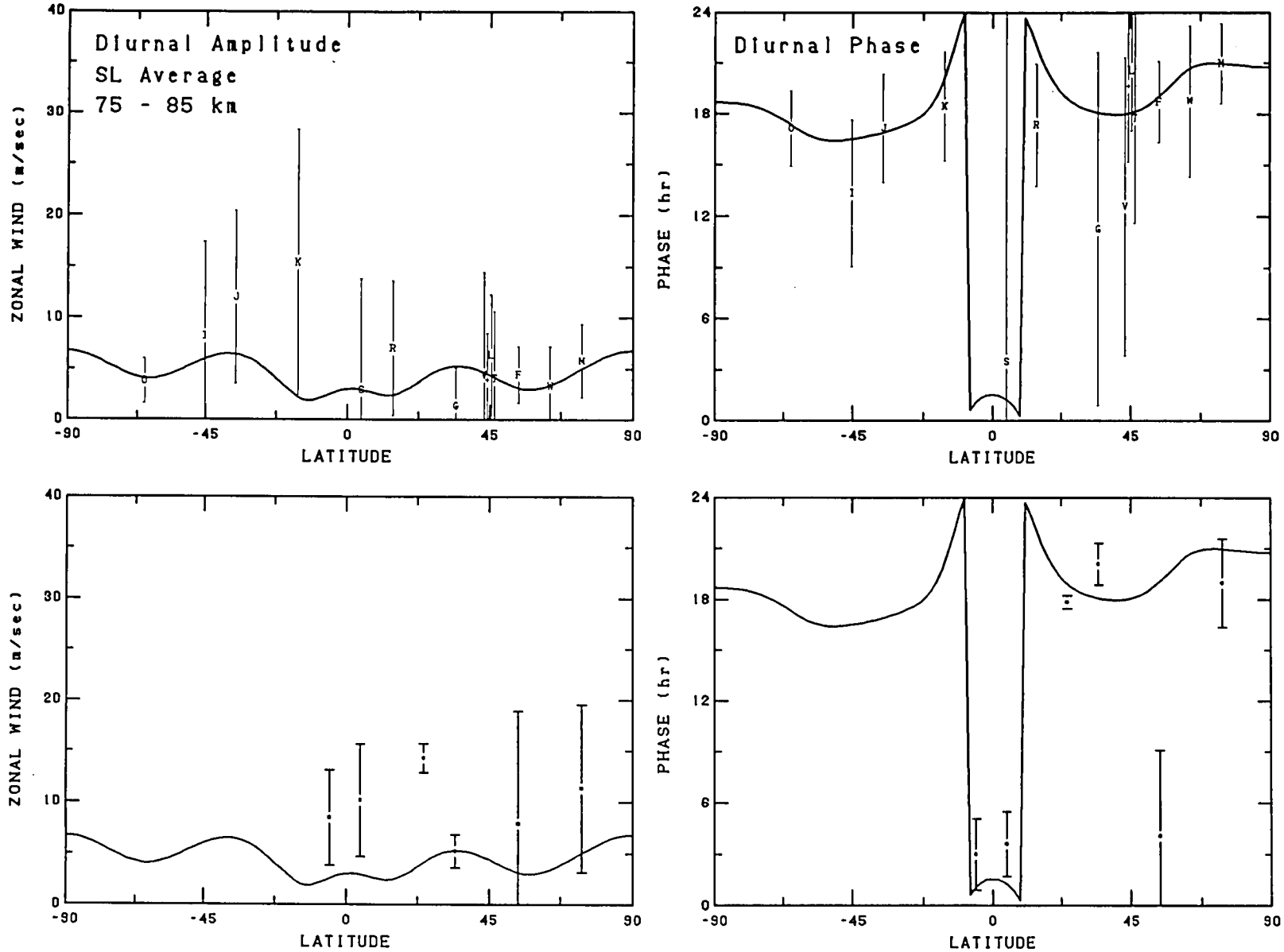

Fig. 3d. Seasonal average diurnal zonal wind amplitude and phase versus latitude for 75 to 85 km. The HWM93 wind (solid line) shown for mid-range conditions. Top row of plots contain MF/Meteor radar data with plot symbols indicated in Table 1. Bottom row contains rocketsonde and IS radar data combined (*).

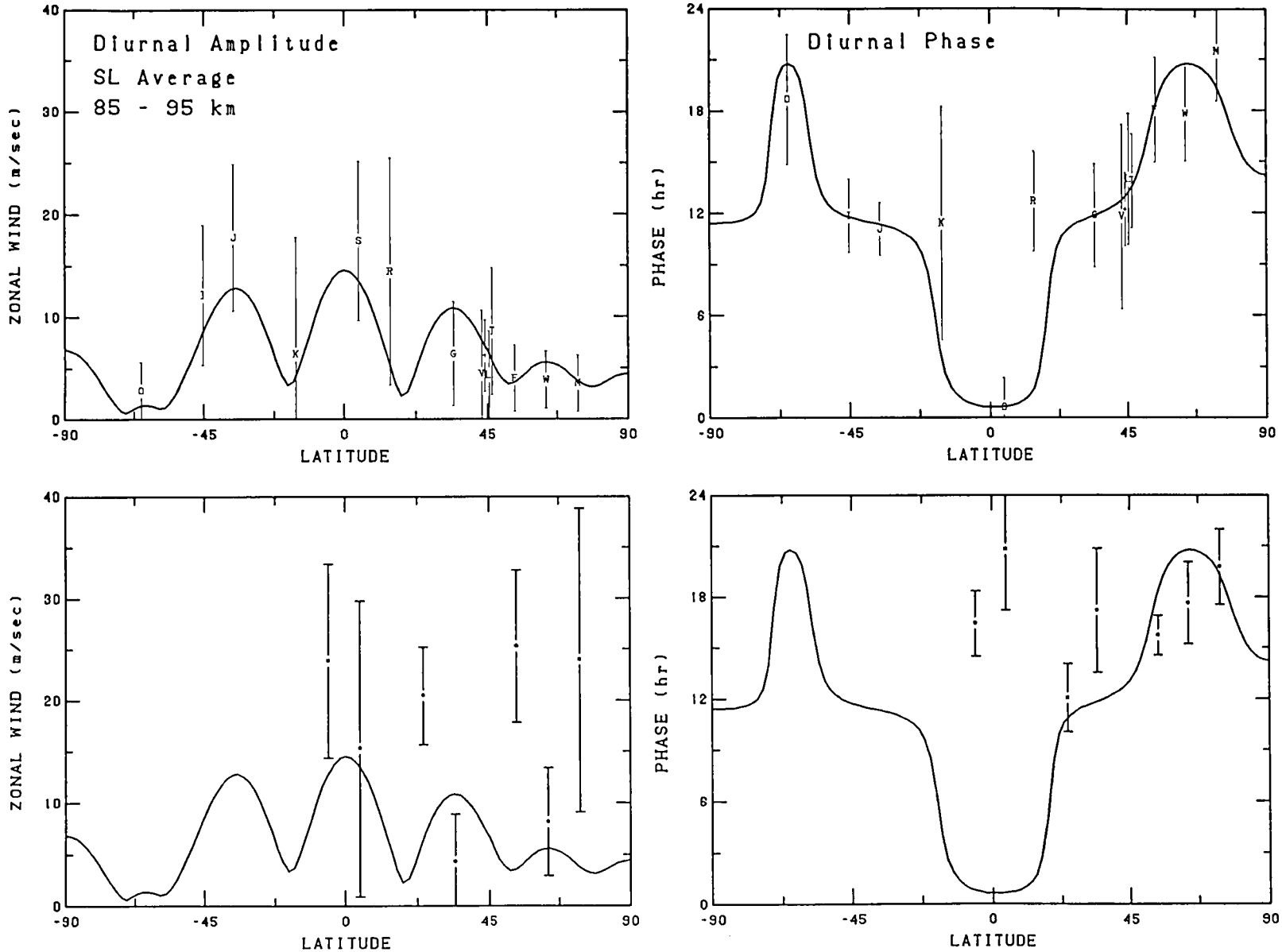

Fig. 3e. Seasonal average diurnal zonal wind amplitude and phase versus latitude for 85 to 95 km. The HWM93 wind (solid line) shown for mid-range conditions. Top row of plots contain MF/Meteor radar data with plot symbols indicated in Table 1. Bottom row contains rocketsonde and IS radar data combined (*).

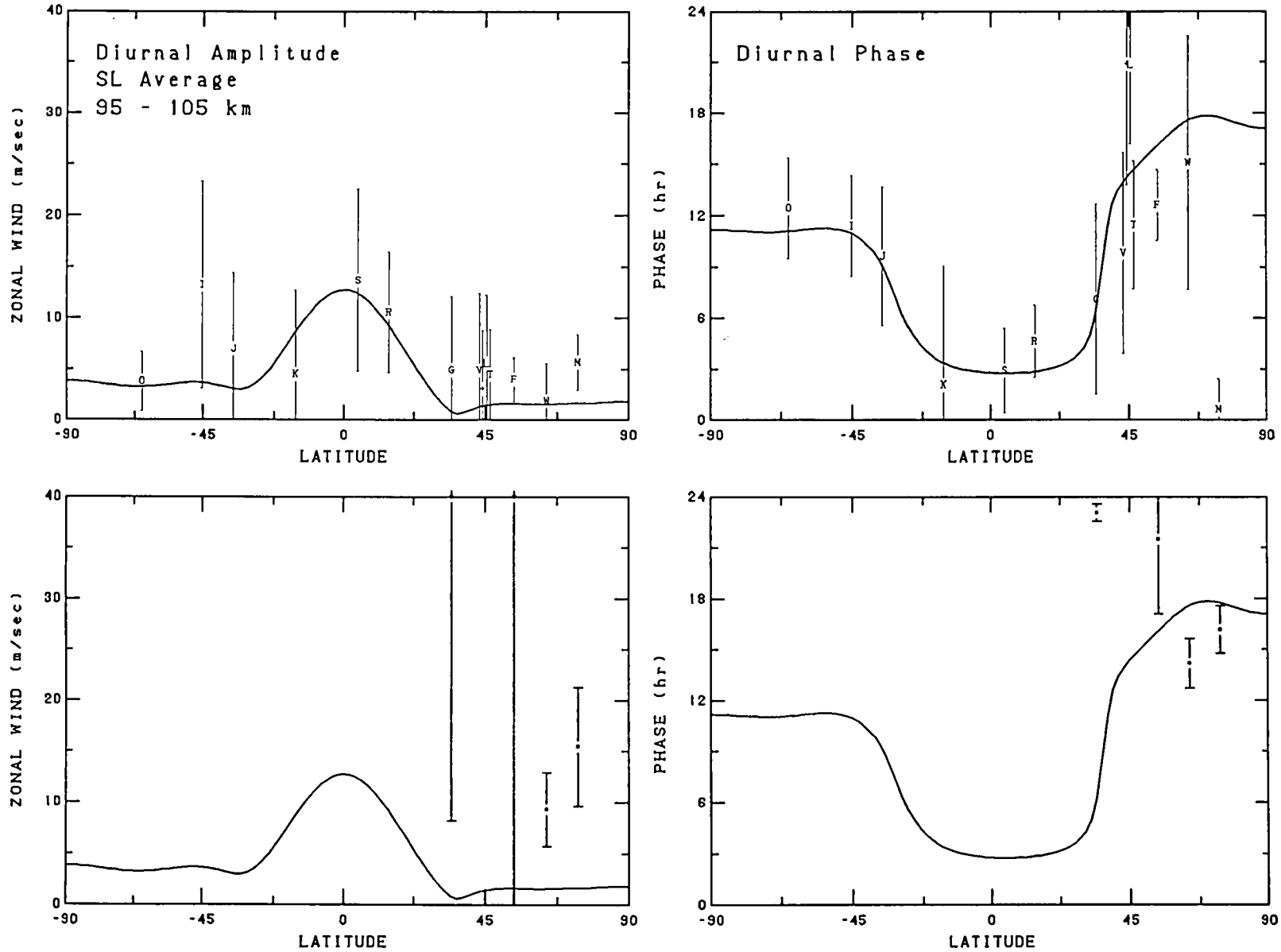

Fig. 3f. Seasonal average diurnal zonal wind amplitude and phase versus latitude for 95 to 105 km. The HWM93 wind (solid line) shown for mid-range conditions. Top row of plots contain MF/Meteor radar data with plot symbols indicated in Table 1. Bottom row contains rocketsonde and IS radar data combined (*).

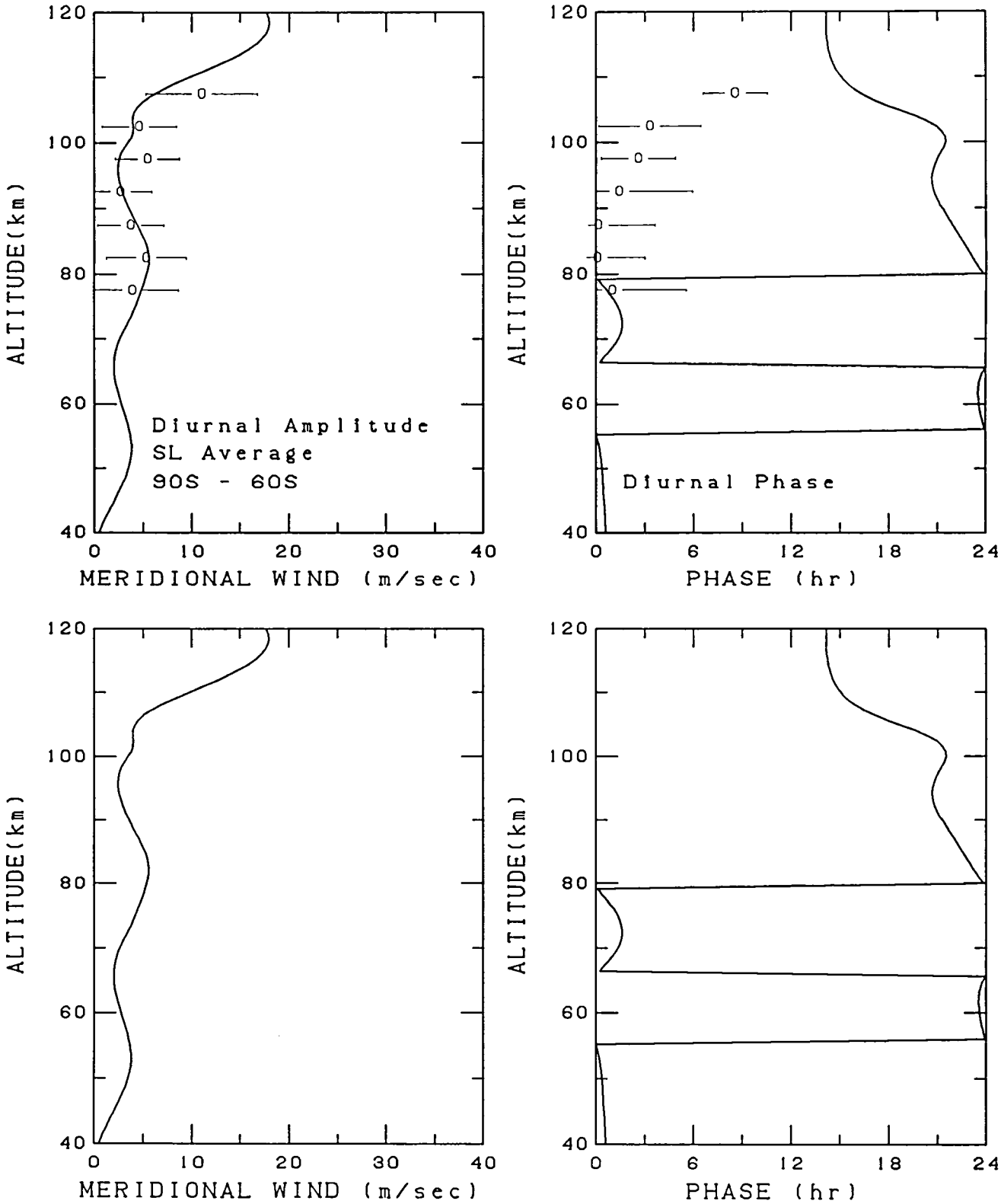

Fig. 4a. Seasonal average diurnal meridional wind amplitude and phase versus altitude for southern high latitudes. The HWM93 wind (solid line) shown for mid-range conditions. Top row of plots contain MF/Meteor radar data with plot symbols indicated in Table 1. Bottom row contains rocketsonde and IS radar data combined (*).

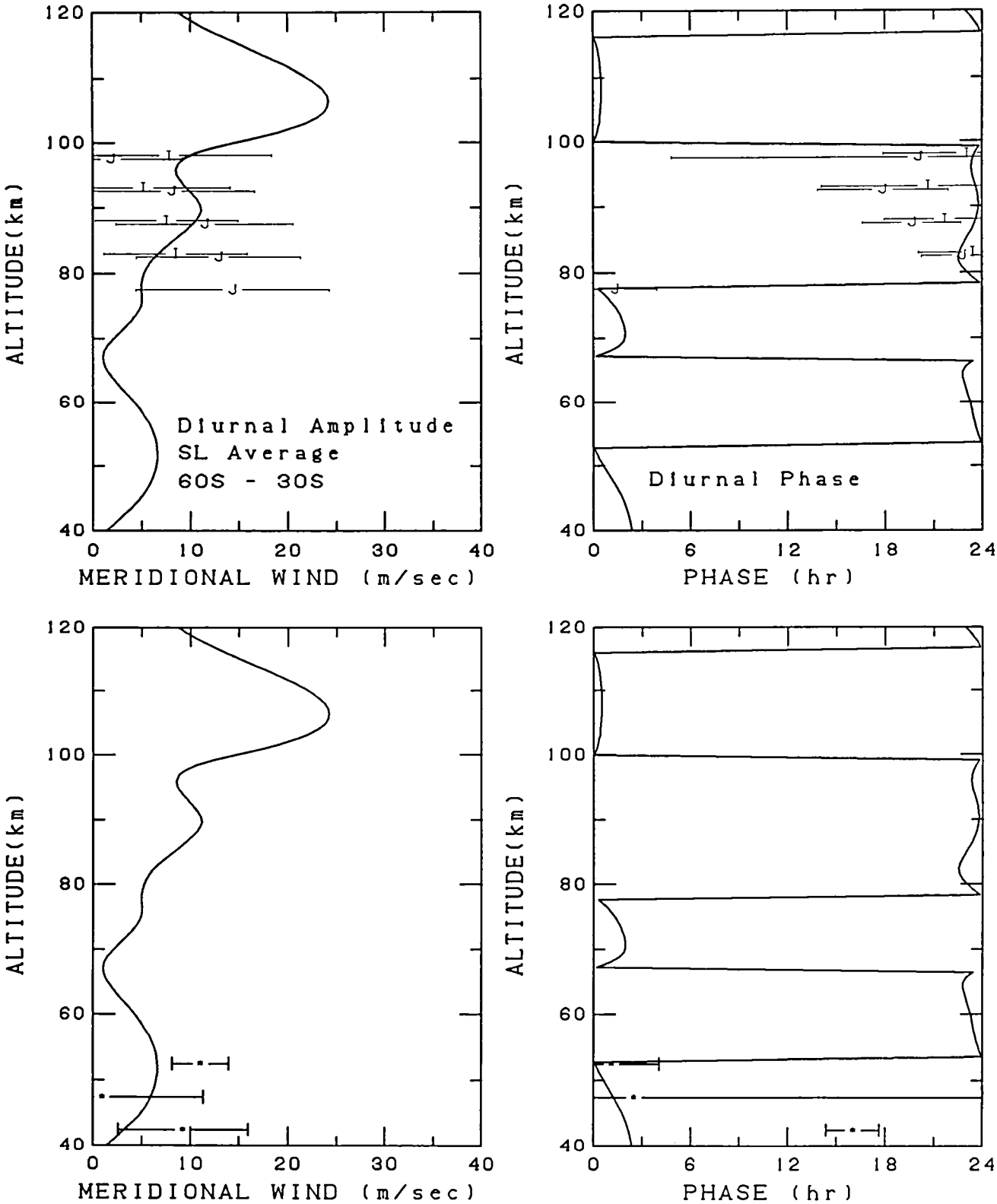

Fig. 4b. Seasonal average diurnal meridional wind amplitude and phase versus altitude for southern middle latitudes. The HWM93 wind (solid line) shown for mid-range conditions. Top row of plots contain MF/Meteor radar data with plot symbols indicated in Table 1. Bottom row contains rocketsonde and IS radar data combined (*).

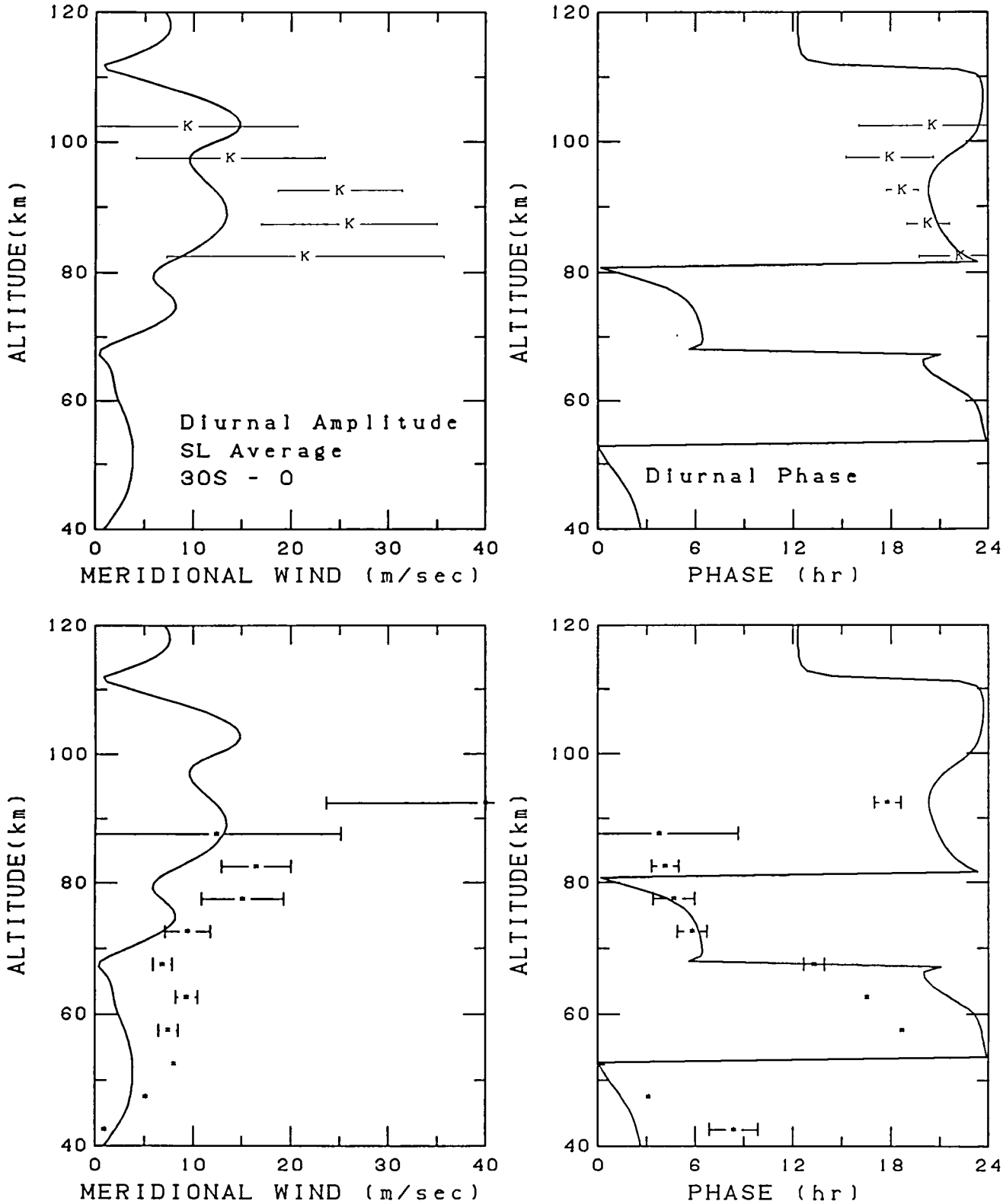

Fig. 4c. Seasonal average diurnal meridional wind amplitude and phase versus altitude for southern low latitudes. The HWM93 wind (solid line) shown for mid-range conditions. Top row of plots contain MF/Meteor radar data with plot symbols indicated in Table 1. Bottom row contains rocketsonde and IS radar data combined (*).

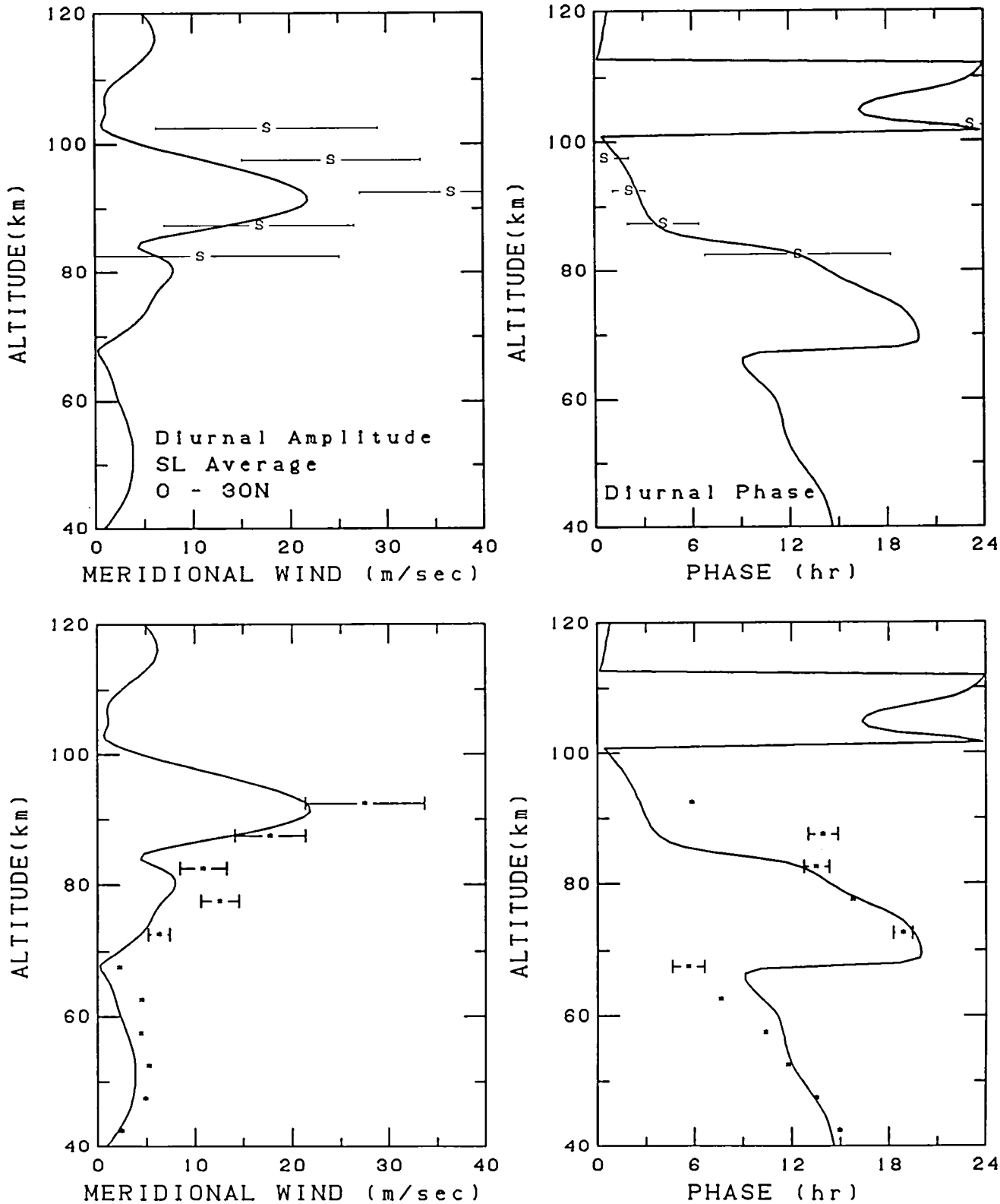

Fig. 4d. Seasonal average diurnal meridional wind amplitude and phase versus altitude for norther low latitudes. The HWM93 wind (solid line) shown for mid-range conditions. Top row of plots contain MF/Meteor radar data with plot symbols indicated in Table 1. Bottom row contains rocketsonde and IS radar data combined (*).

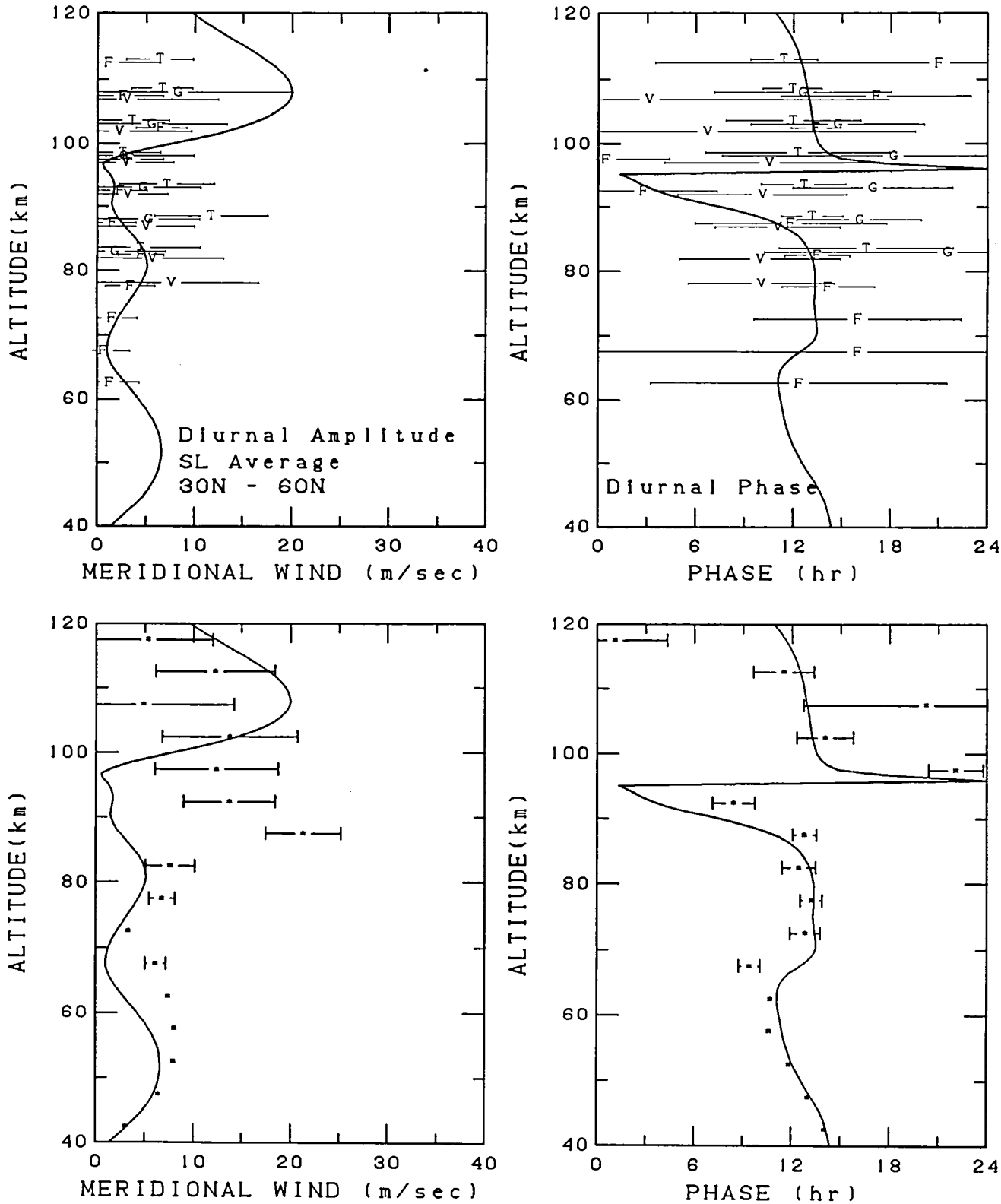

Fig. 4e. Seasonal average diurnal meridional wind amplitude and phase versus altitude for northern middle latitudes. The HWM93 wind (solid line) shown for mid-range conditions. Top row of plots contain MF/Meteor radar data with plot symbols indicated in Table 1. Bottom row contains rocketsonde and IS radar data combined (*).

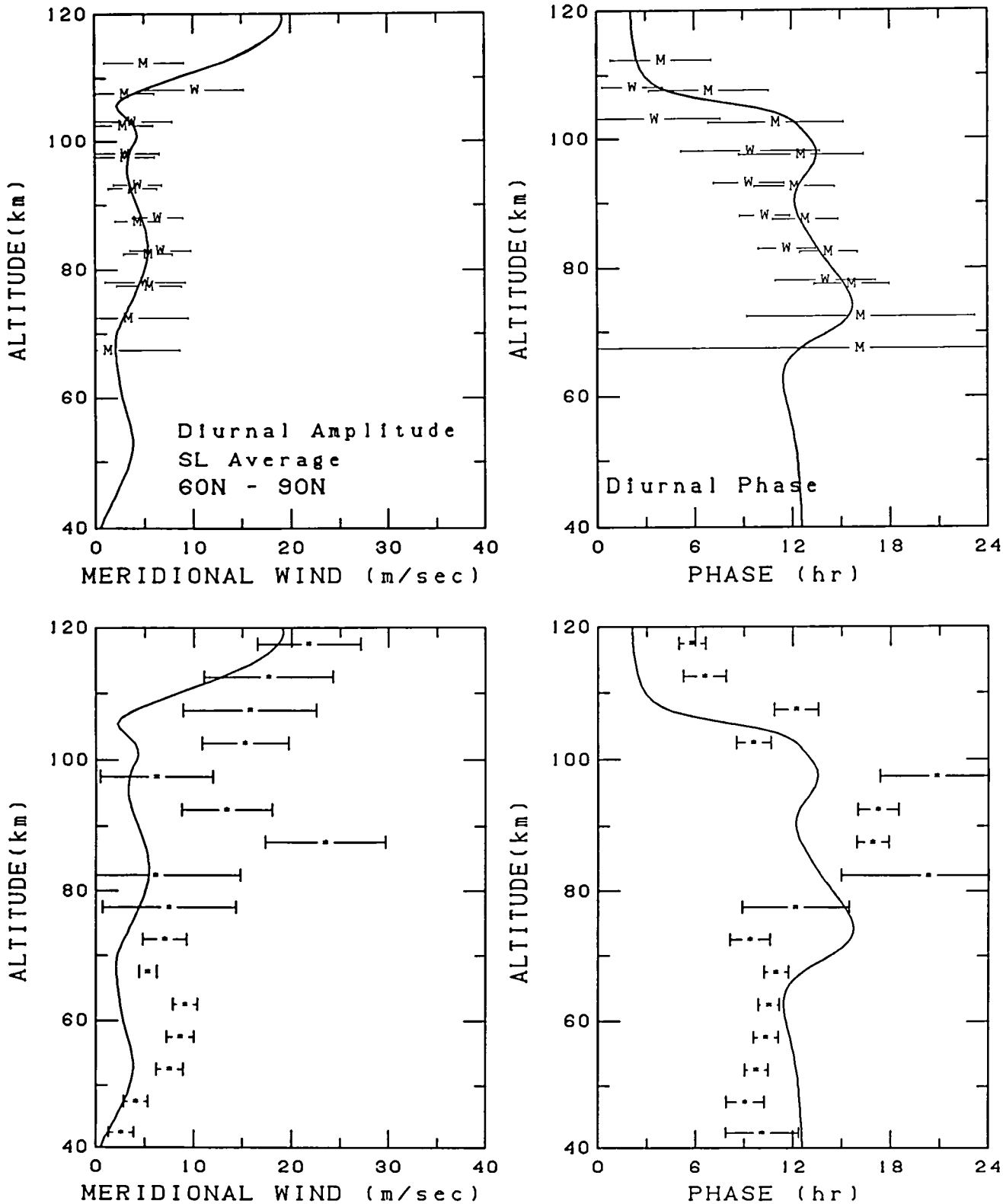

Fig. 4f. Seasonal average diurnal meridional wind amplitude and phase versus altitude for northern high latitudes. The HWM93 wind (solid line) shown for mid-range conditions. Top row of plots contain MF/Meteor radar data with plot symbols indicated in Table 1. Bottom row contains rocketsonde and IS radar data combined (*).

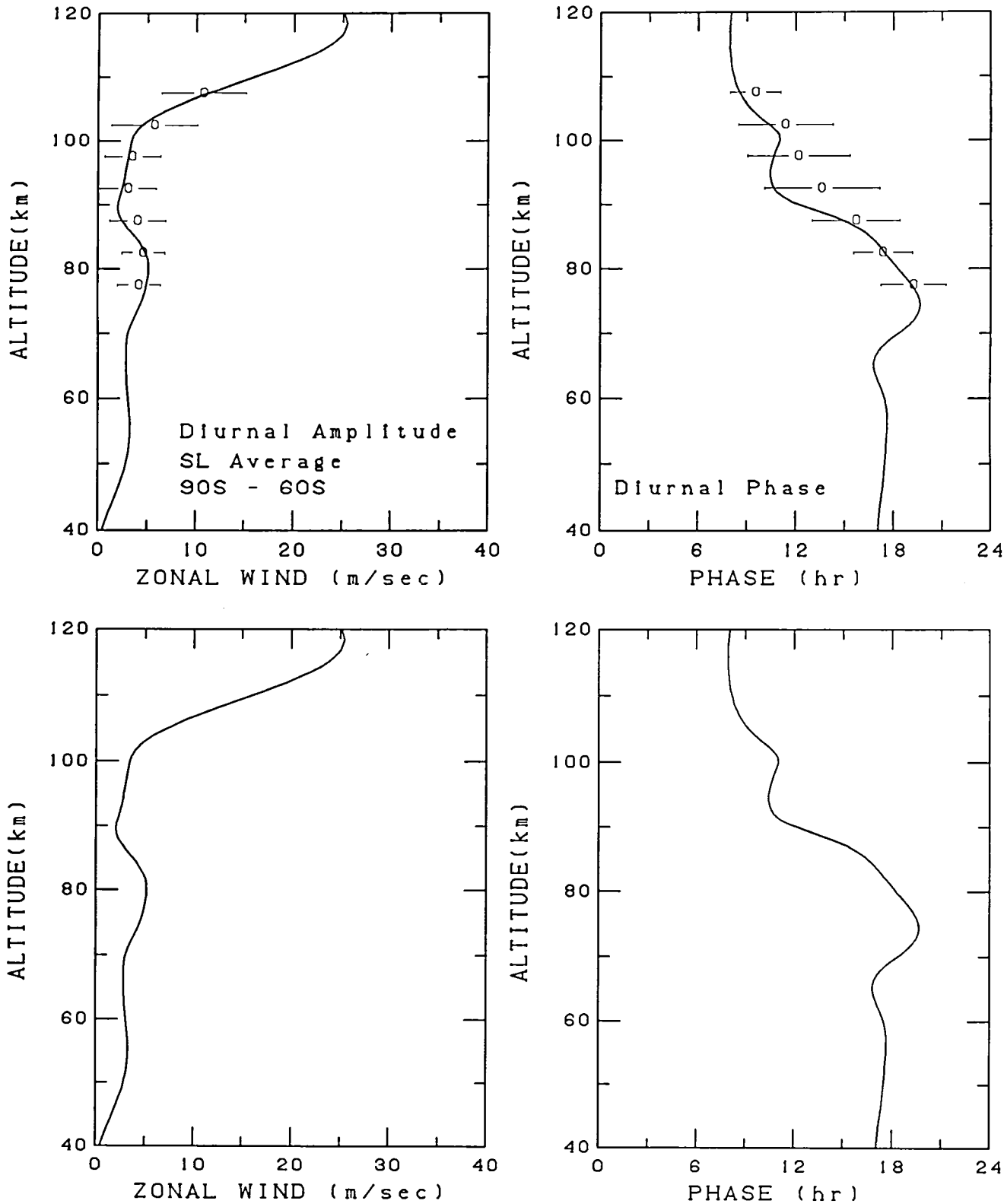

Fig. 5a. Seasonal average diurnal zonal wind amplitude and phase versus latitude for southern high latitudes. The HWM93 wind (solid line) shown for mid-range conditions. Top row of plots contain MF/Meteor radar data with plot symbols indicated in Table 1. Bottom row contains rocketsonde and IS radar data combined (*).

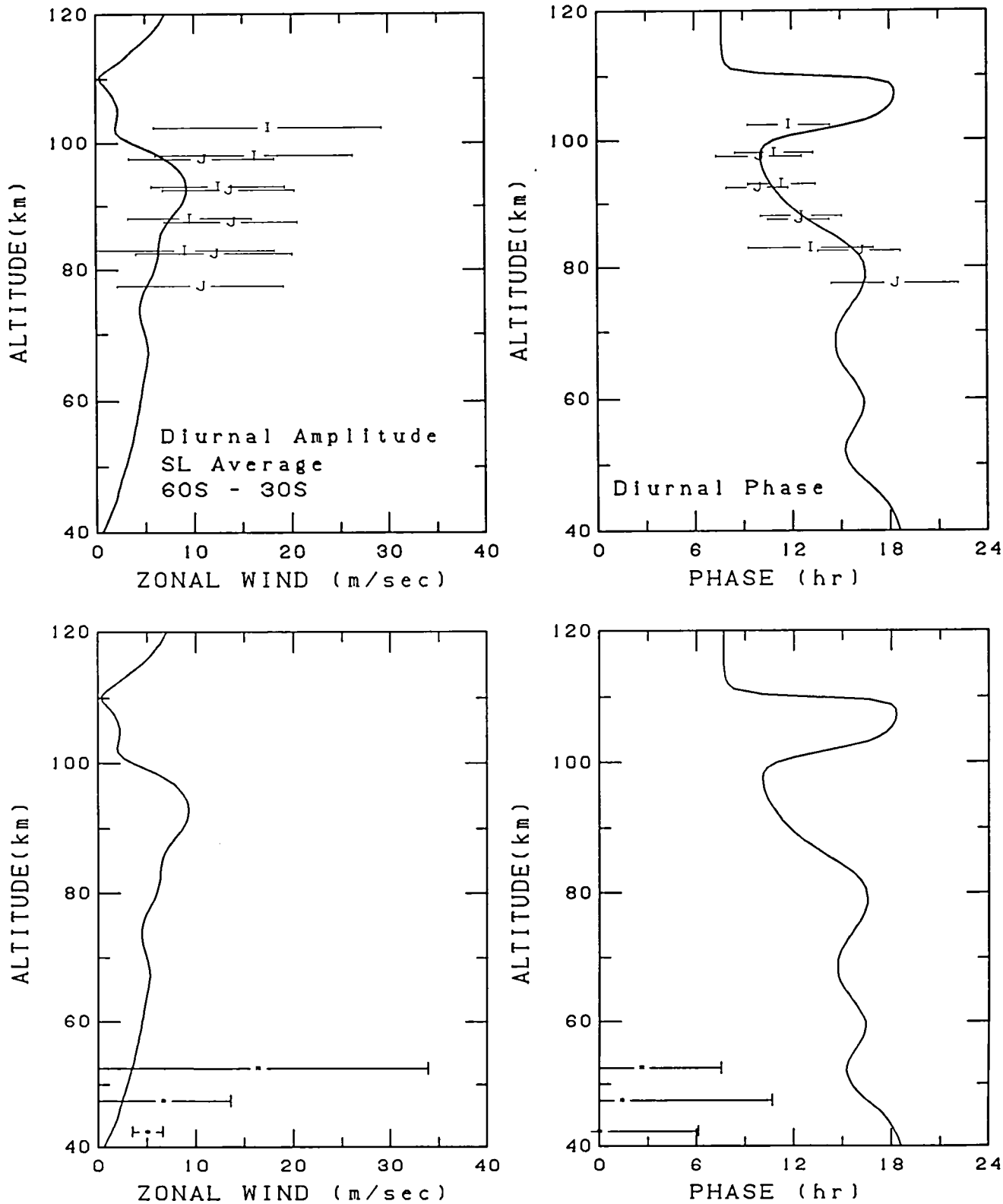

Fig. 5b. Seasonal average diurnal zonal wind amplitude and phase versus latitude for southern middle latitudes. The HWM93 wind (solid line) shown for mid-range conditions. Top row of plots contain MF/Meteor radar data with plot symbols indicated in Table 1. Bottom row contains rocketsonde and IS radar data combined (*).

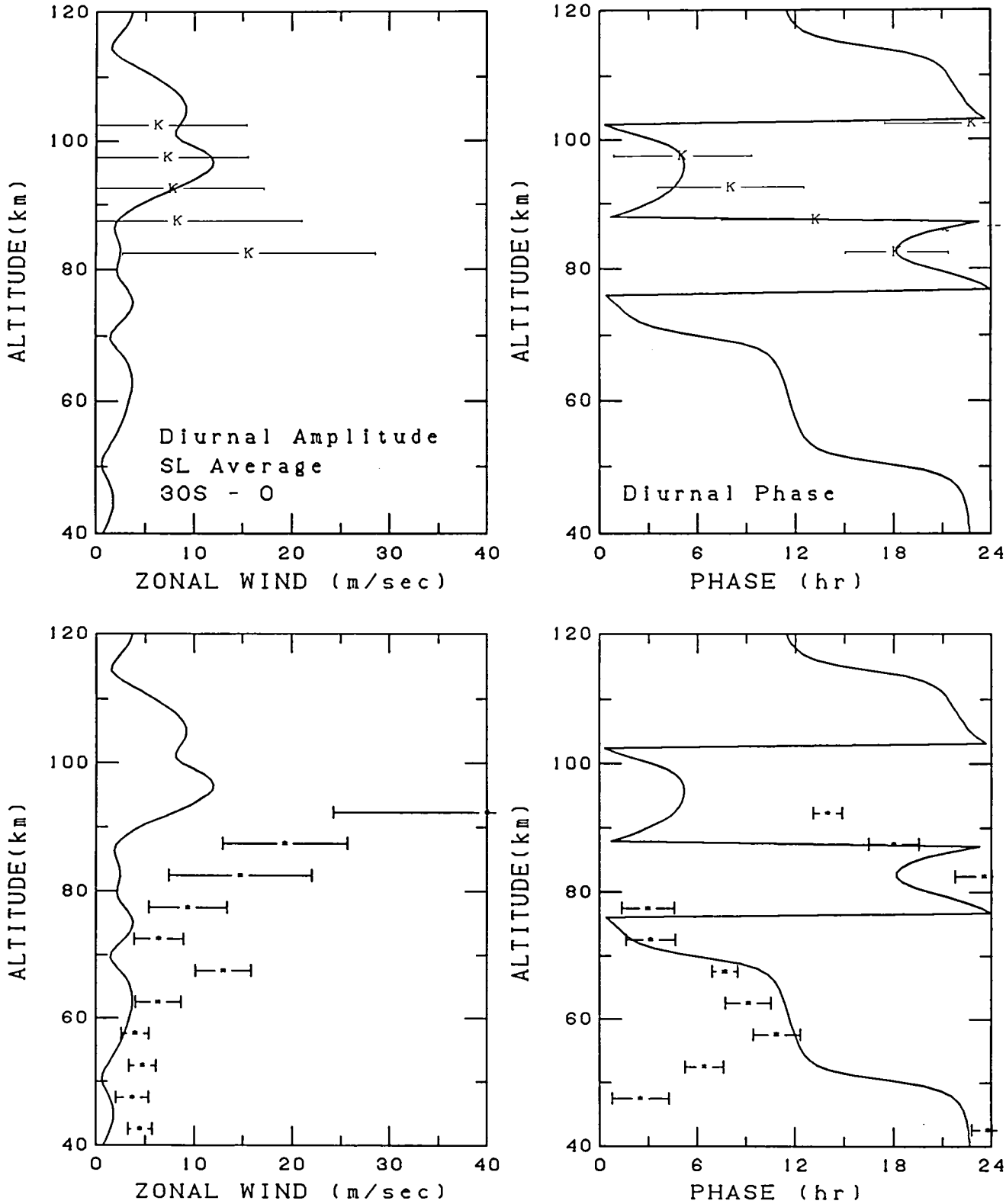

Fig. 5c. Seasonal average diurnal zonal wind amplitude and phase versus latitude for southern low latitudes. The HWM93 wind (solid line) shown for mid-range conditions. Top row of plots contain MF/Meteor radar data with plot symbols indicated in Table 1. Bottom row contains rocketsonde and IS radar data combined (*).

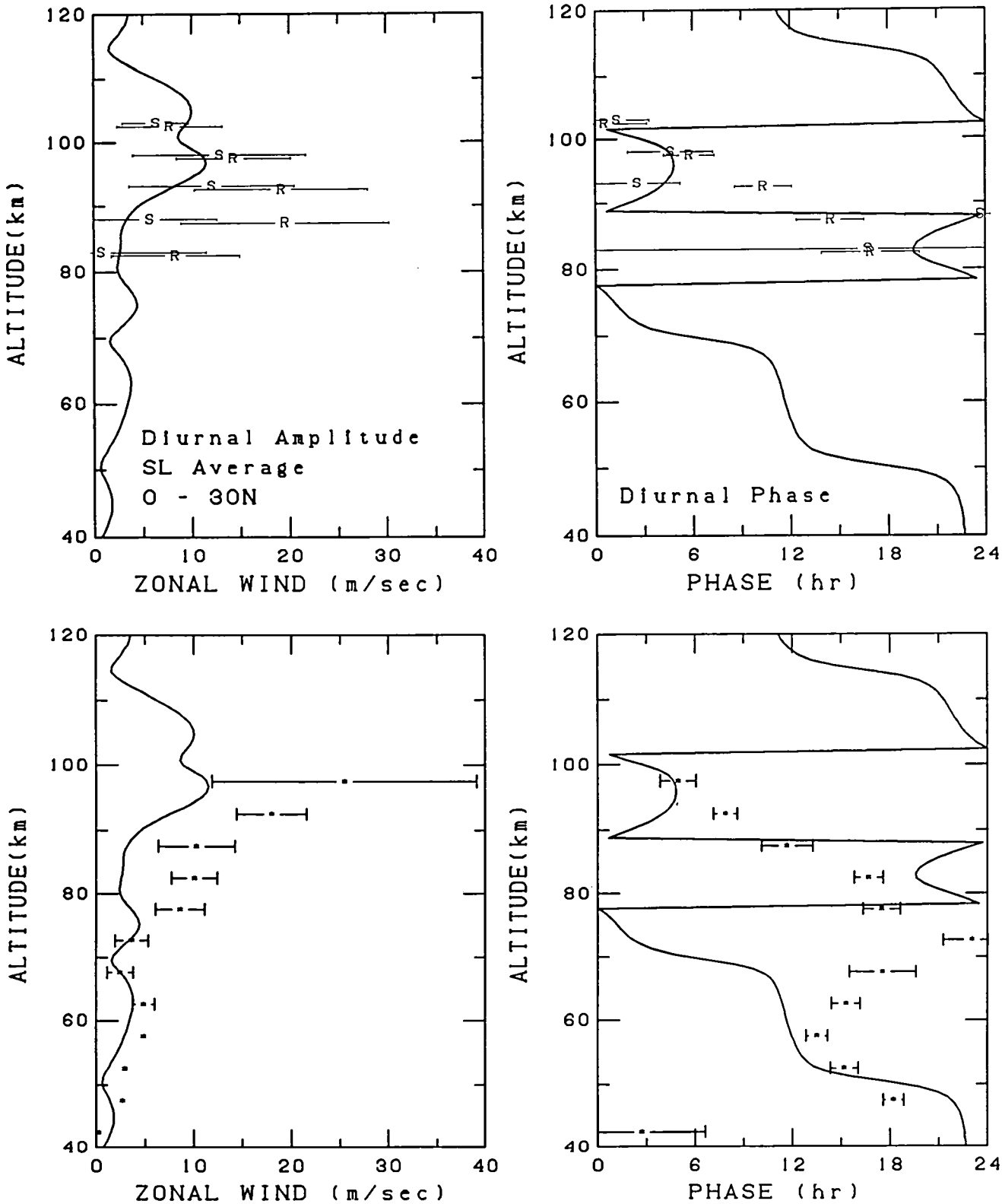

Fig. 5d. Seasonal average diurnal zonal wind amplitude and phase versus latitude for northern low latitudes. The HWM93 wind (solid line) shown for mid-range conditions. Top row of plots contain MF/Meteor radar data with plot symbols indicated in Table 1. Bottom row contains rocketsonde and IS radar data combined (*).

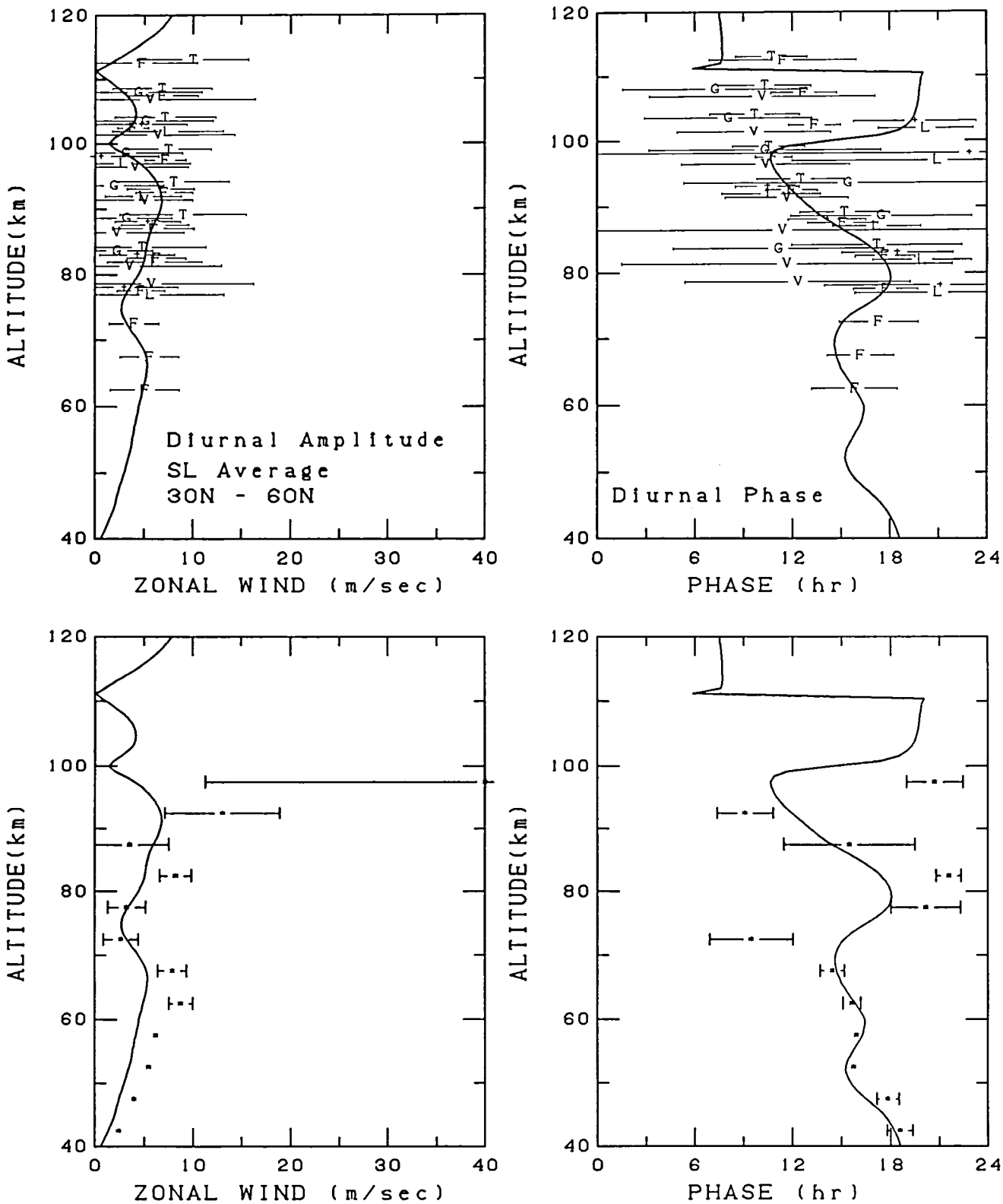

Fig. 5e. Seasonal average diurnal zonal wind amplitude and phase versus latitude for northern middle latitudes. The HWM93 wind (solid line) shown for mid-range conditions. Top row of plots contain MF/Meteor radar data with plot symbols indicated in Table 1. Bottom row contains rocketsonde and IS radar data combined (*).

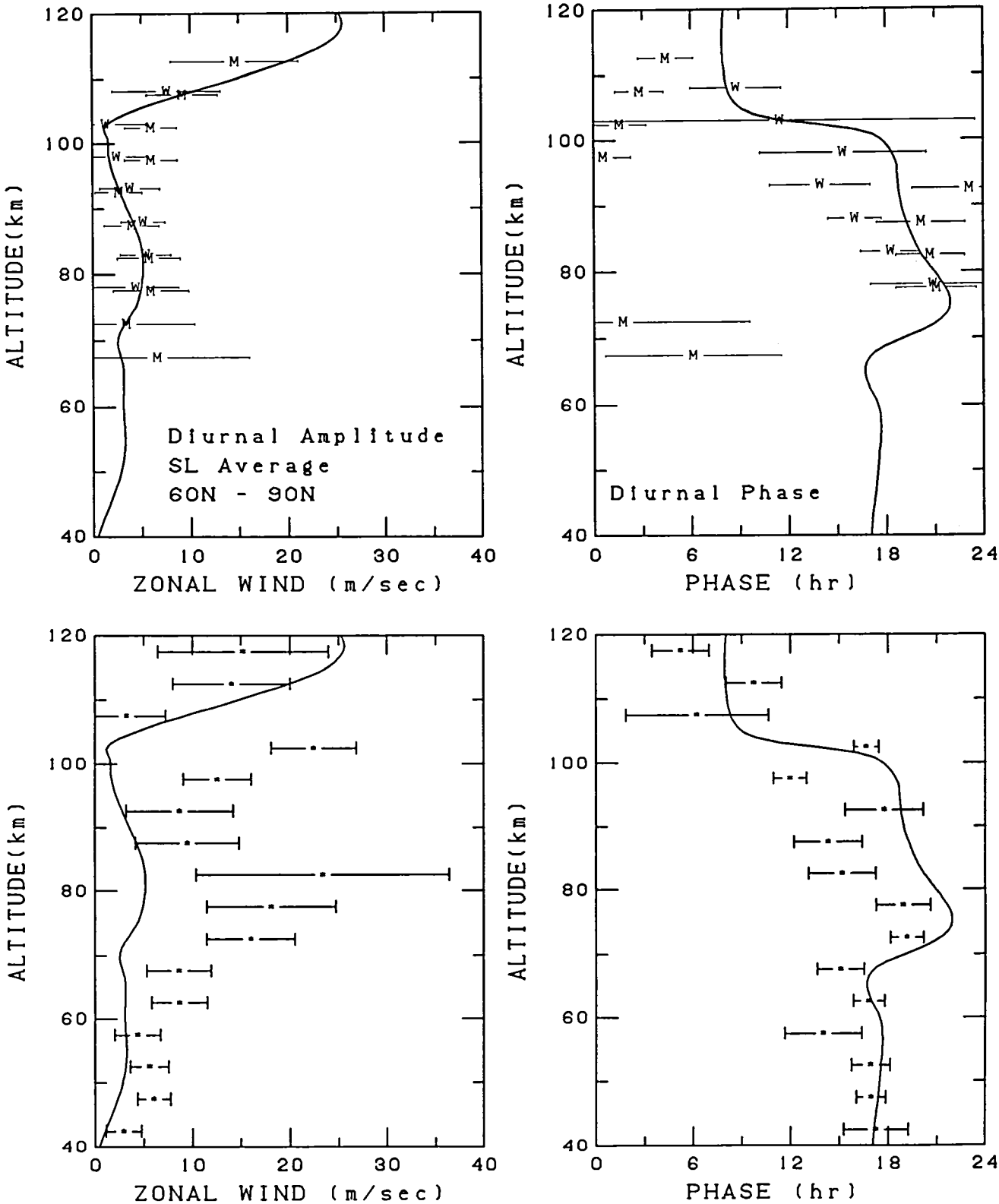

Fig. 5f. Seasonal average diurnal zonal wind amplitude and phase versus latitude for northern high latitudes. The HWM93 wind (solid line) shown for mid-range conditions. Top row of plots contain MF/Meteor radar data with plot symbols indicated in Table 1. Bottom row contains rocketsonde and IS radar data combined (*).

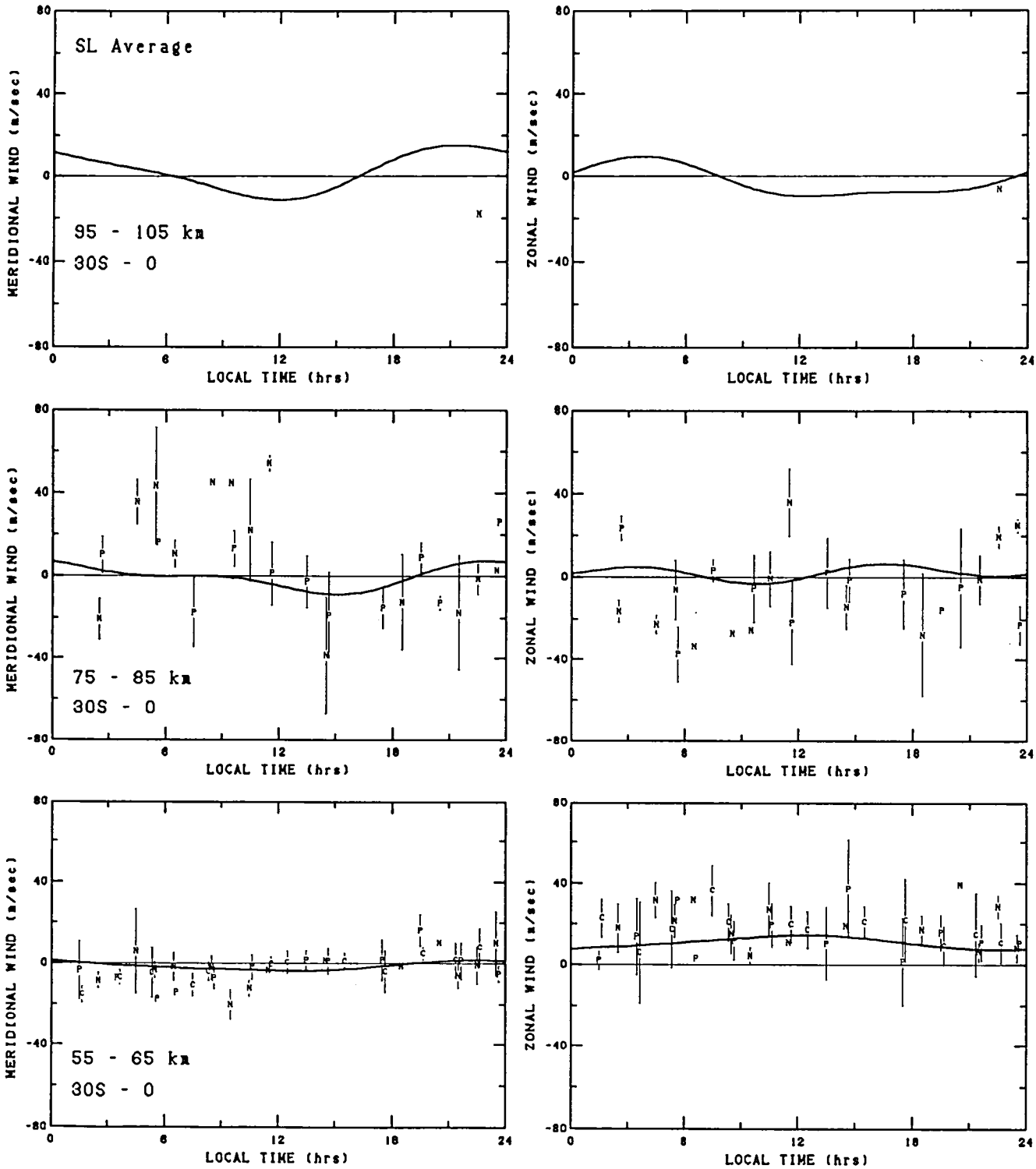

Fig. 6a. Meridional and zonal wind versus local time for selected altitude regions at southern low latitudes. The HWM93 wind (solid line) shown for mid-range conditions. Plot symbols indicated in Table 1.

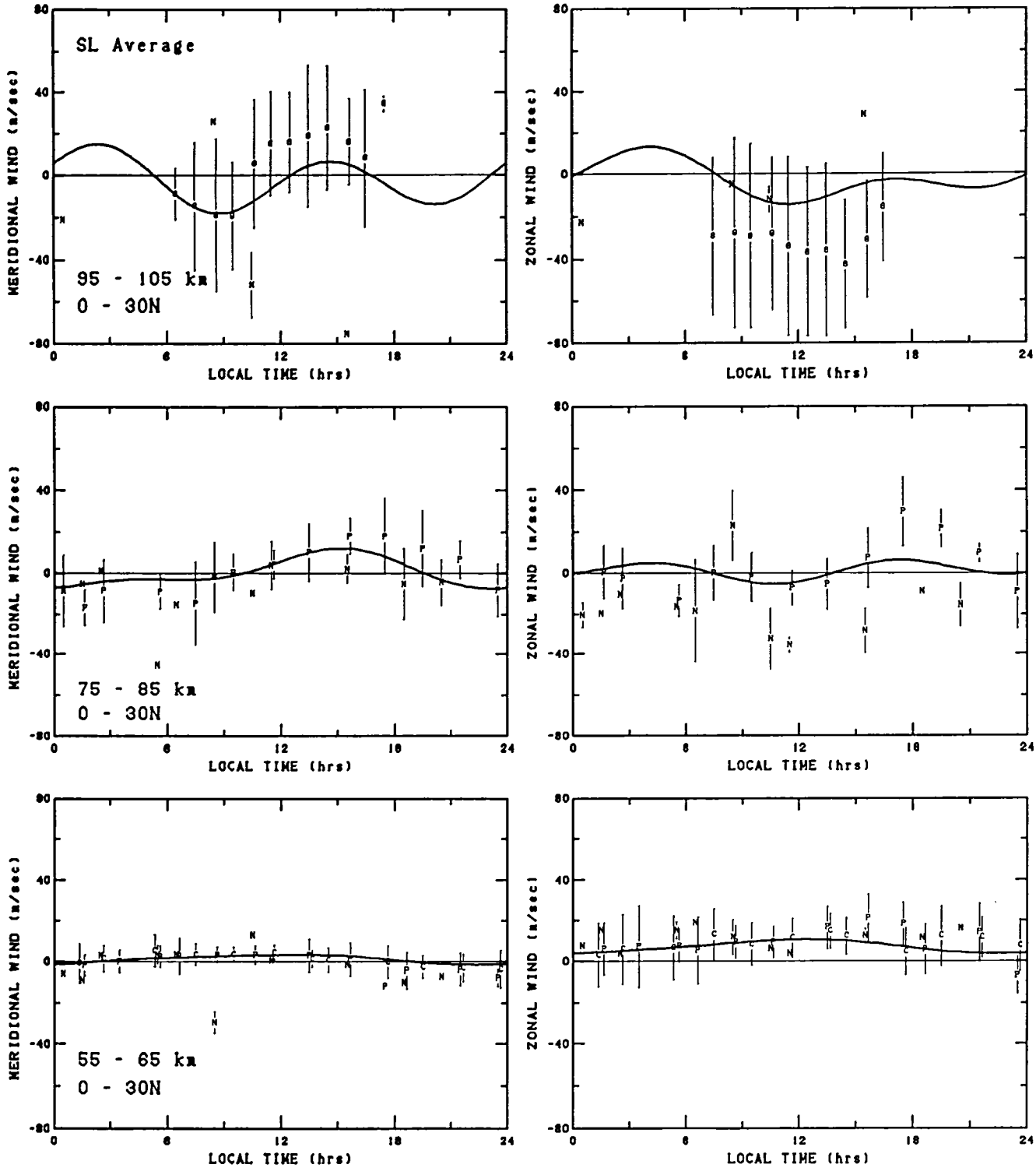

Fig. 6b. Meridional and zonal wind versus local time for selected altitude regions at northern low latitudes. The HWM93 wind (solid line) shown for mid-range conditions. Plot symbols indicated in Table 1.

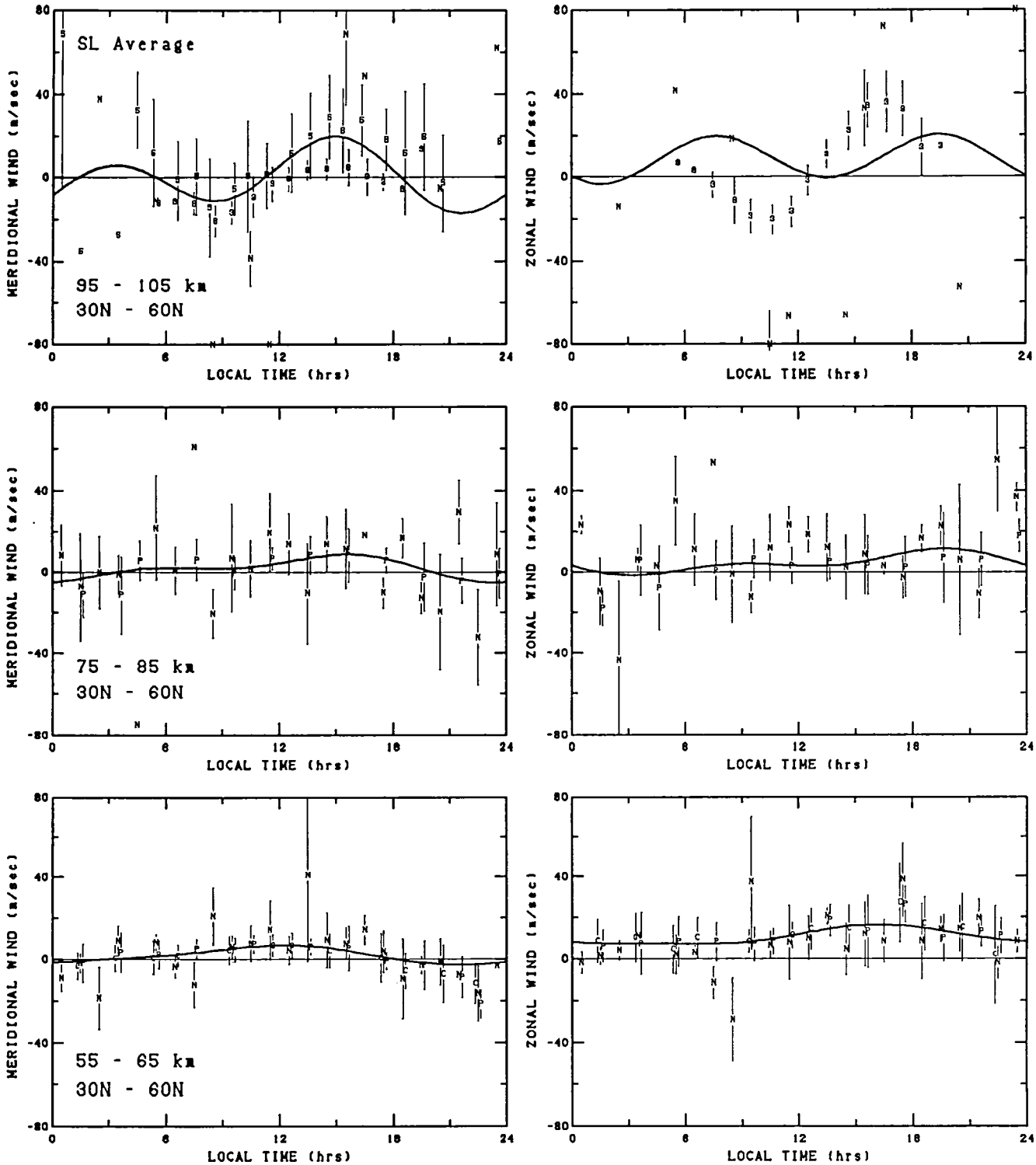

Fig. 6c. Meridional and zonal wind versus local time for selected altitude regions at northern middle latitudes. The HWM93 wind (solid line) shown for mid-range conditions. Plot symbols indicated in Table 1.

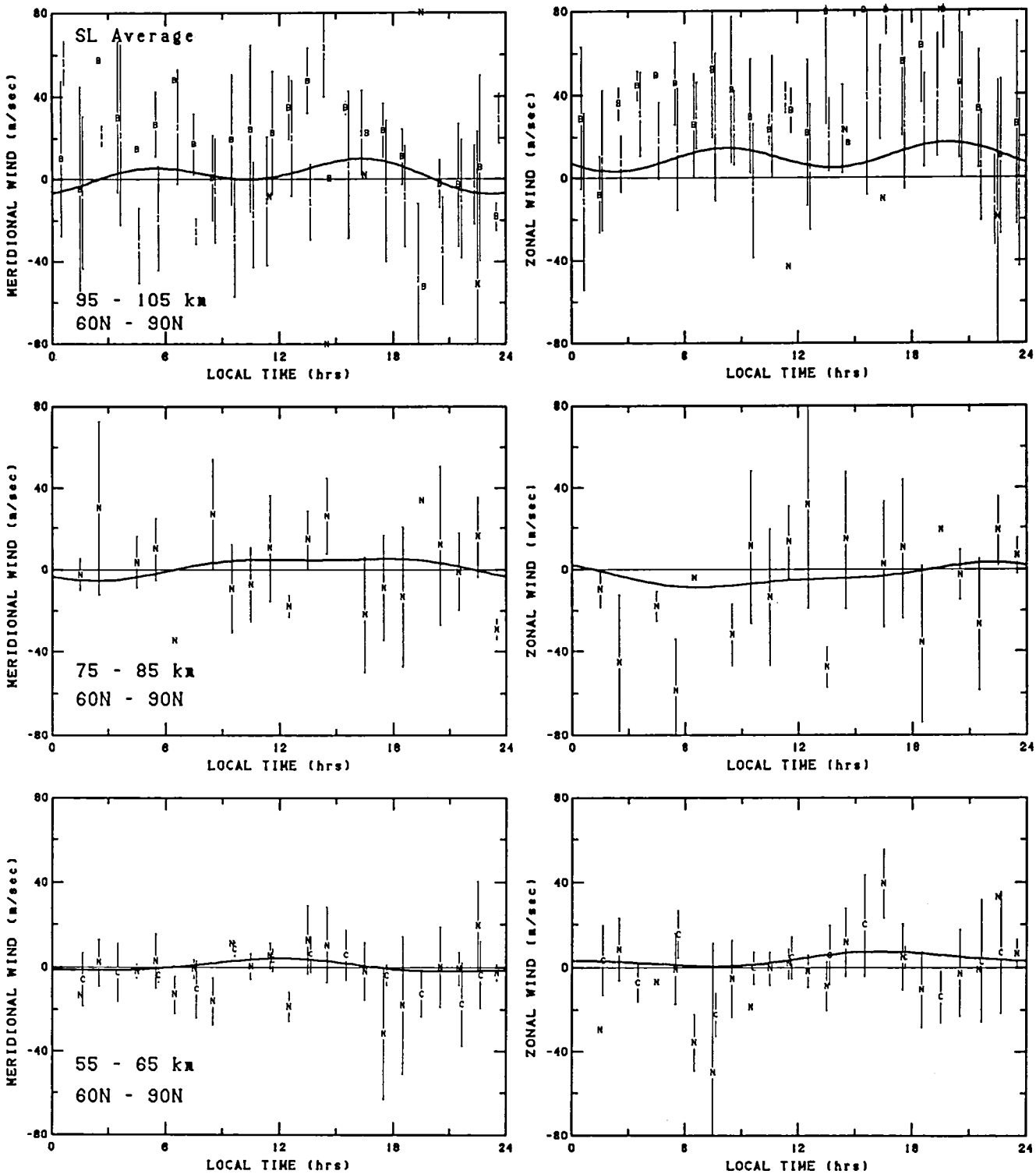

Fig. 6d. Meridional and zonal wind versus local time for selected altitude regions at northern high latitudes. The HWM93 wind (solid line) shown for mid-range conditions. Plot symbols indicated in Table 1.

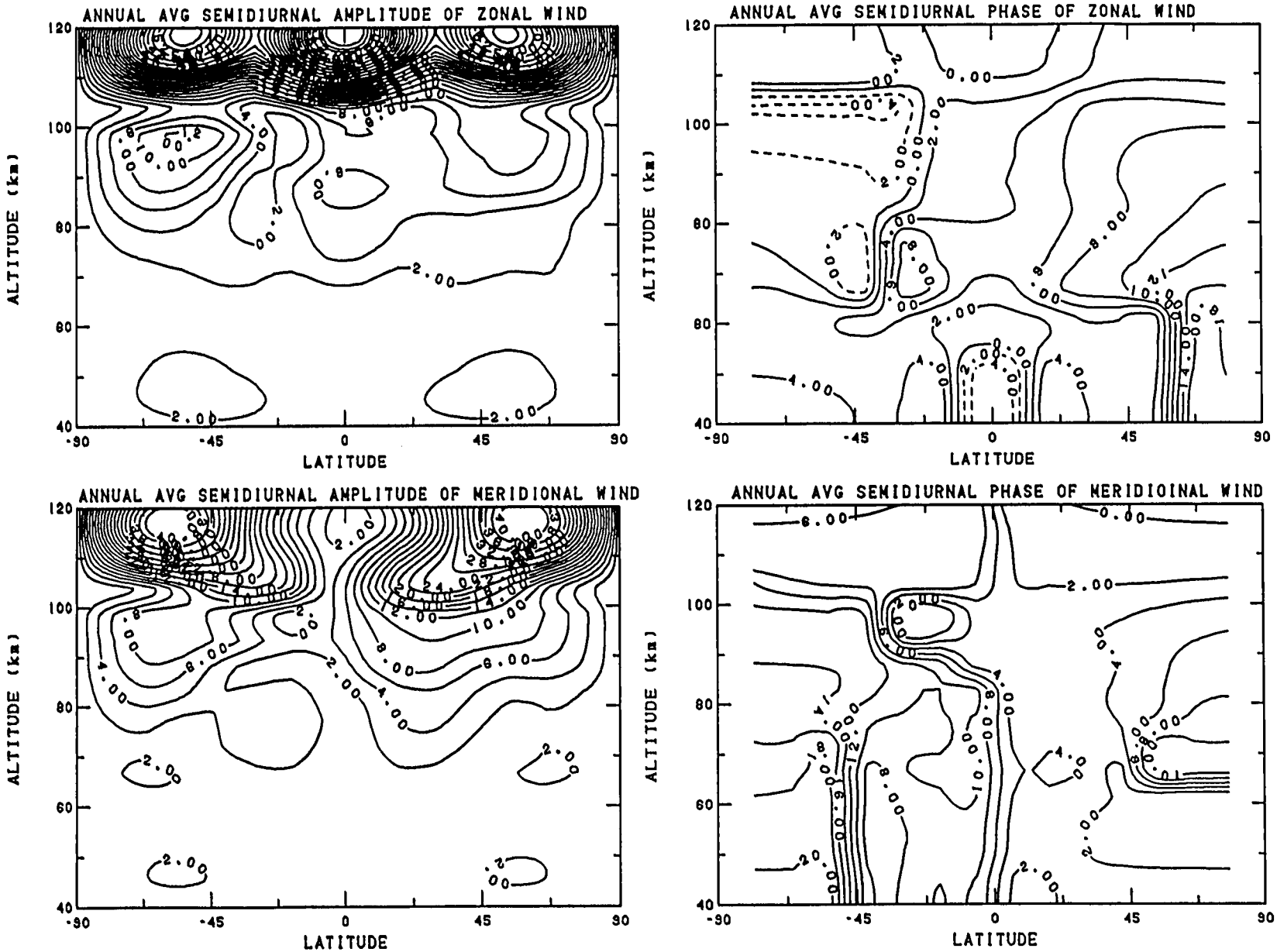

Fig. 7. Contour plots in altitude versus latitude of the seasonal average semidiurnal wind amplitude and phase (negative phase dashed) for zonal wind (upper panels) and meridional wind (lower panels).

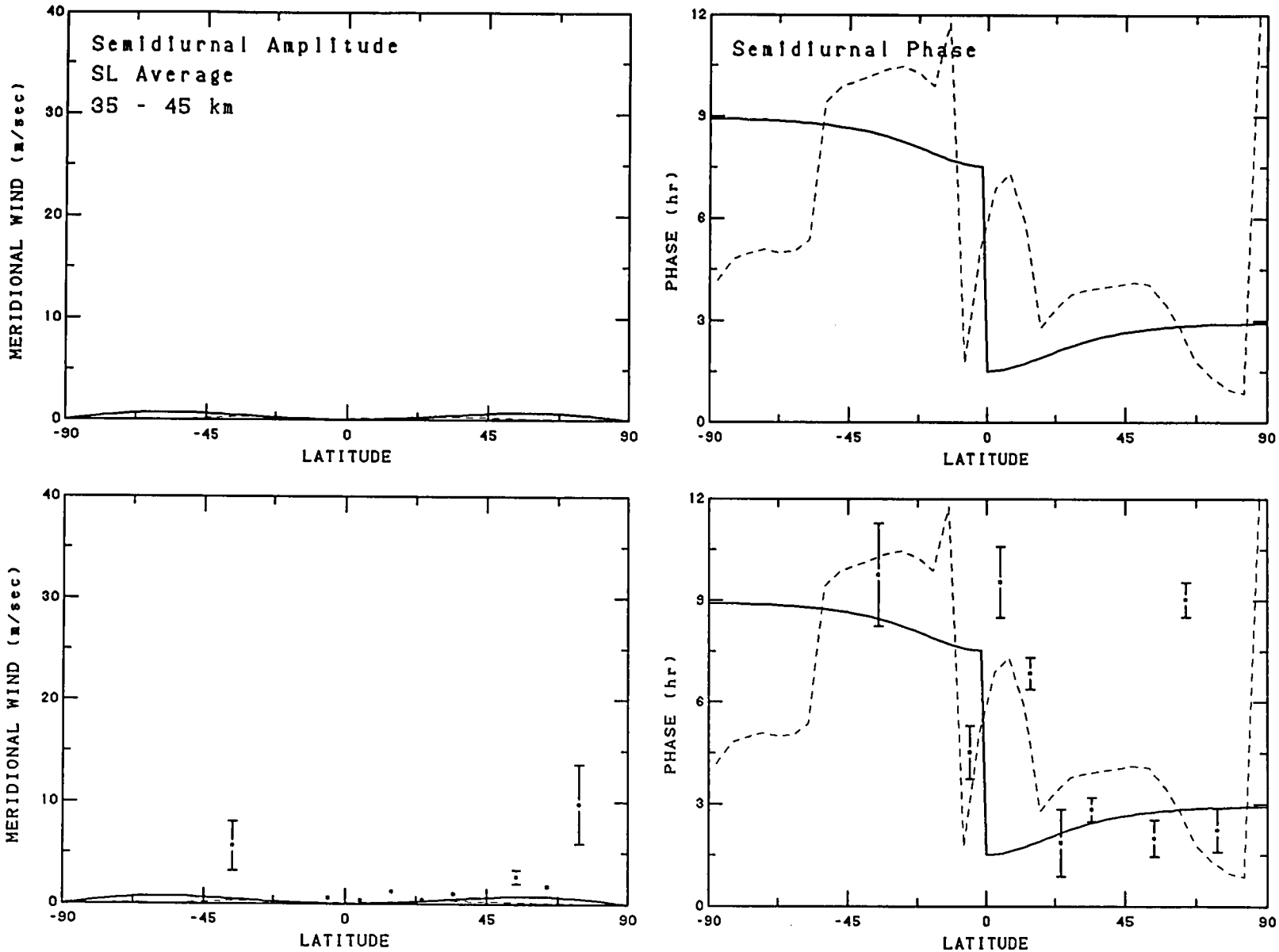

Fig. 8a. Seasonal average semidiurnal meridional wind amplitude and phase versus latitude for 35 to 45 km. The HWM93 wind (solid line) and FV89 (dashed) shown for mid-range conditions. Top row of plots contain MF/Meteor radar data with plot symbols indicated in Table 1. Bottom row contains rocketsonde and IS radar data combined (*).

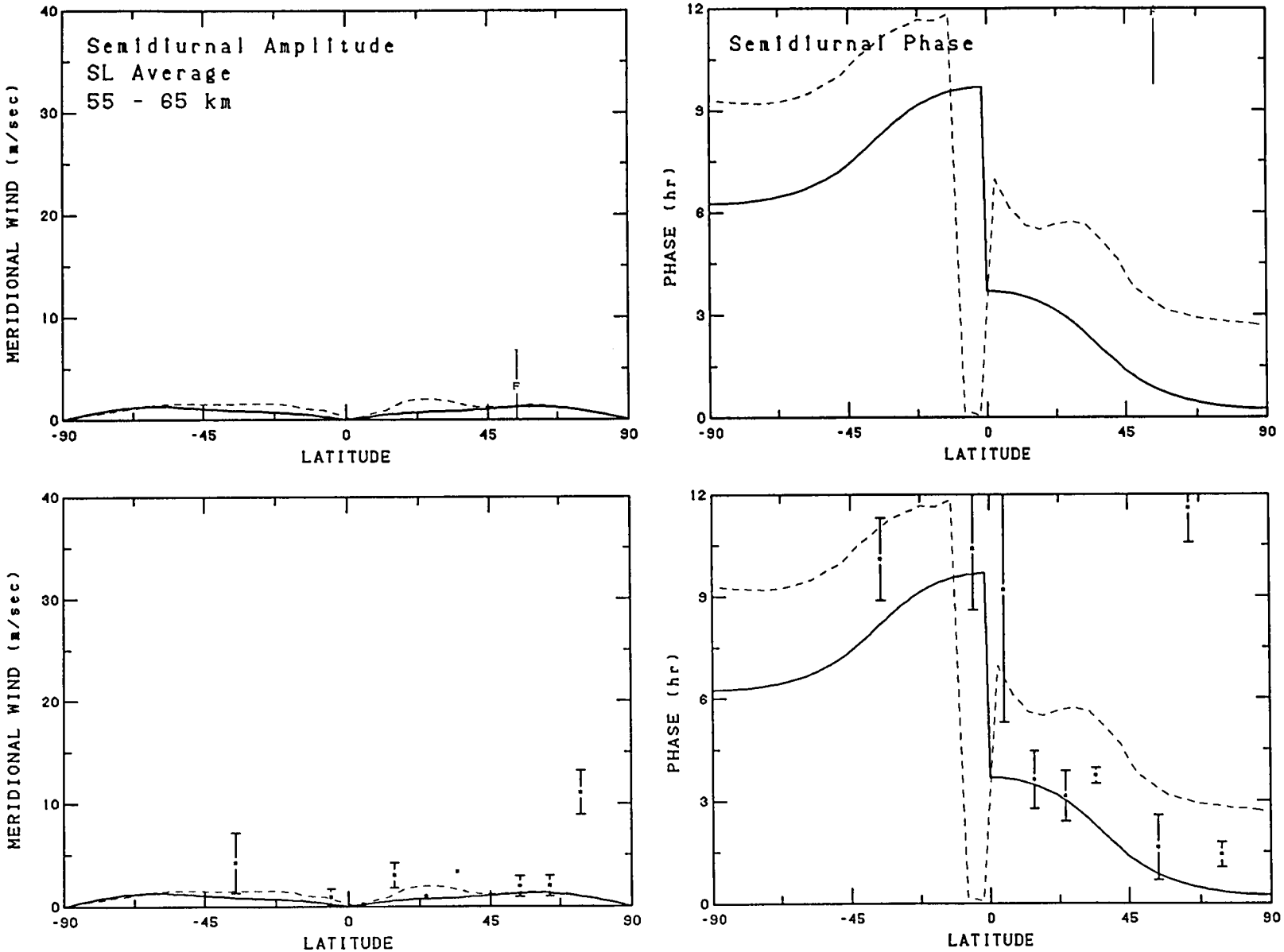

Fig. 8b. Seasonal average semidiurnal meridional wind amplitude and phase versus latitude for 55 to 65 km. The HWM93 wind (solid line) and FV89 (dashed) shown for mid-range conditions. Top row of plots contain MF/Meteor radar data with plot symbols indicated in Table 1. Bottom row contains rocketsonde and IS radar data combined (*).

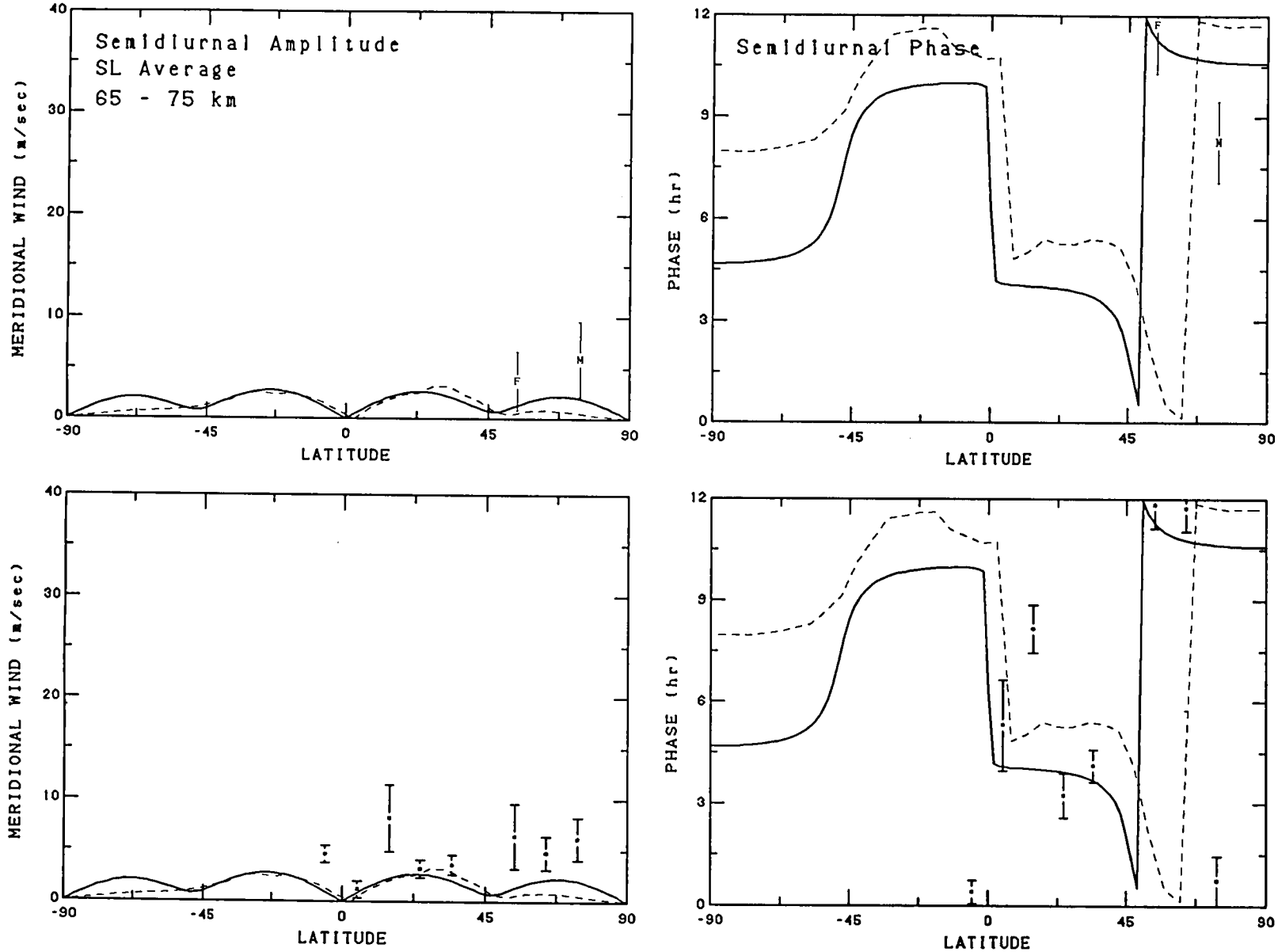

Fig. 8c. Seasonal average semidiurnal meridional wind amplitude and phase versus latitude for 65 to 75 km. The HWM93 wind (solid line) and FV89 (dashed) shown for mid-range conditions. Top row of plots contain MF/Meteor radar data with plot symbols indicated in Table 1. Bottom row contains rocketsonde and IS radar data combined (*).

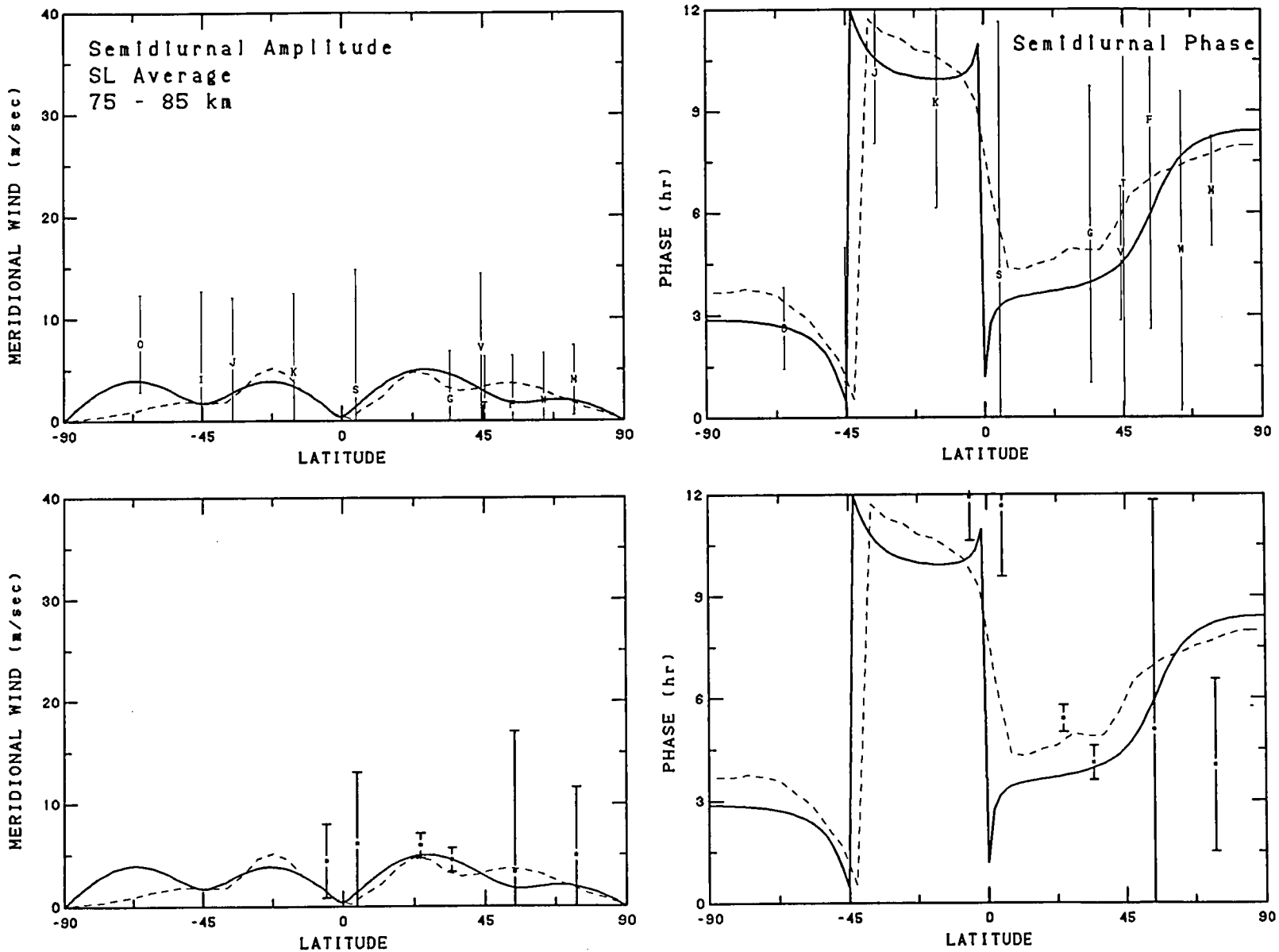

Fig. 8d. Seasonal average semidiurnal meridional wind amplitude and phase versus latitude for 75 to 85 km. The HWM93 wind (solid line) and FV89 (dashed) shown for mid-range conditions. Top row of plots contain MF/Meteor radar data with plot symbols indicated in Table 1. Bottom row contains rocketsonde and IS radar data combined (*).

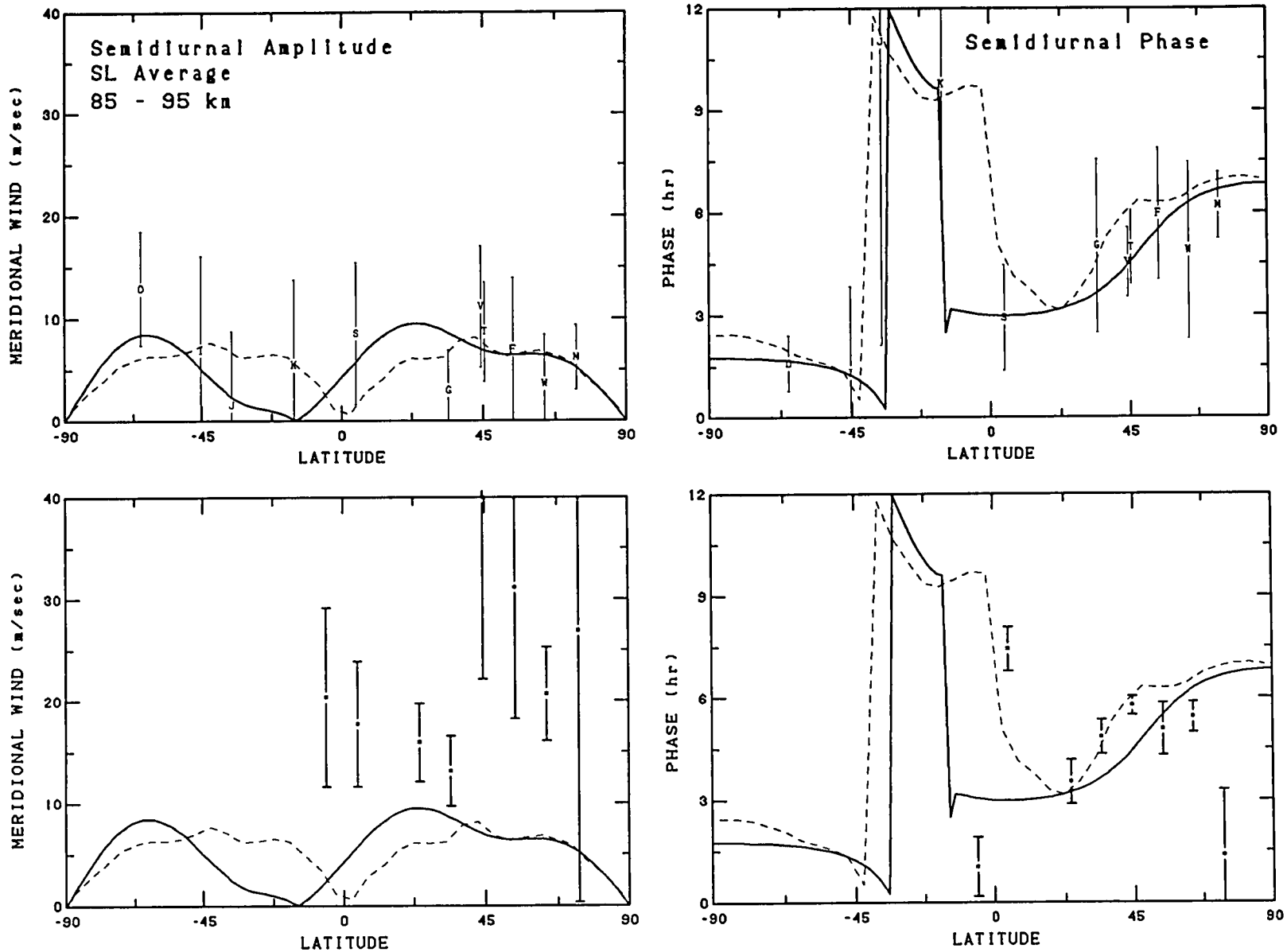

Fig. 8e. Seasonal average semidiurnal meridional wind amplitude and phase versus latitude for 85 to 95 km. The HWM93 wind (solid line) and FV89 (dashed) shown for mid-range conditions. Top row of plots contain MF/Meteor radar data with plot symbols indicated in Table 1. Bottom row contains rocketsonde and IS radar data combined (*).

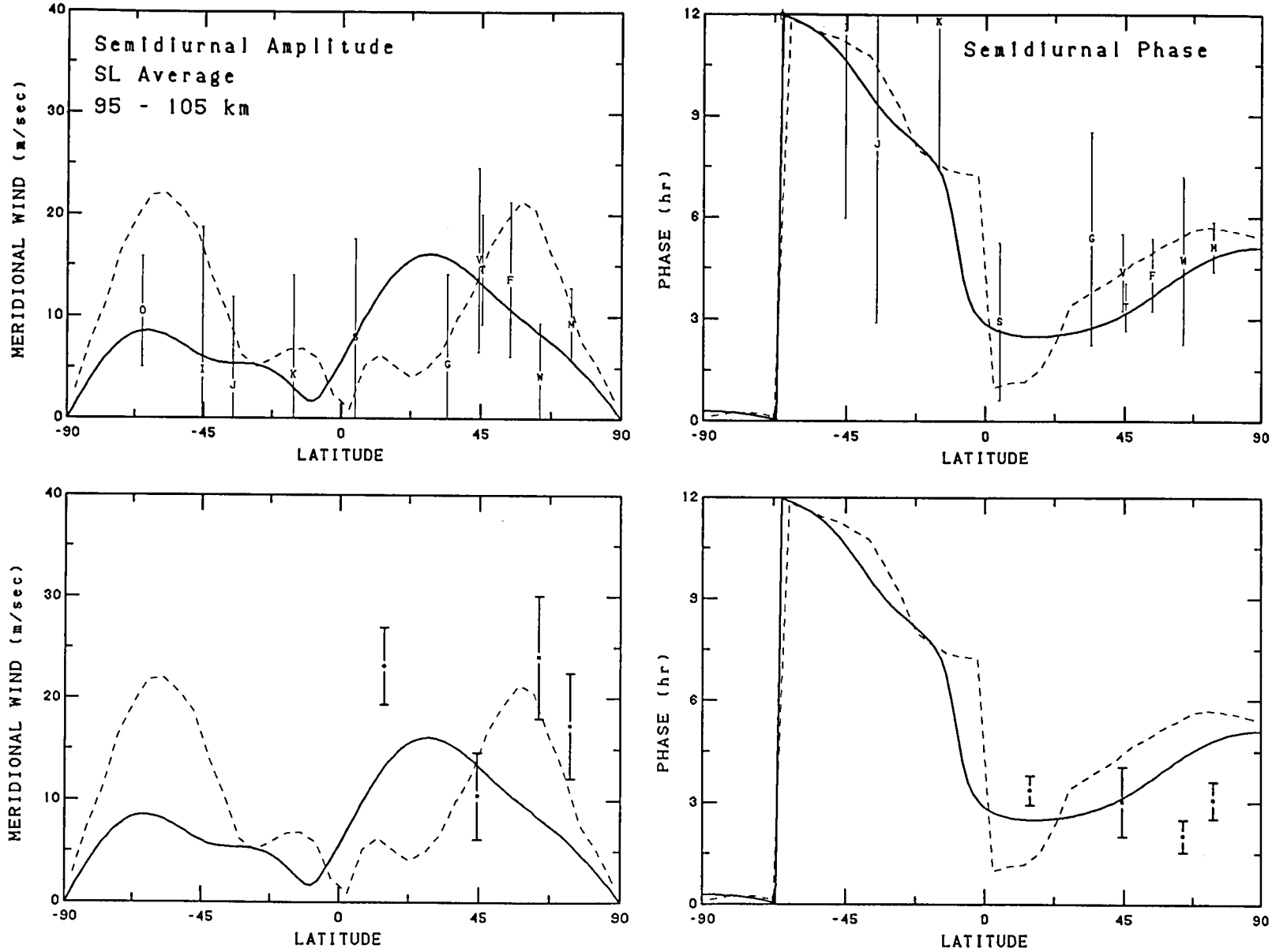

Fig. 8f. Seasonal average semidiurnal meridional wind amplitude and phase versus latitude for 95 to 105 km. The HWM93 wind (solid line) and FV89 (dashed) shown for mid-range conditions. Top row of plots contain MF/Meteor radar data with plot symbols indicated in Table 1. Bottom row contains rocketsonde and IS radar data combined (*).

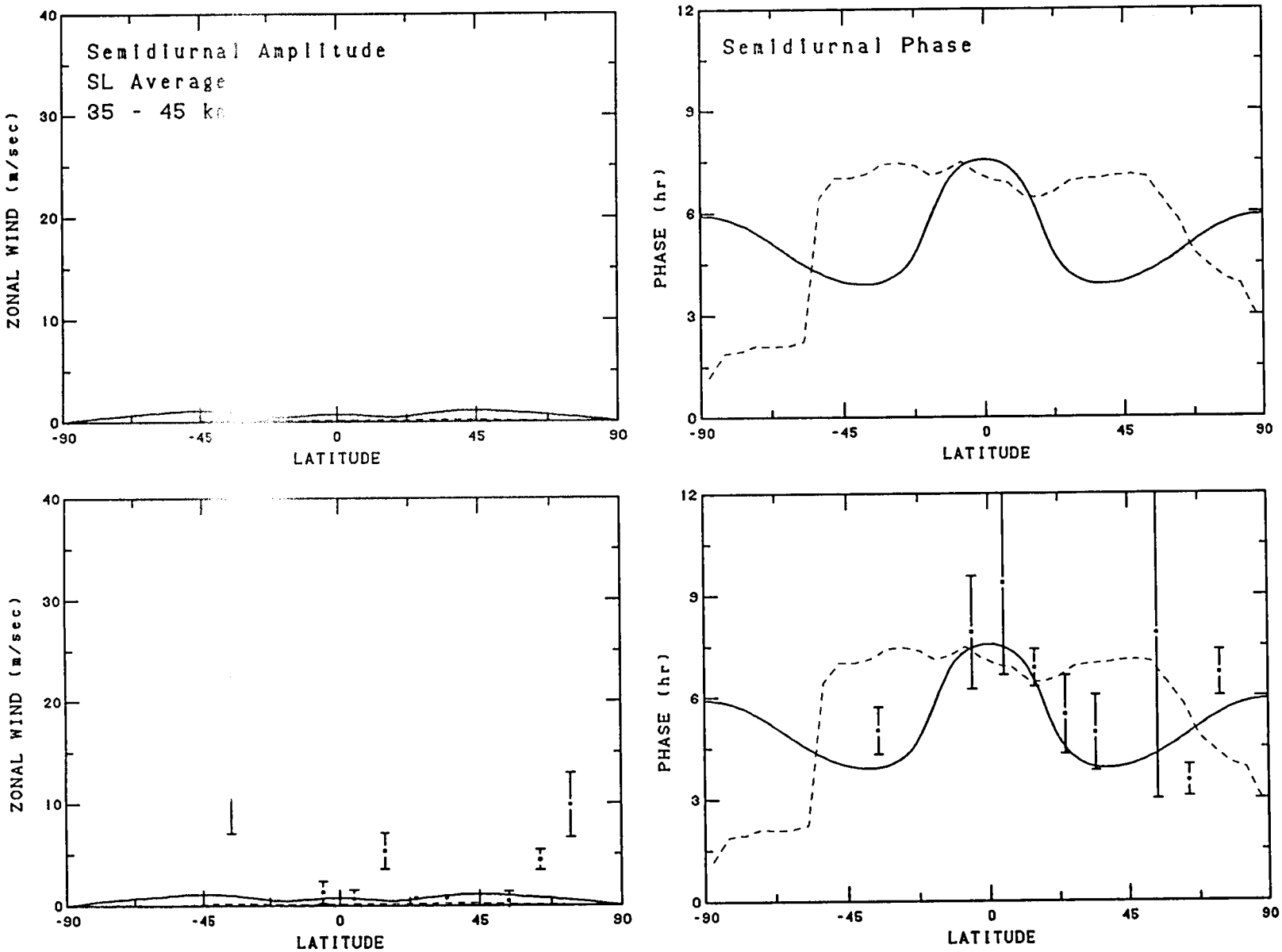

Fig. 9a. Seasonal average semidiurnal zonal wind amplitude and phase versus latitude for 35 to 45 km. The HWM93 wind (solid line) and FV89 (dashed) shown for mid-range conditions. Top row of plots contain MF/Meteor radar data with plot symbols as indicated in Table 1. Bottom row contains rocketsonde and IS radar data combined (*).

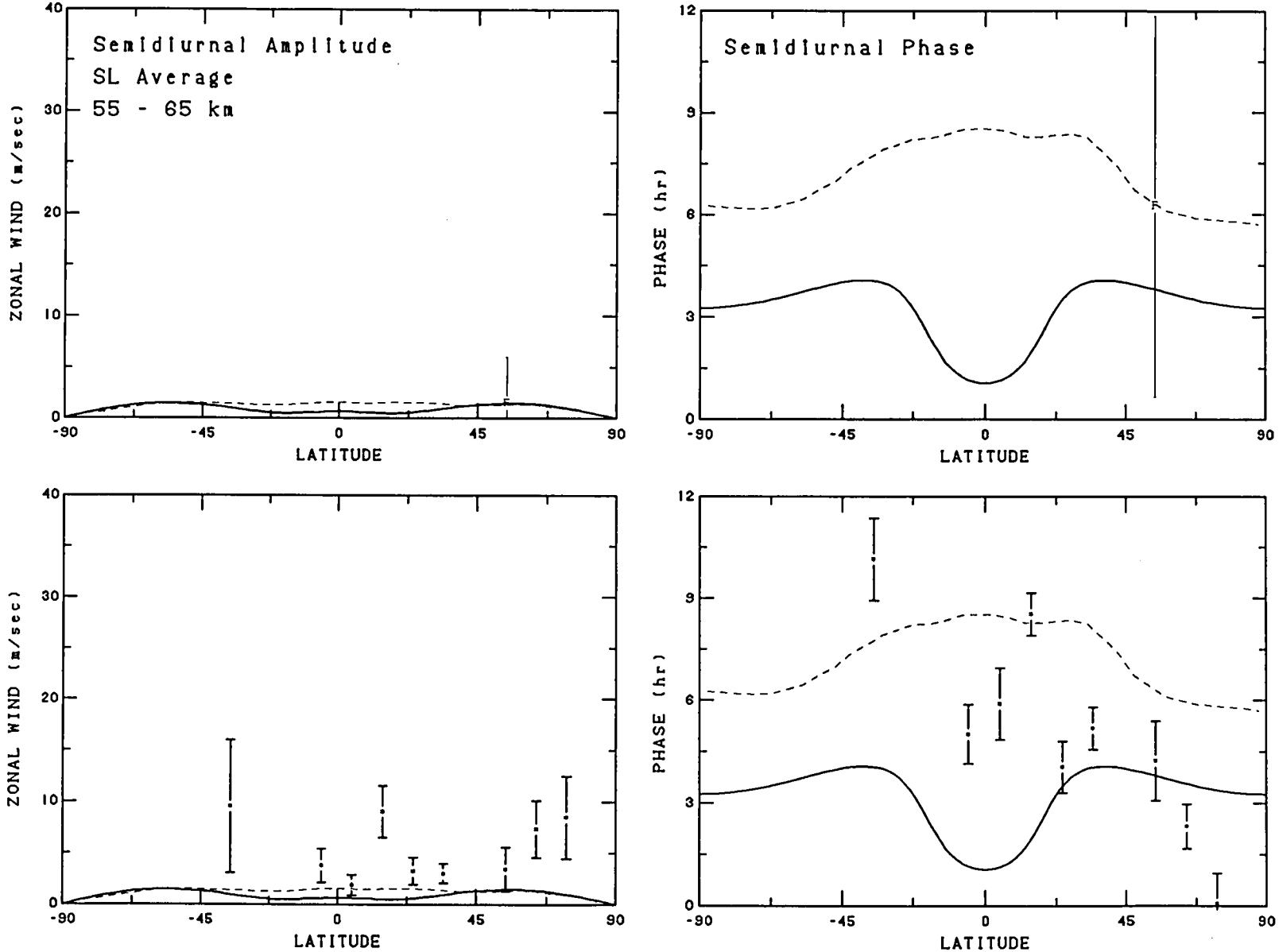

Fig. 9b. Seasonal average semidiurnal zonal wind amplitude and phase versus latitude for 55 to 65 km. The HWM93 wind (solid line) and FV89 (dashed) shown for mid-range conditions. Top row of plots contain MF/Meteor radar data with plot symbols as indicated in Table 1. Bottom row contains rocketsonde and IS radar data combined (*).

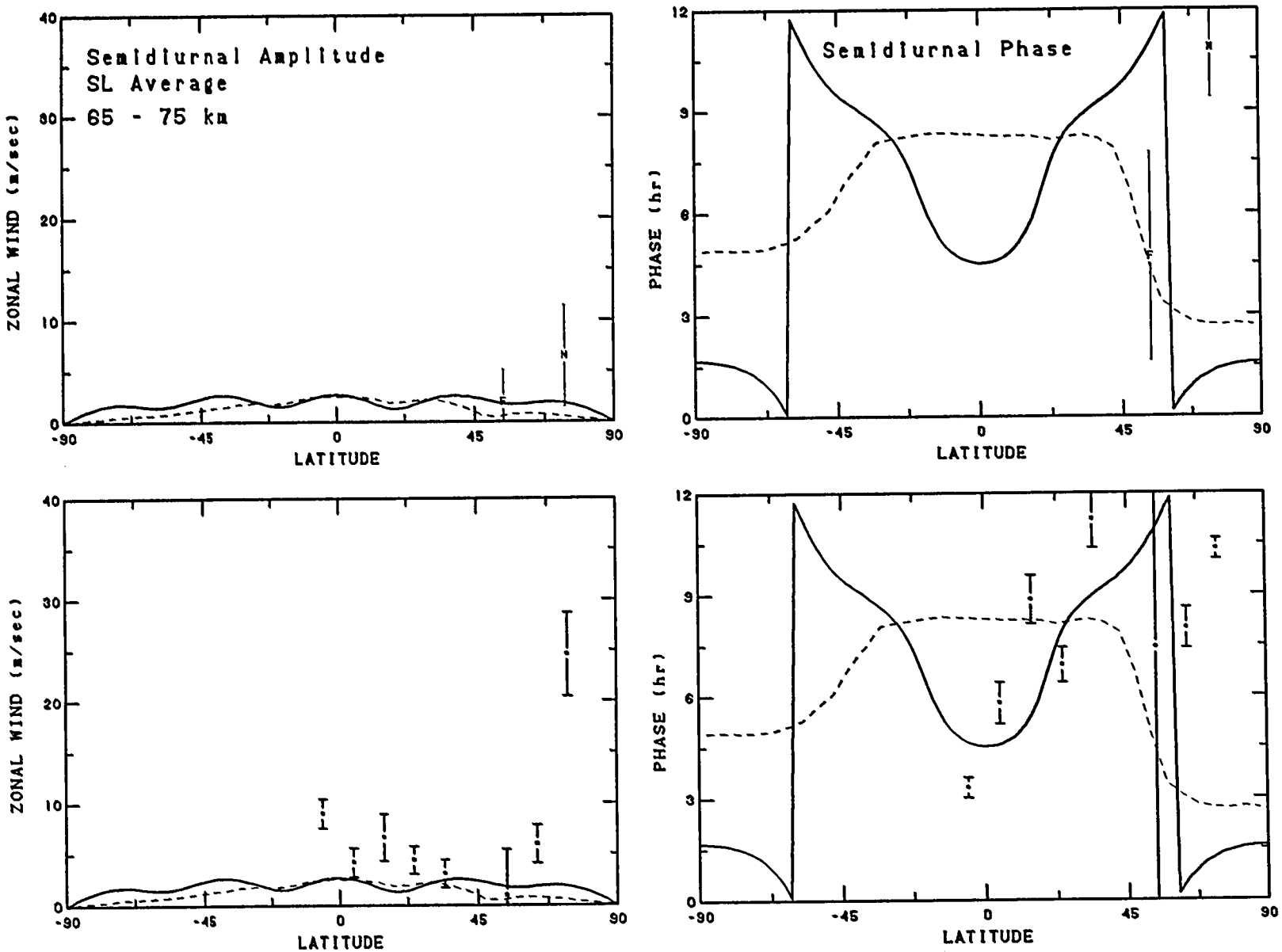

Fig. 9c. Seasonal average semidiurnal zonal wind amplitude and phase versus latitude for 65 to 75 km. The HWM93 wind (solid line) and FV89 (dashed) shown for mid-range conditions. Top row of plots contain MF/Meteor radar data with plot symbols as indicated in Table 1. Bottom row contains rocketsonde and IS radar data combined (*).

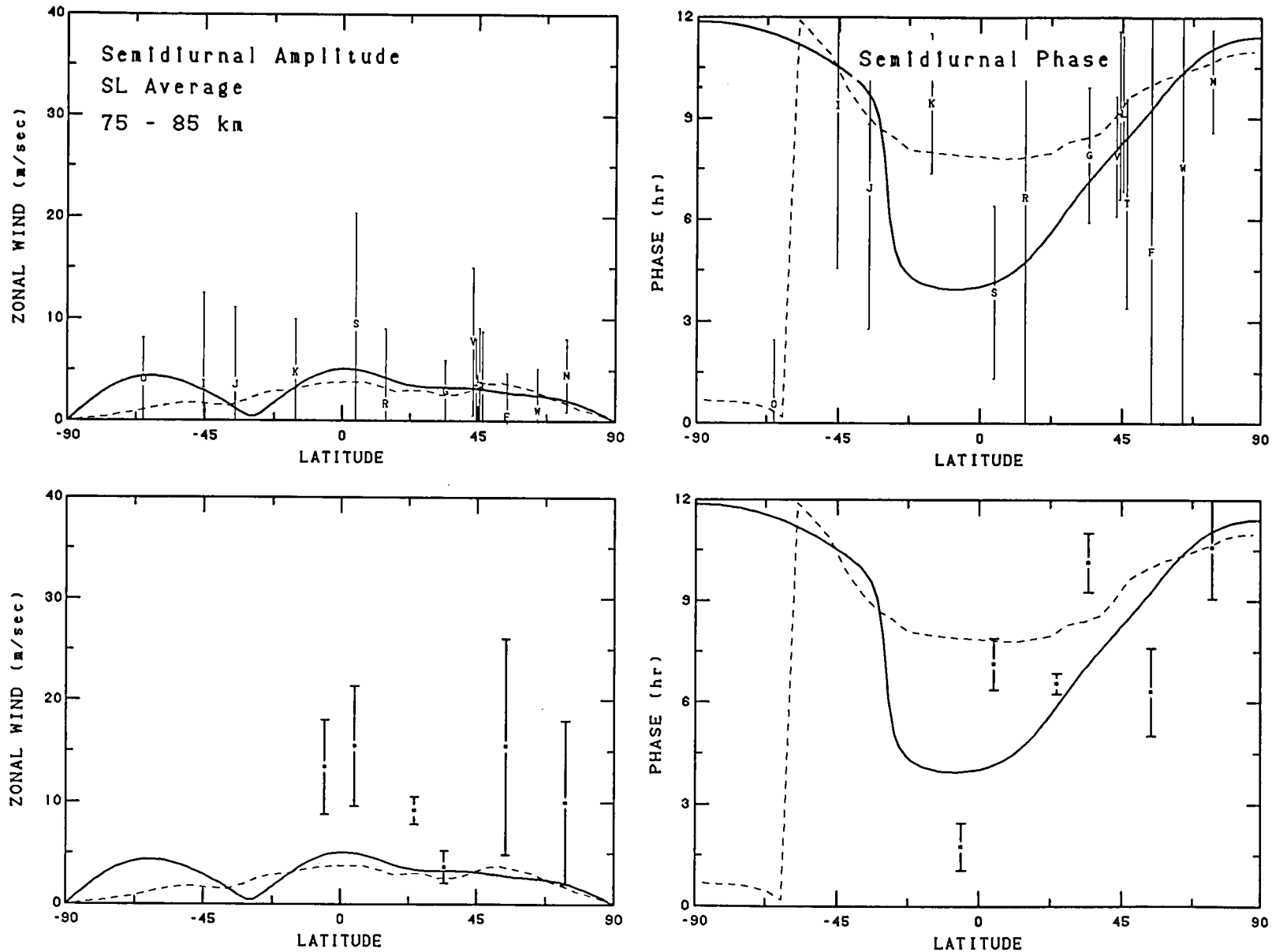

Fig. 9d. Seasonal average semidiurnal zonal wind amplitude and phase versus latitude for 75 to 85 km. The HWM93 wind (solid line) and FV89 (dashed) shown for mid-range conditions. Top row of plots contain MF/Meteor radar data with plot symbols as indicated in Table 1. Bottom row contains rocketsonde and IS radar data combined (*).

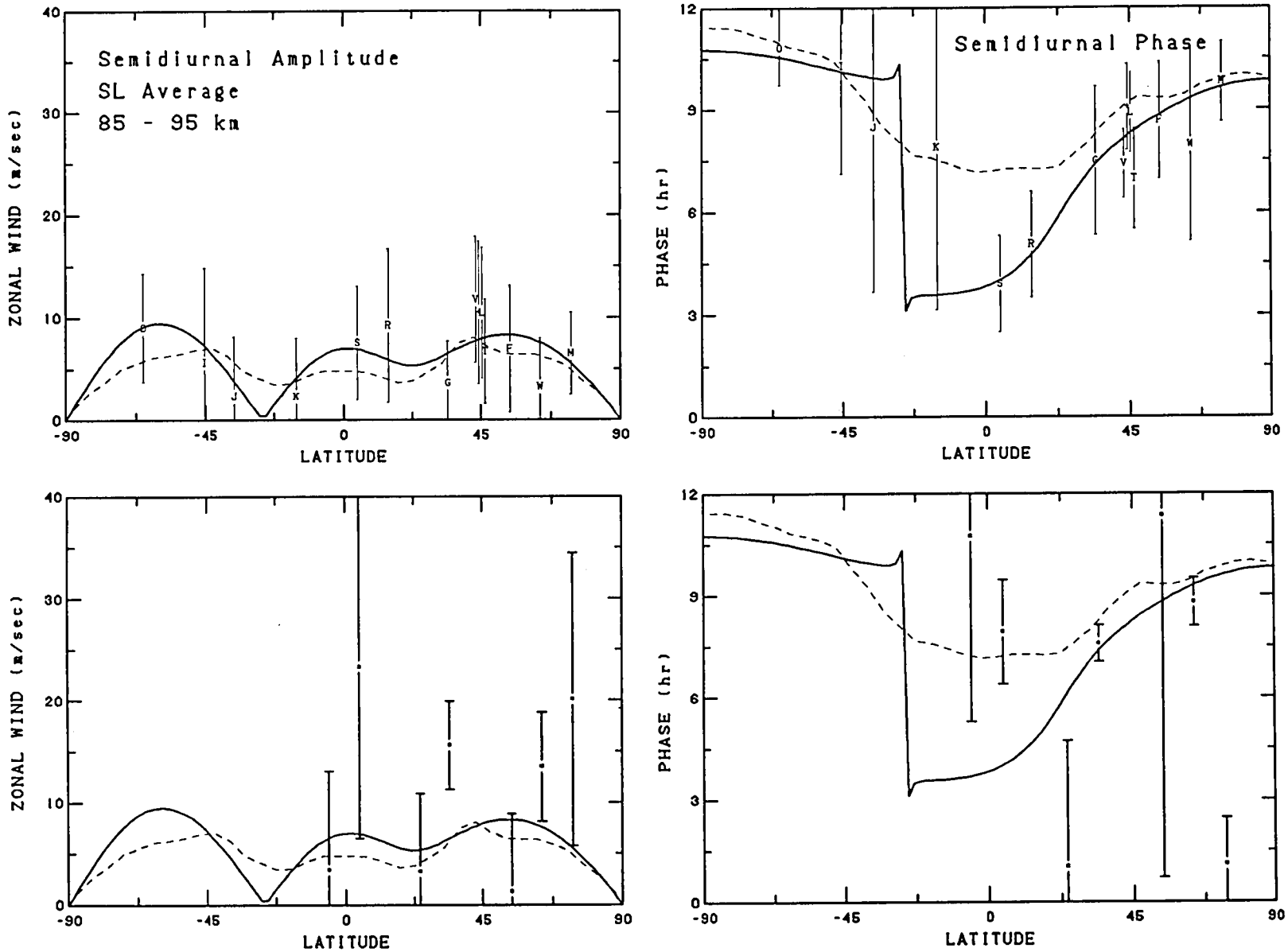

Fig. 9e. Seasonal average semidiurnal zonal wind amplitude and phase versus latitude for 85 to 95 km. The HWM93 wind (solid line) and FV89 (dashed) shown for mid-range conditions. Top row of plots contain MF/Meteor radar data with plot symbols as indicated in Table 1. Bottom row contains rocketsonde and IS radar data combined (*).

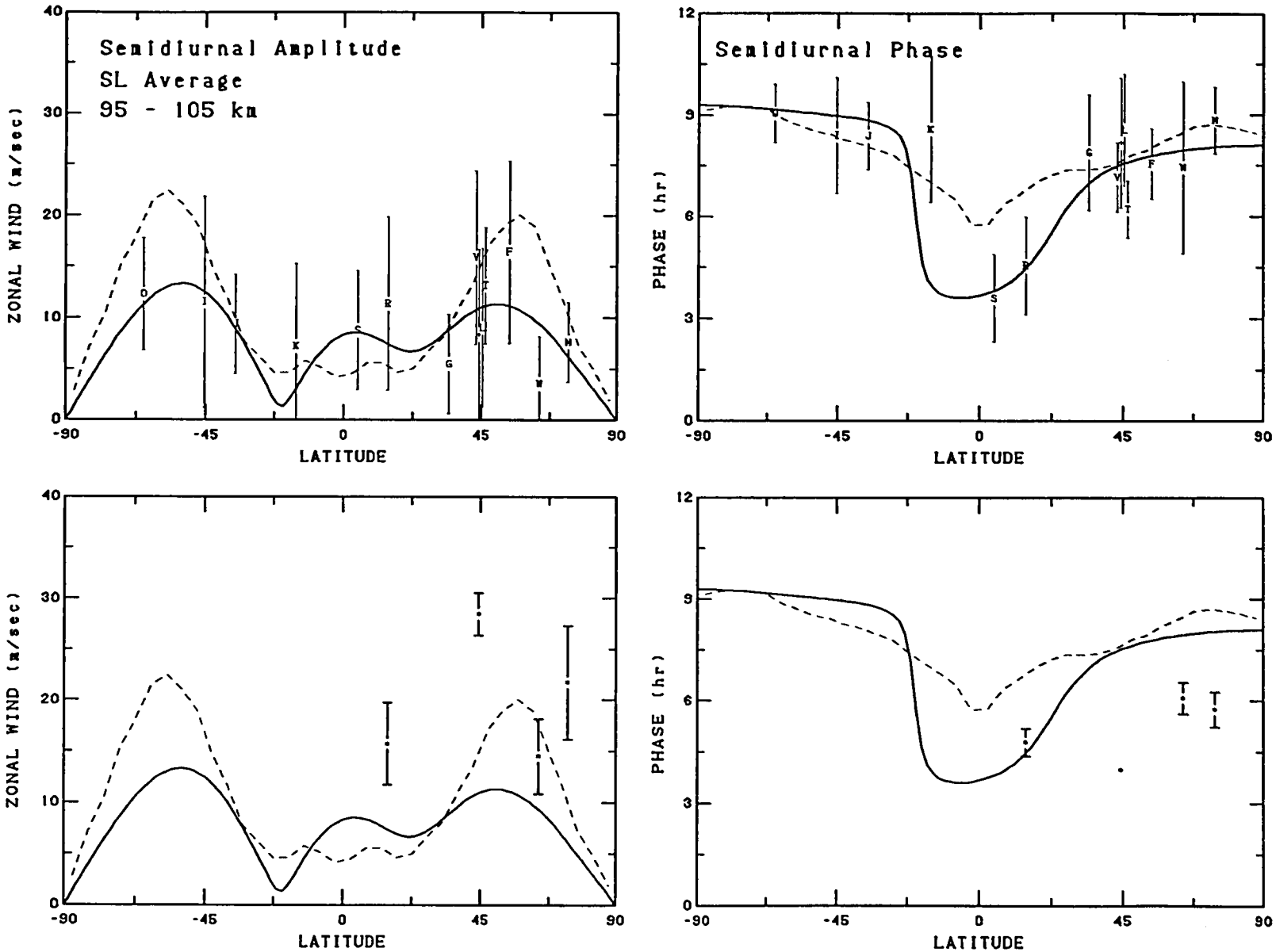

Fig. 9f. Seasonal average semidiurnal zonal wind amplitude and phase versus latitude for 95 to 105 km. The HWM93 wind (solid line) and FV89 (dashed) shown for mid-range conditions. Top row of plots contain MF/Meteor radar data with plot symbols as indicated in Table 1. Bottom row contains rocketsonde and IS radar data combined (*).

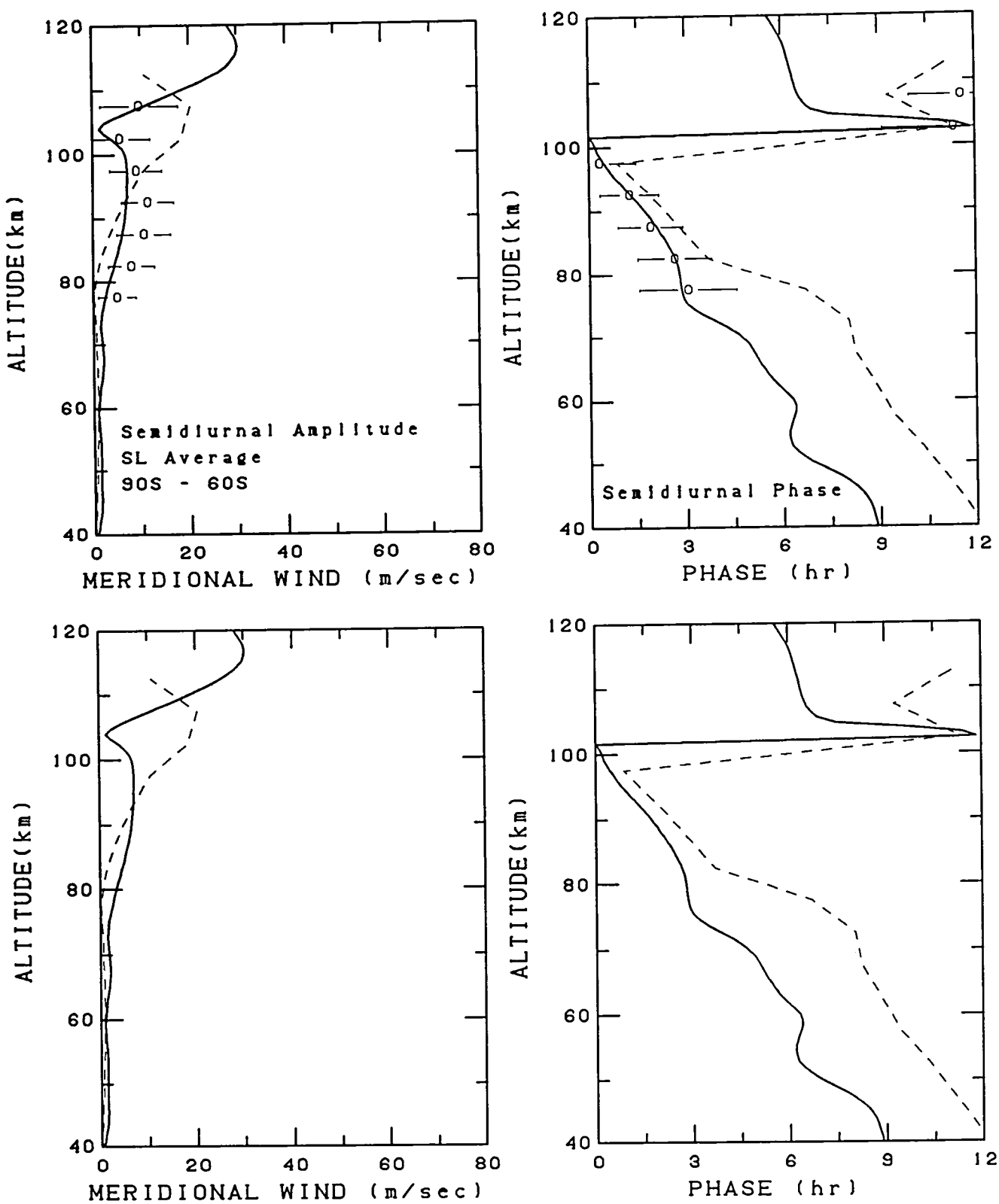

Fig. 10a. Seasonal average semidiurnal meridional wind amplitude and phase versus altitude for southern high latitudes. The HWM93 wind (solid line) and FV89 (dashed) shown for mid-range conditions. Top row of plots contain MF/Meteor radar data with symbols indicated in Table 1. Bottom row contains rocketsonde and IS radar data combined (*).

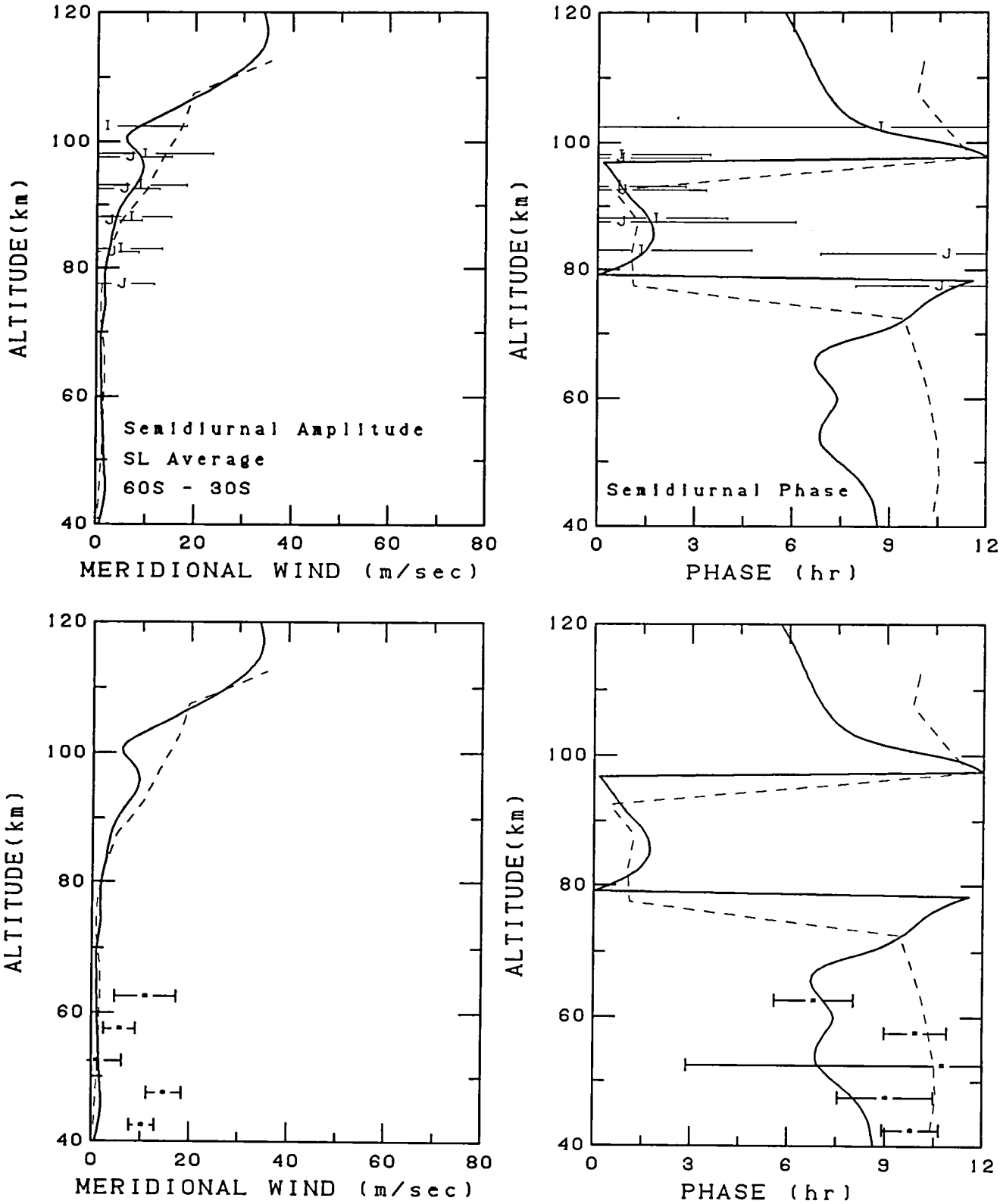

Fig. 10b. Seasonal average semidiurnal meridional wind amplitude and phase versus altitude for southern middle latitudes. The HWM93 wind (solid line) and FV89 (dashed) shown for mid-range conditions. Top row of plots contain MF/Meteor radar data with symbols indicated in Table 1. Bottom row contains rocketsonde and IS radar data combined (*).

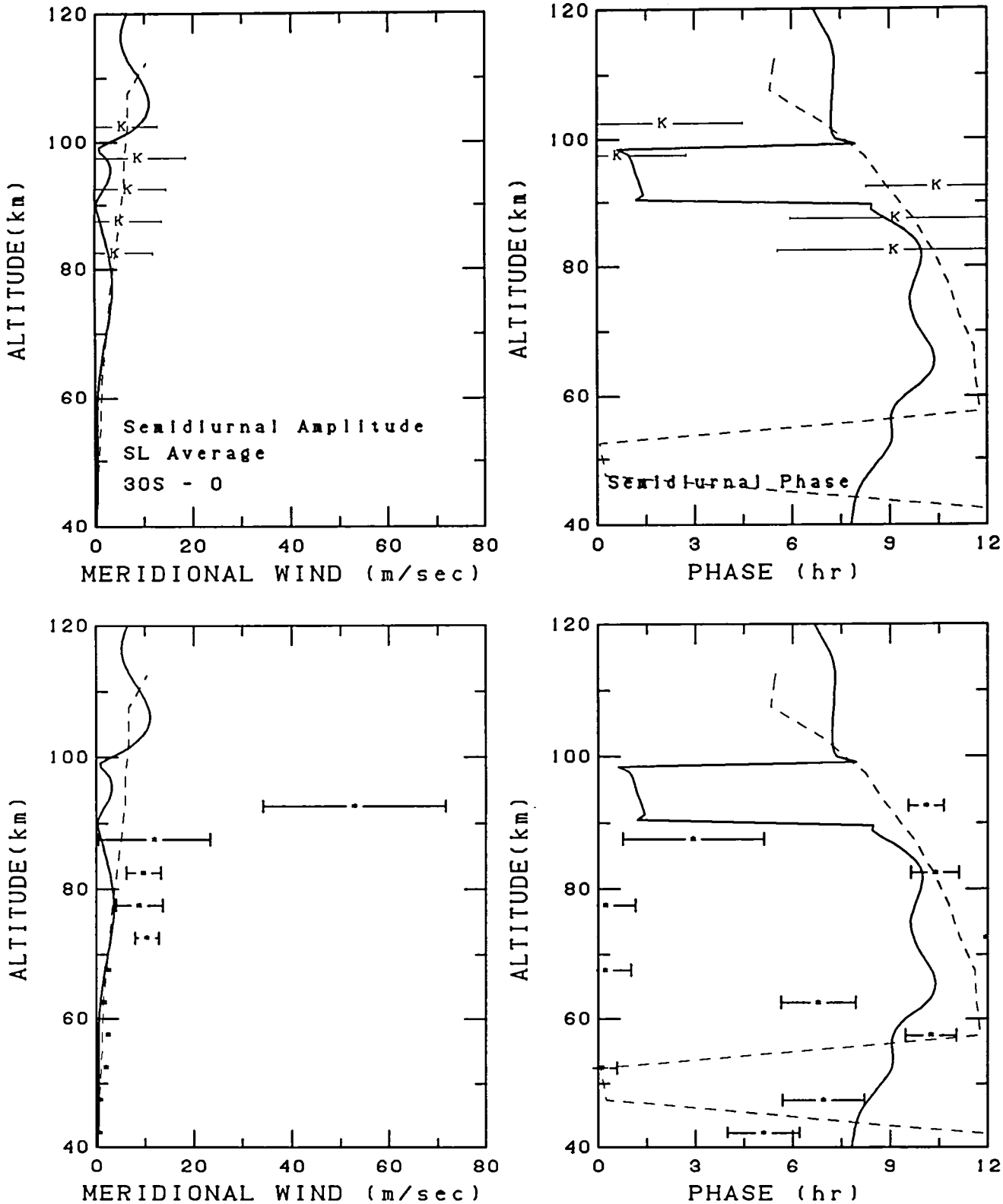

Fig. 10c. Seasonal average semidiurnal meridional wind amplitude and phase versus altitude for southern low latitudes. The HWM93 wind (solid line) and FV89 (dashed) shown for mid-range conditions. Top row of plots contain MF/Meteor radar data with symbols indicated in Table 1. Bottom row contains rocketsonde and IS radar data combined (*).

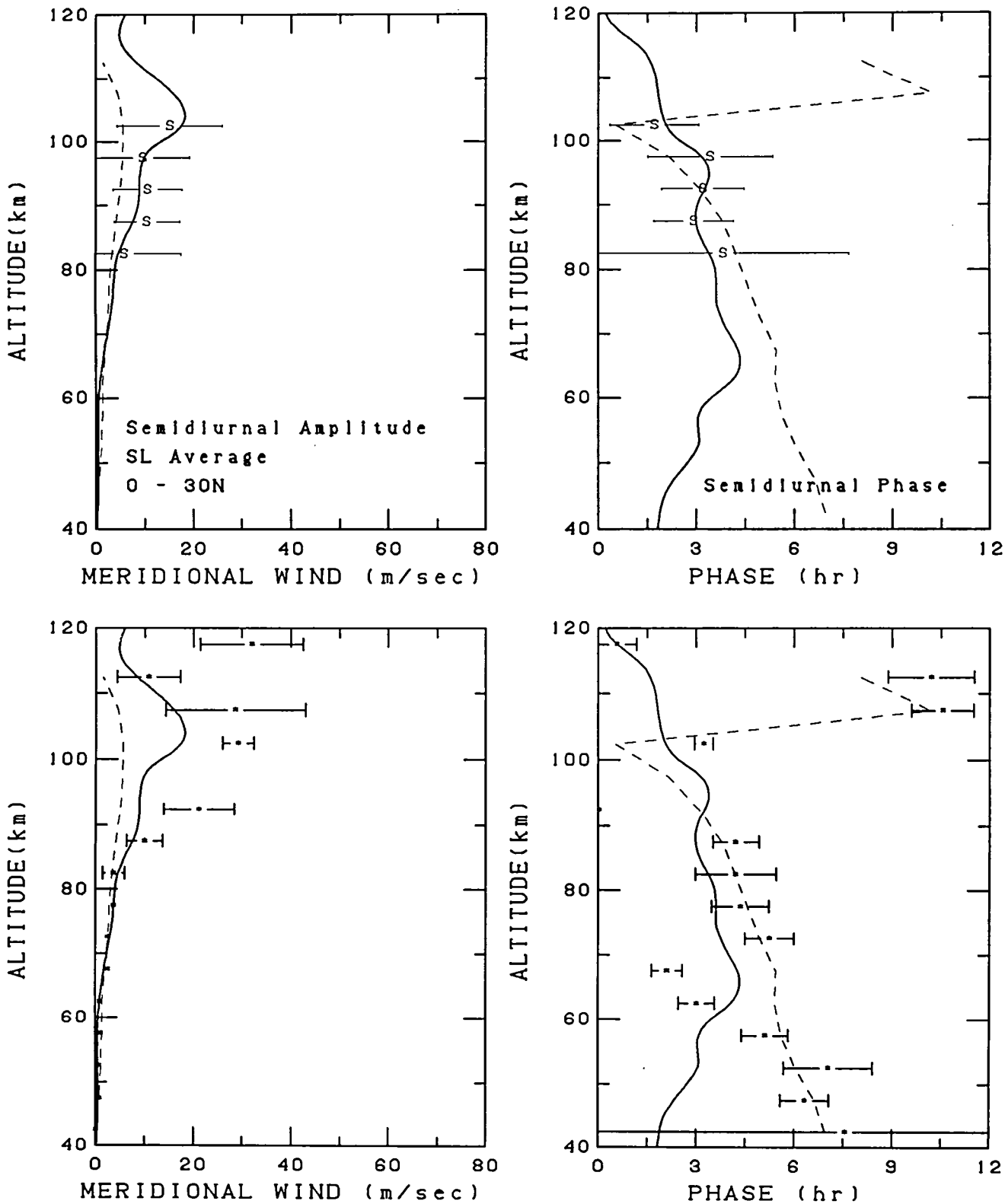

Fig. 10d. Seasonal average semidiurnal meridional wind amplitude and phase versus altitude for northern low latitudes. The HWM93 wind (solid line) and FV89 (dashed) shown for mid-range conditions. Top row of plots contain MF/Meteor radar data with symbols indicated in Table 1. Bottom row contains rocketsonde and IS radar data combined (*).

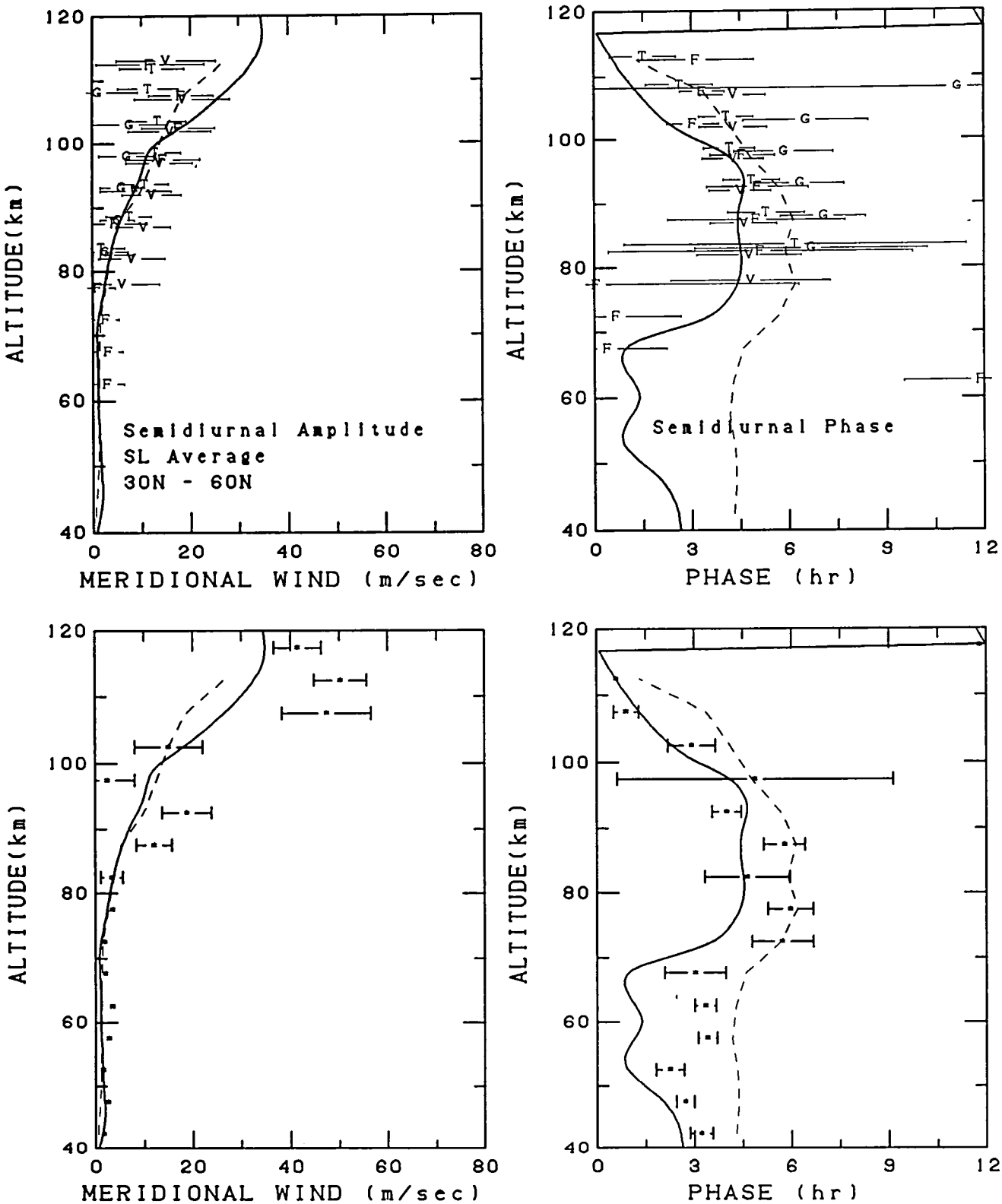

Fig. 10e. Seasonal average semidiurnal meridional wind amplitude and phase versus altitude for northern middle latitudes. The HWM93 wind (solid line) and FV89 (dashed) shown for mid-range conditions. Top row of plots contain MF/Meteor radar data with symbols indicated in Table 1. Bottom row contains rocketsonde and IS radar data combined (*).

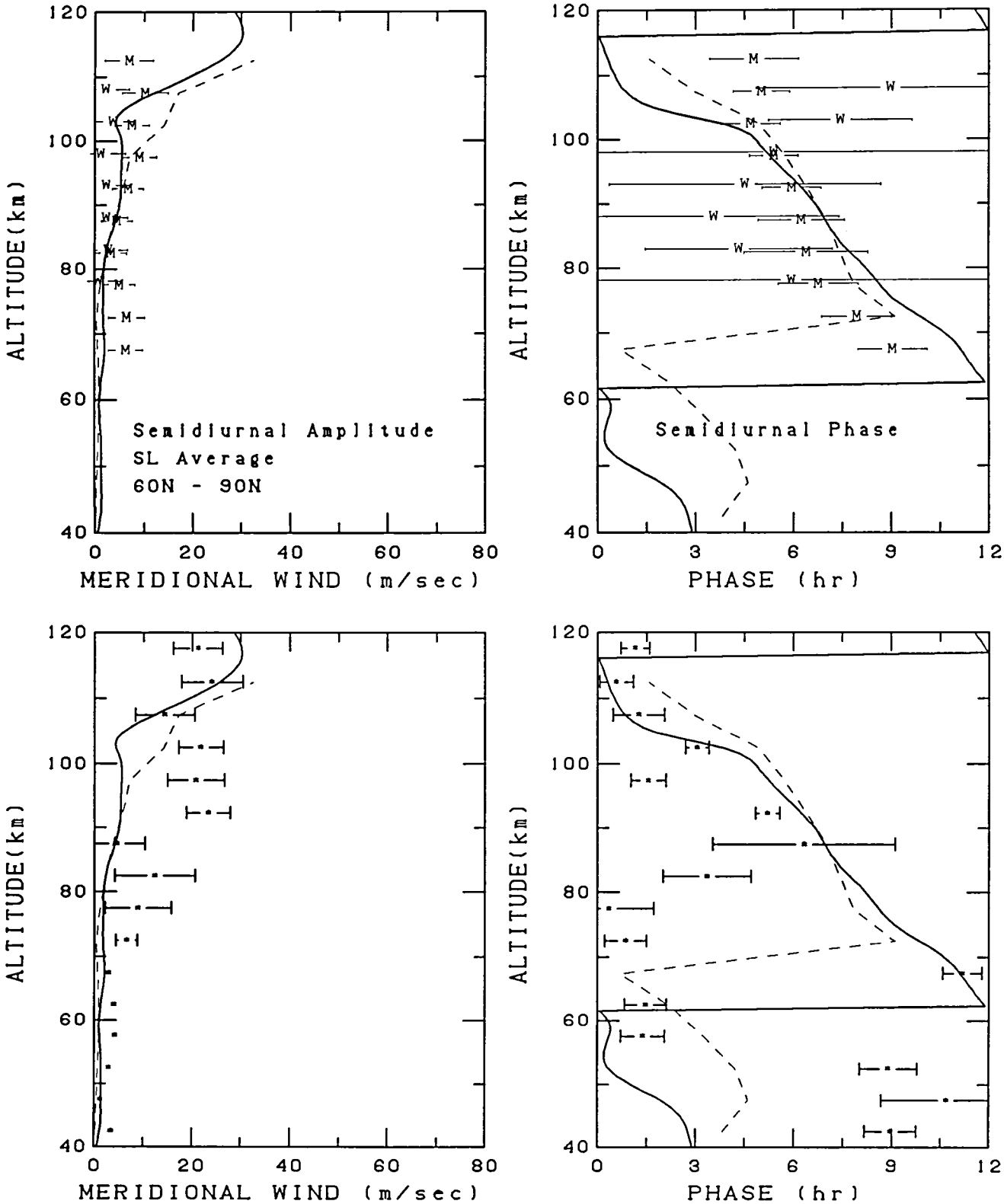

Fig. 10f. Seasonal average semidiurnal meridional wind amplitude and phase versus altitude for norhtern high latitudes. The HWM93 wind (solid line) and FV89 (dashed) shown for mid-range conditions. Top row of plots contain MF/Meteor radar data with indicated in Table 1. Bottom row contains rocketsonde and IS radar data combined (*).

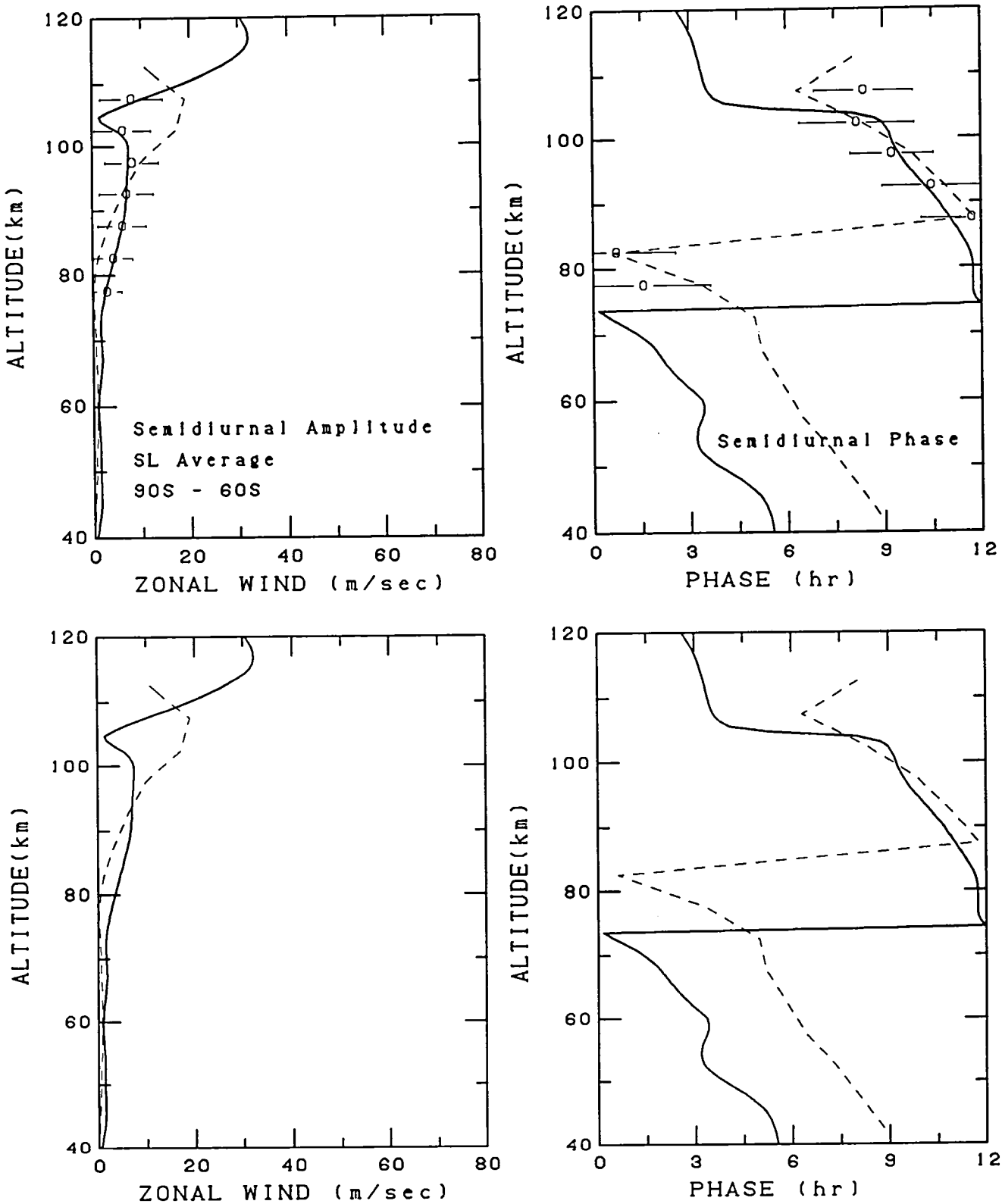

Fig. 11a. Seasonal average semidiurnal zonal wind amplitude and phase versus latitude for southern high latitudes. The HWM93 wind (solid line) and FV89 (dashed) shown for mid-range conditions. Top row of plots contain MF/Meteor radar data with symbols indicated in Table 1. Bottom row contains rocketsonde and IS radar data combined (*).

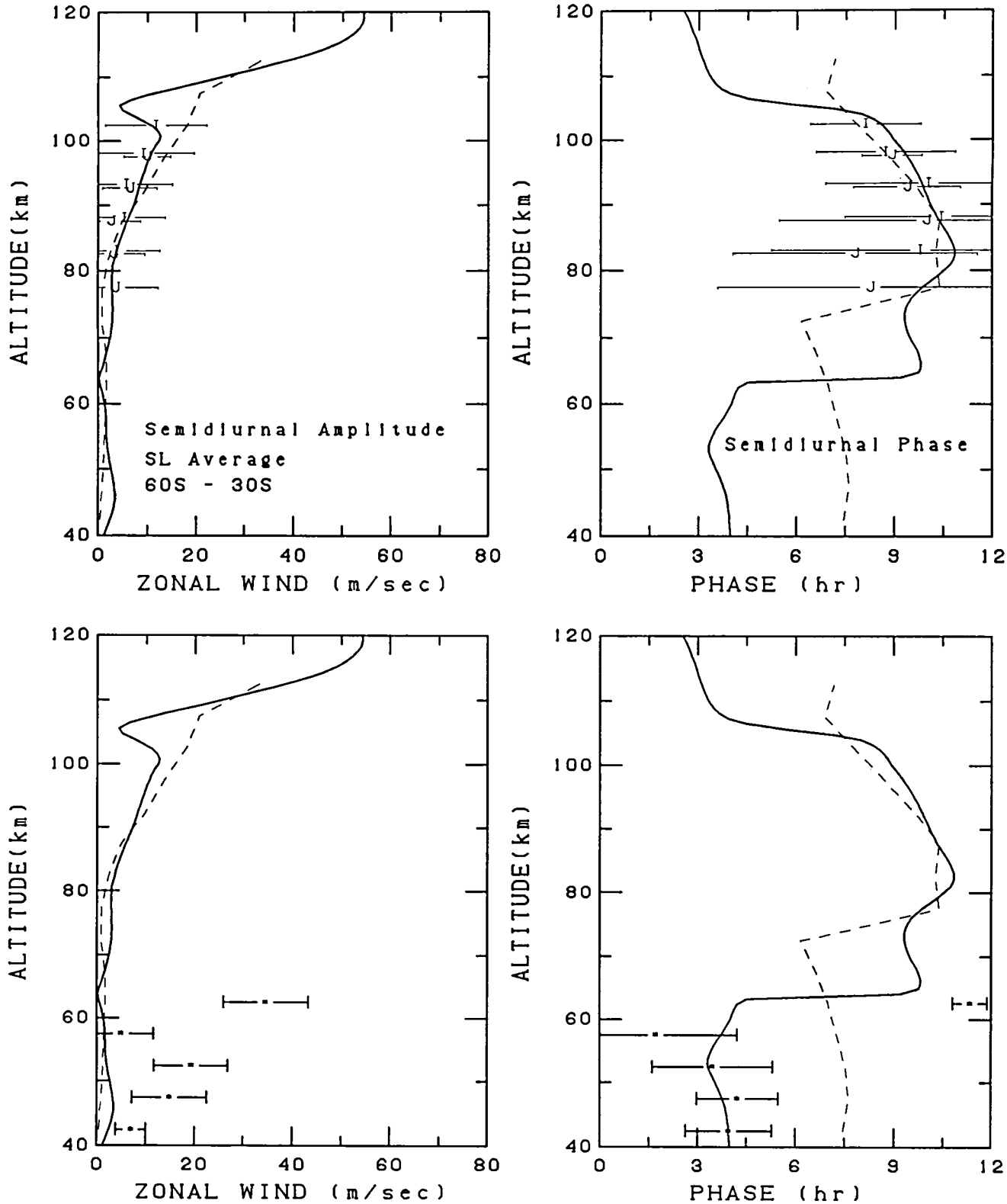

Fig. 11b. Seasonal average semidiurnal zonal wind amplitude and phase versus latitude for southern middle latitudes. The HWM93 wind (solid line) and FV89 (dashed) shown for mid-range conditions. Top row of plots contain MF/Meteor radar data with symbols indicated in Table 1. Bottom row contains rocketsonde and IS radar data combined (*).

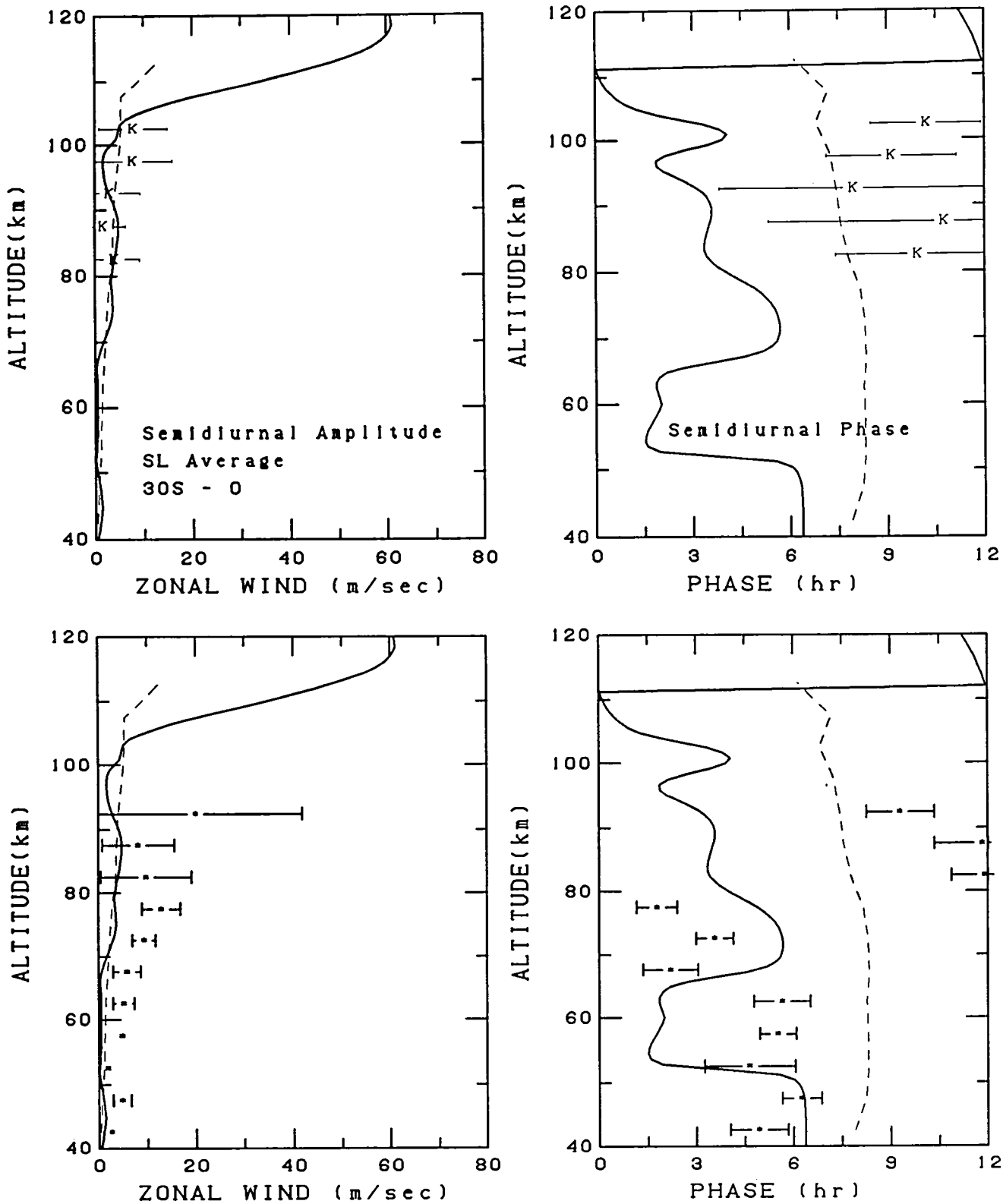

Fig. 11c. Seasonal average semidiurnal zonal wind amplitude and phase versus latitude for southern low latitudes. The HWM93 wind (solid line) and FV89 (dashed) shown for mid-range conditions. Top row of plots contain MF/Meteor radar data with symbols indicated in Table 1. Bottom row contains rocketsonde and IS radar data combined (*).

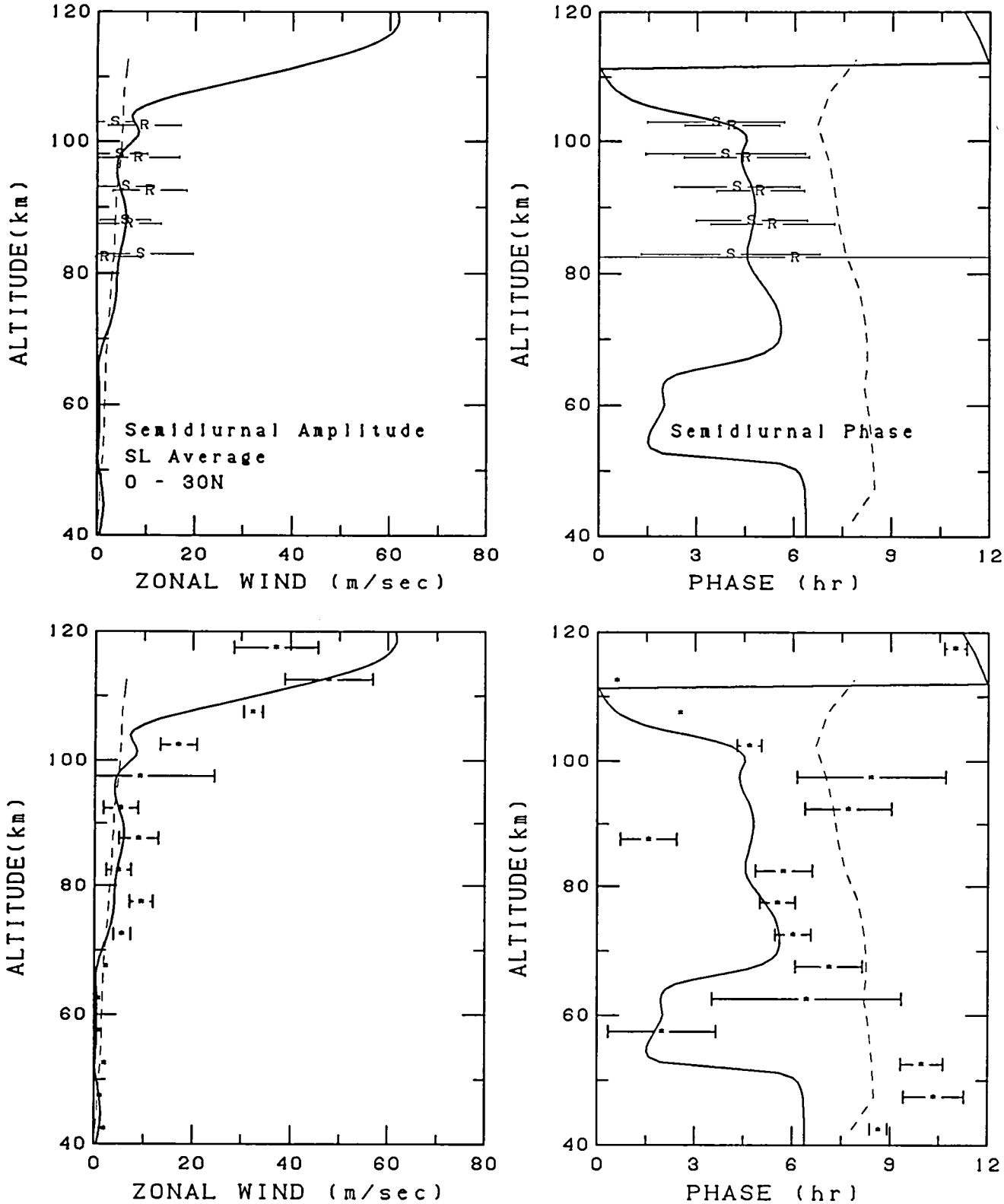

Fig. 11d. Seasonal average semidiurnal zonal wind amplitude and phase versus latitude for northern low latitudes. The HWM93 wind (solid line) and FV89 (dashed) shown for mid-range conditions. Top row of plots contain MF/Meteor radar data with symbols indicated in Table 1. Bottom row contains rocketsonde and IS radar data combined (*).

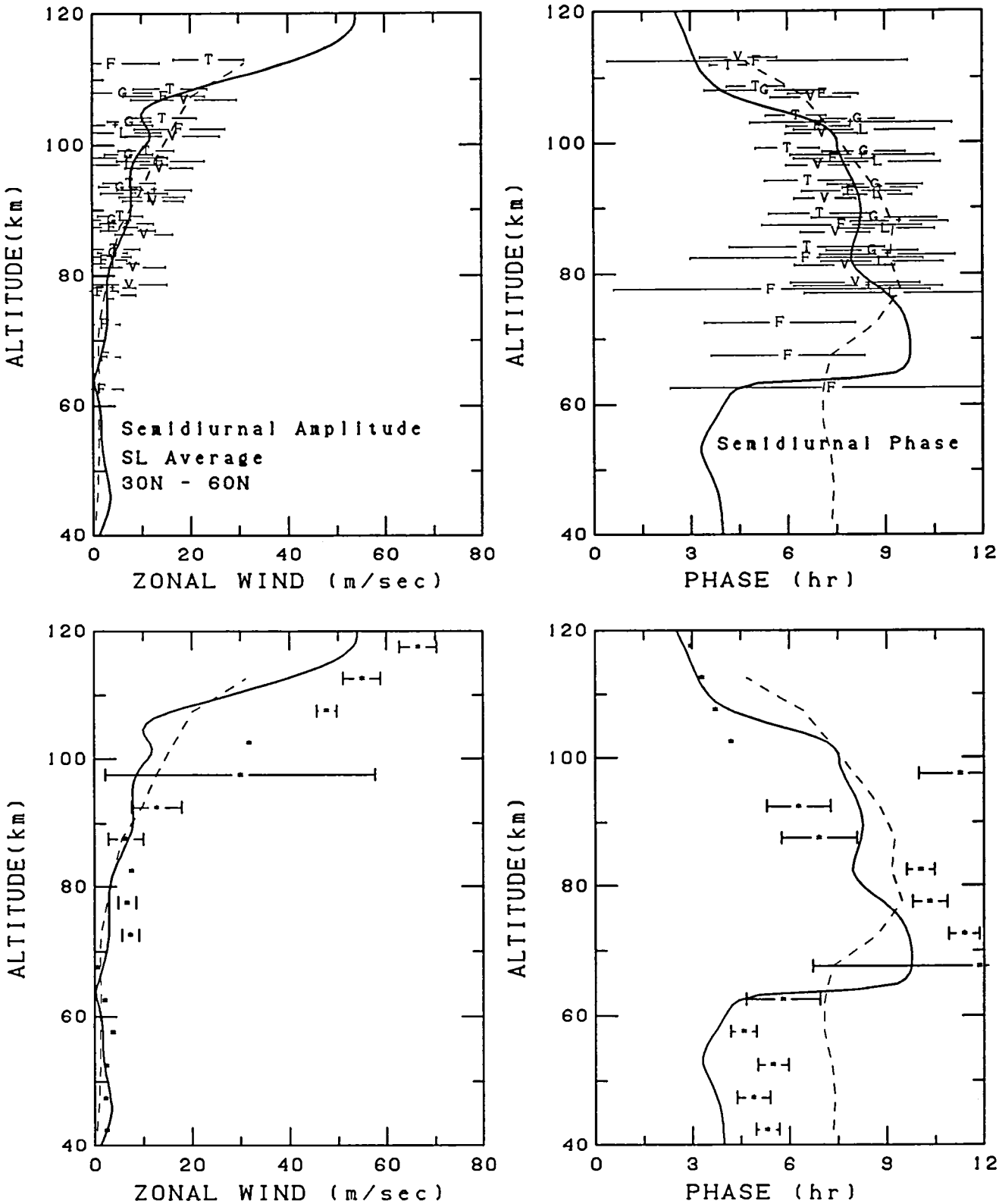

Fig. 11e. Seasonal average semidiurnal zonal wind amplitude and phase versus latitude for northern middle latitudes. The HWM93 wind (solid line) and FV89 (dashed) shown for mid-range conditions. Top row of plots contain MF/Meteor radar data with symbols indicated in Table 1. Bottom row contains rocketsonde and IS radar data combined (*).

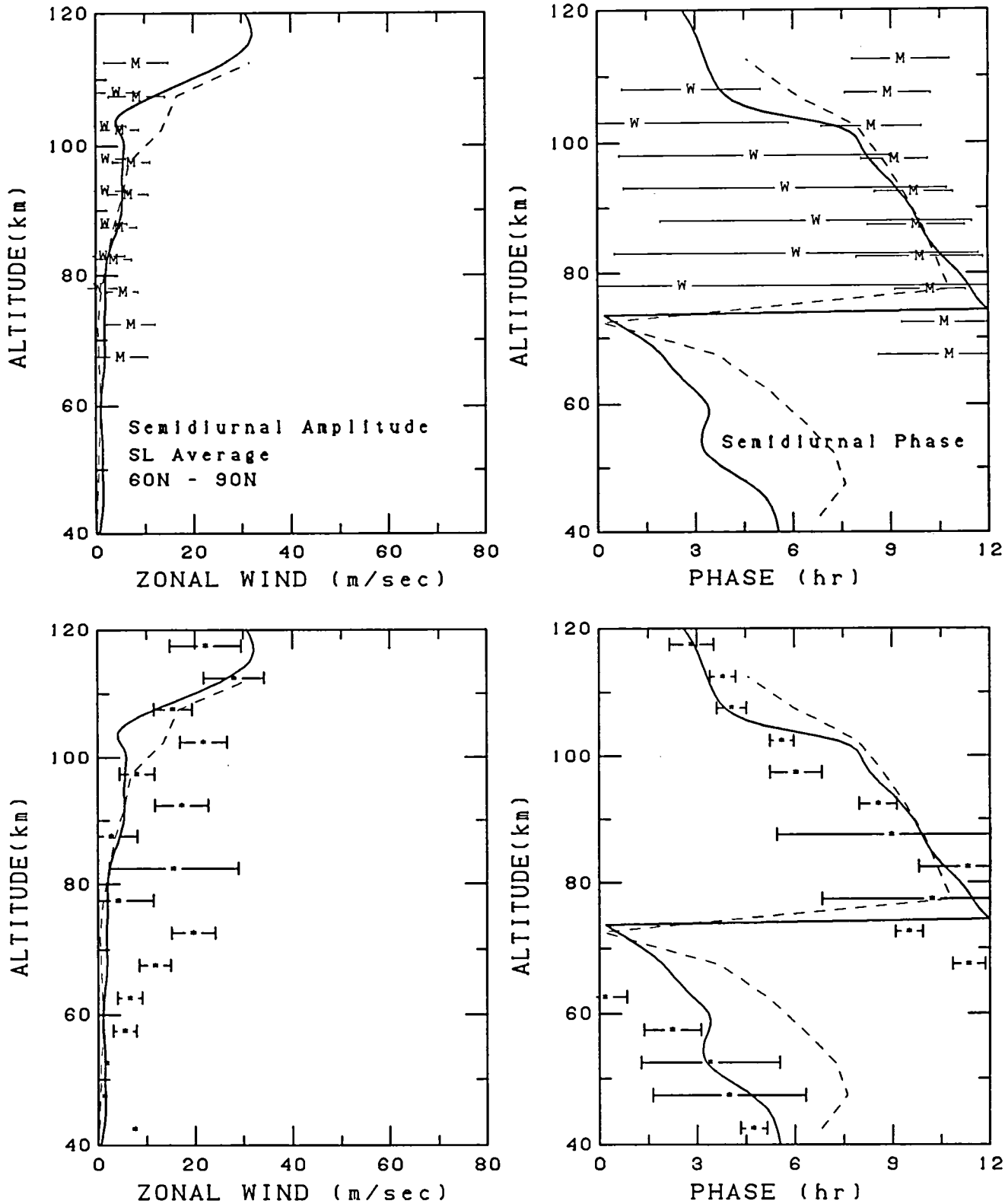

Fig. 11f. Seasonal average semidiurnal zonal wind amplitude and phase versus latitude for northern high latitudes. The HWM93 wind (solid line) and FV89 (dashed) shown for mid-range conditions. Top row of plots contain MF/Meteor radar data with symbols indicated in Table 1. Bottom row contains rocketsonde and IS radar data combined (*).

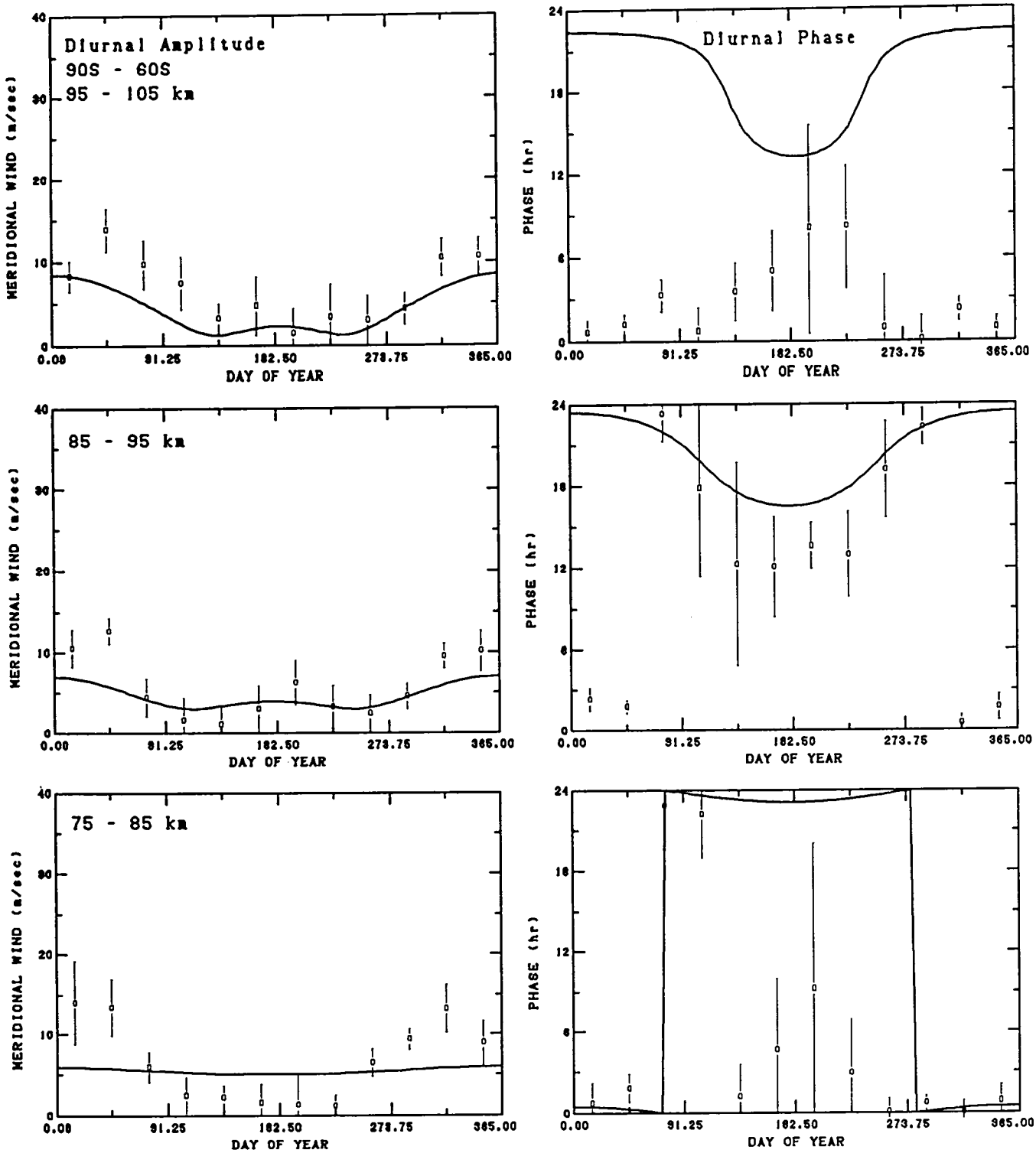

Fig. 13a. Diurnal meridional wind amplitude and phase versus day of year for selected altitudes at southern high latitudes. The HWM93 model (solid line) shown for mid_range conditions. Plot symbols indicate source as given in Table 1.

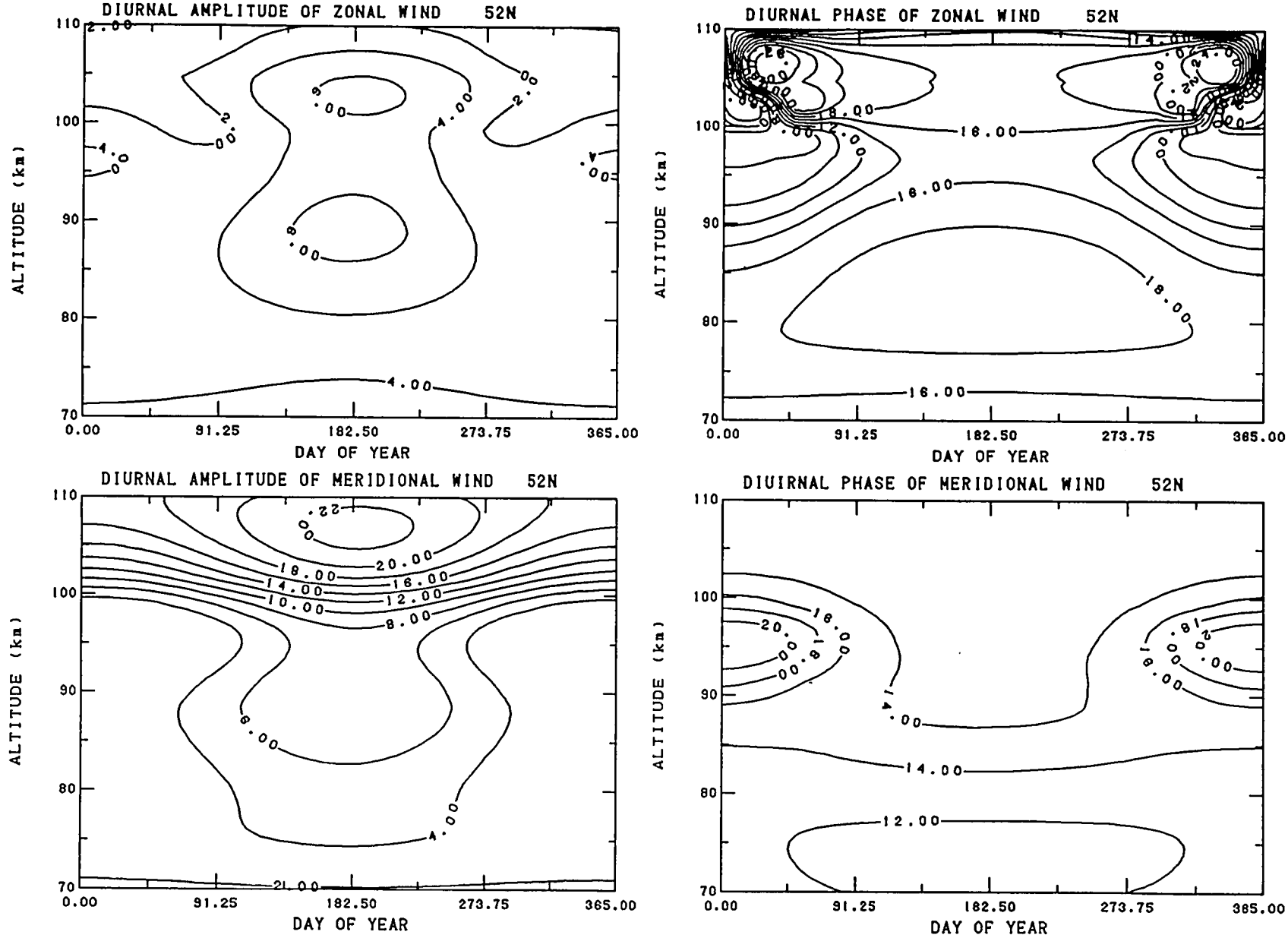

Fig. 12a. Contour plots in altitude versus day of year of the diurnal amplitude and phase (dashed negative) of the zonal and meridional wind at 52N latitude.

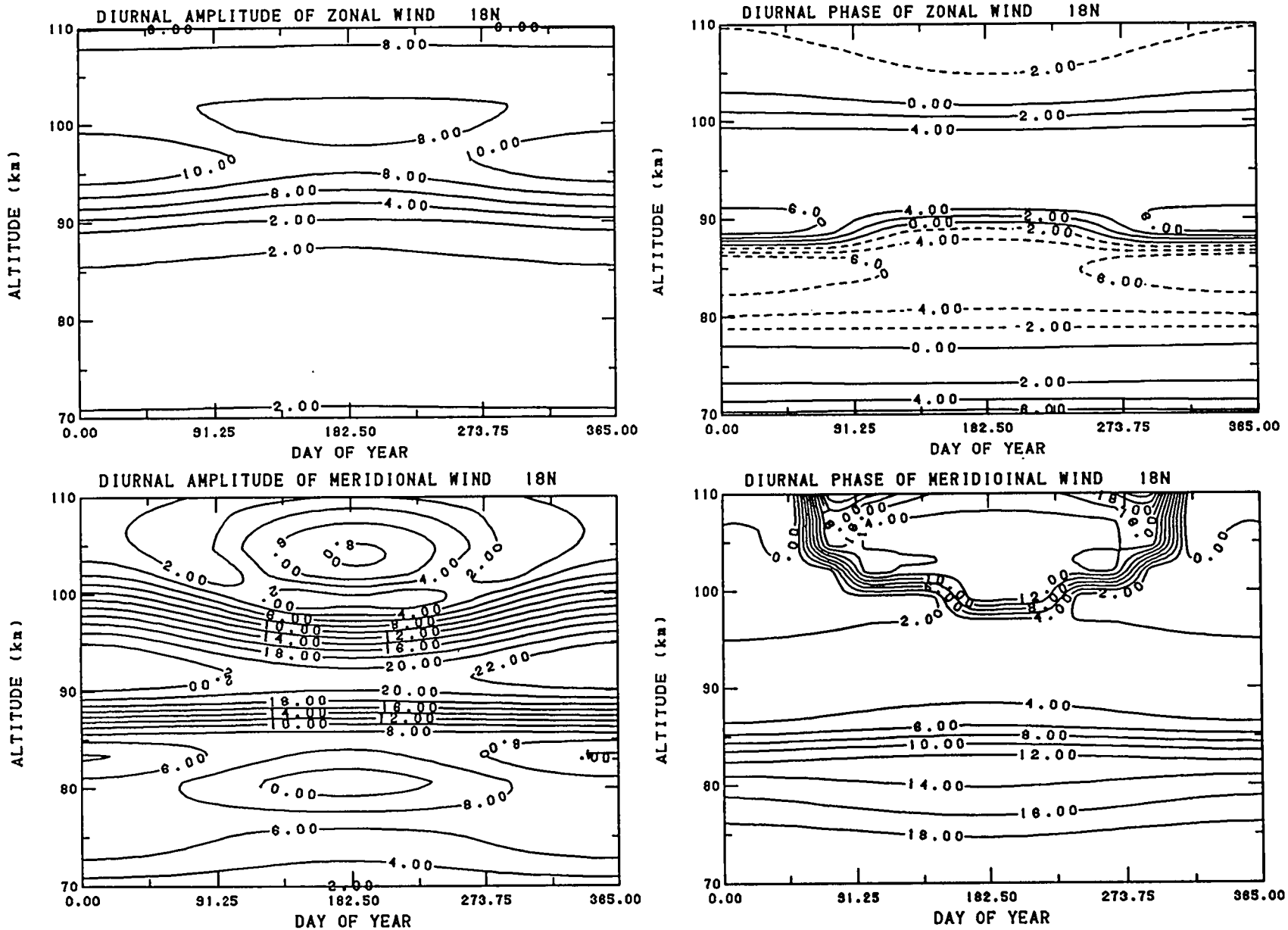

Fig. 12b. Contour plots in altitude versus day of year of the diurnal amplitude and phase (dashed negative) of the zonal and meridional wind at 18 N latitude.

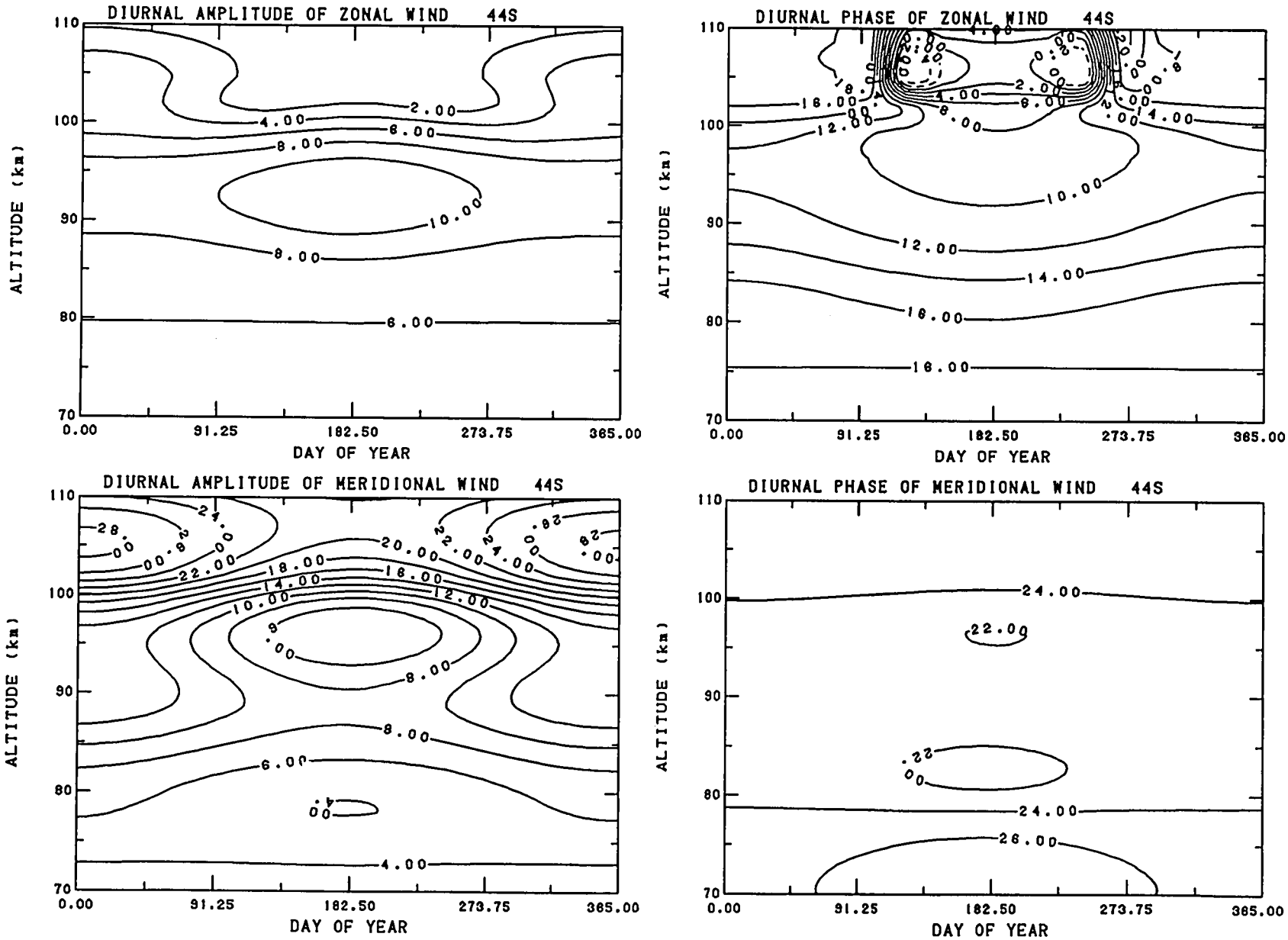

Fig. 12c. Contour plots in altitude versus day of year of the diurnal amplitude and phase (dashed negative) of the zonal and meridional wind at 44S latitude.

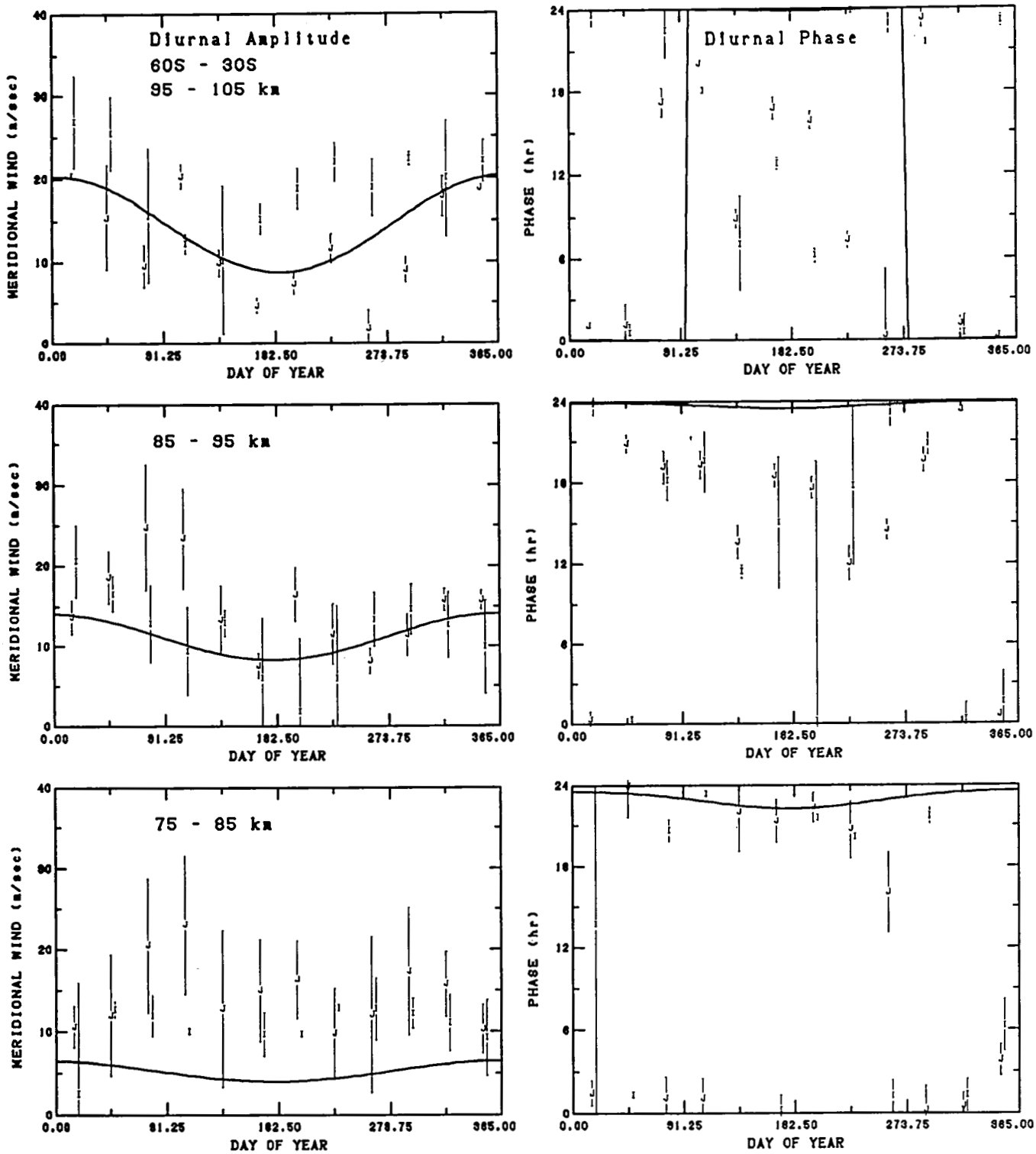

Fig. 13b. Diurnal meridional wind amplitude and phase versus day of year for selected altitudes at southern middle latitudes. The HWM93 model (solid line) shown for mid_range conditions. Plot symbols indicate source as given in Table 1.

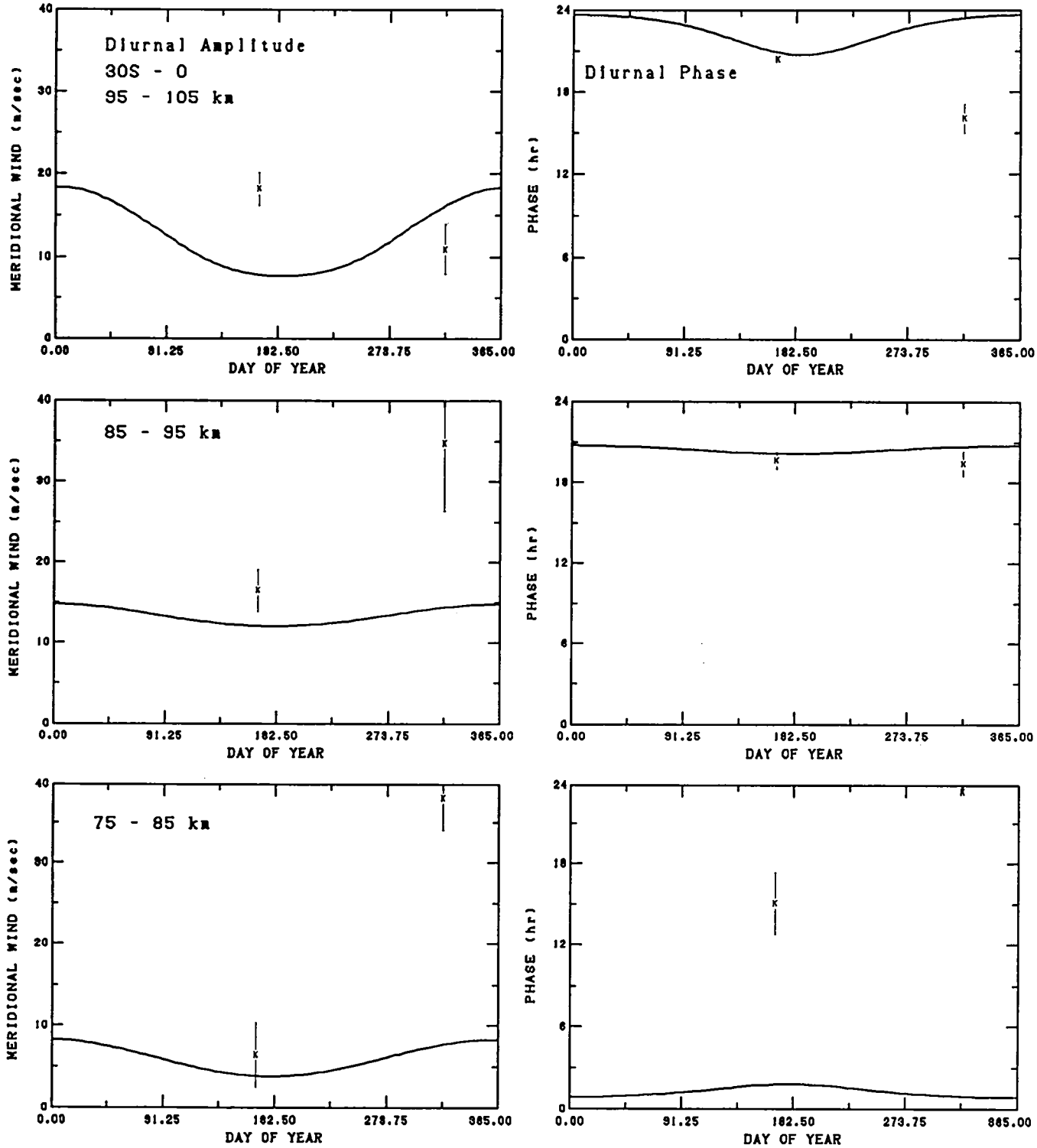

Fig. 13c. Diurnal meridional wind amplitude and phase versus day of year for selected altitudes at southern low latitudes. The HWM93 model (solid line) shown for mid_range conditions. Plot symbols indicate source as given in Table 1.

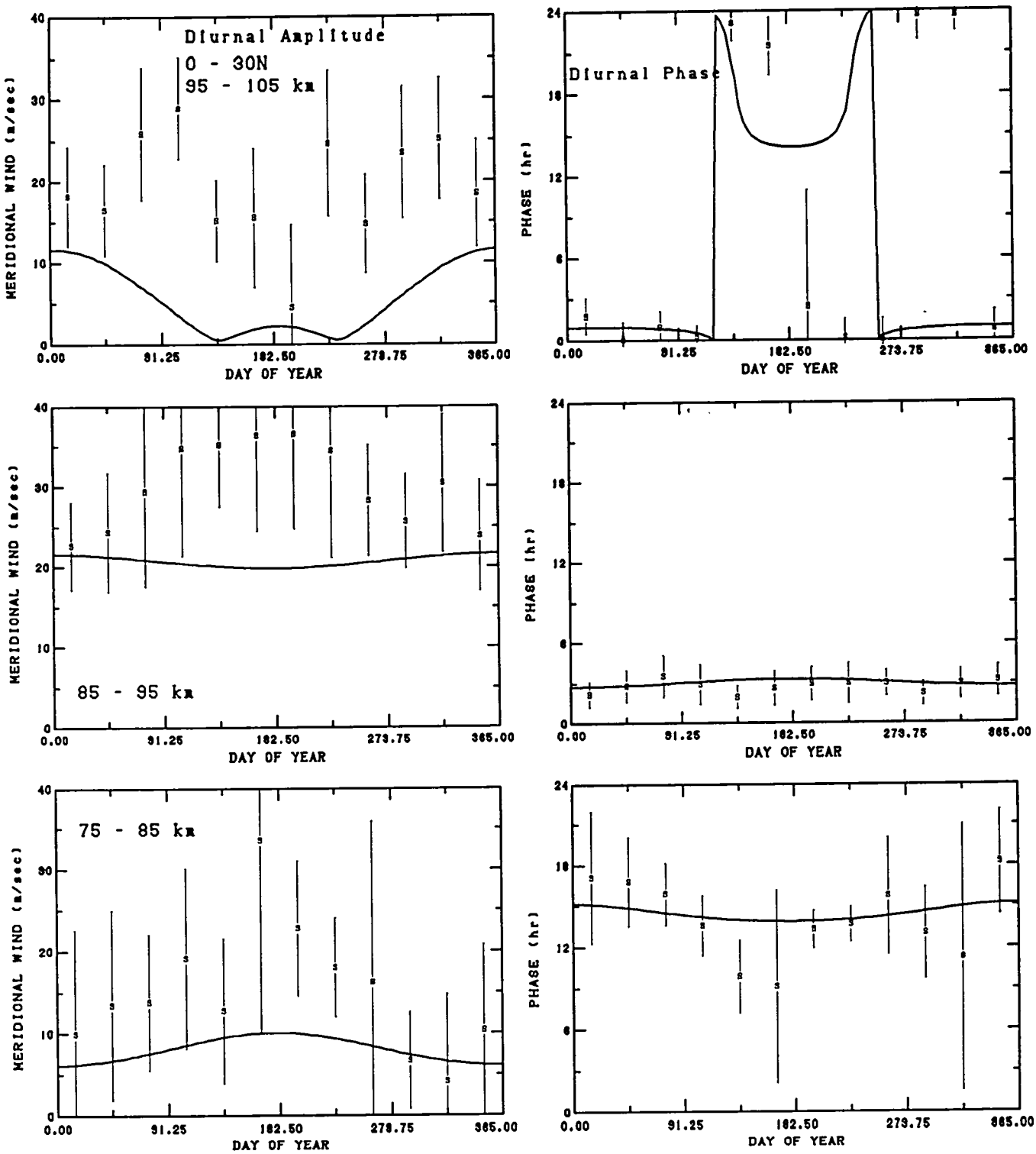

Fig. 13d. Diurnal meridional wind amplitude and phase versus day of year for selected altitudes at northern low latitudes. The HWM93 model (solid line) shown for mid_range conditions. Plot symbols indicate source as given in Table 1.

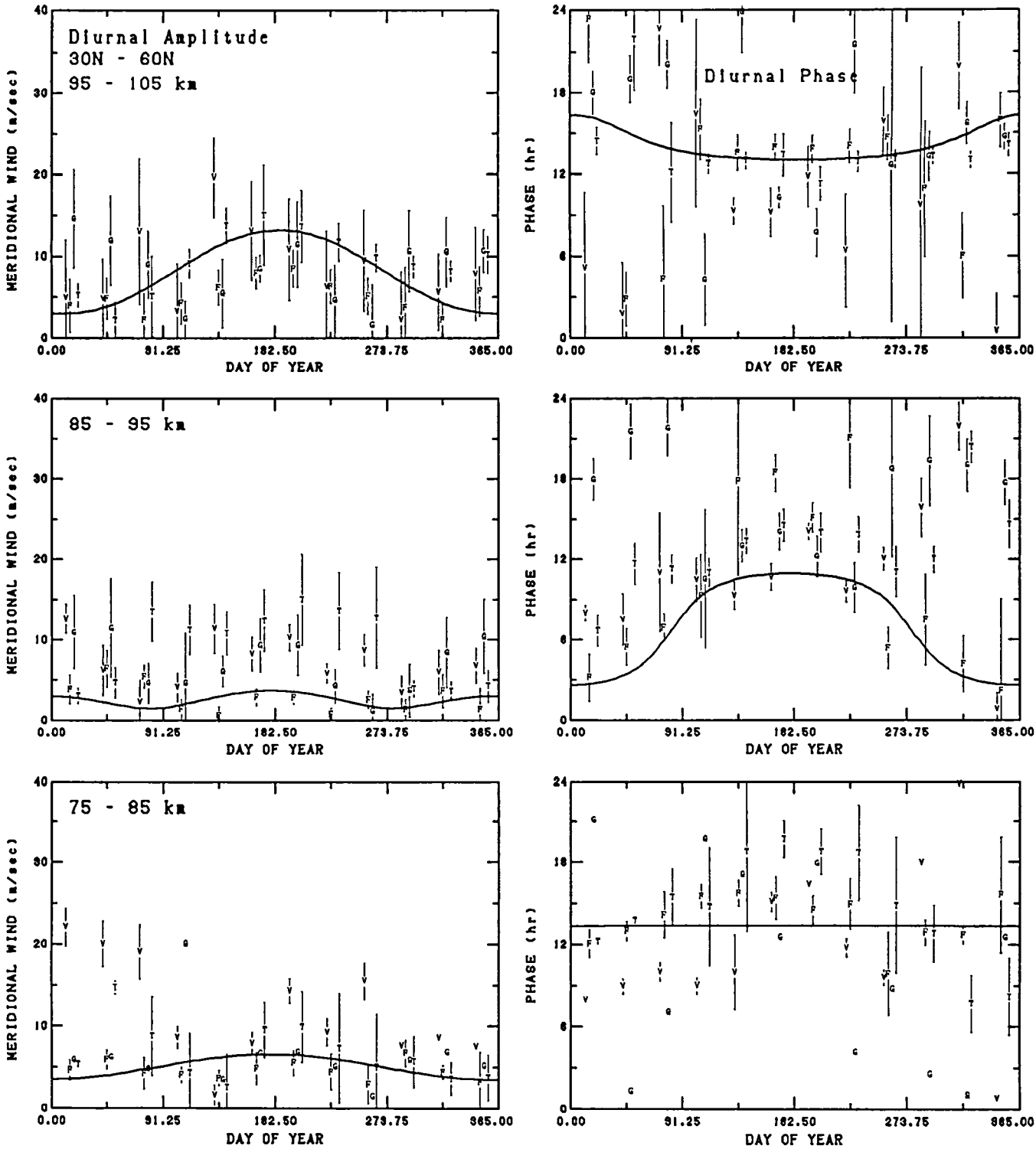

Fig. 13e. Diurnal meridional wind amplitude and phase versus day of year for selected altitudes at northern middle latitudes. The HWM93 model (solid line) shown for mid_range conditions. Plot symbols indicate source as given in Table 1.

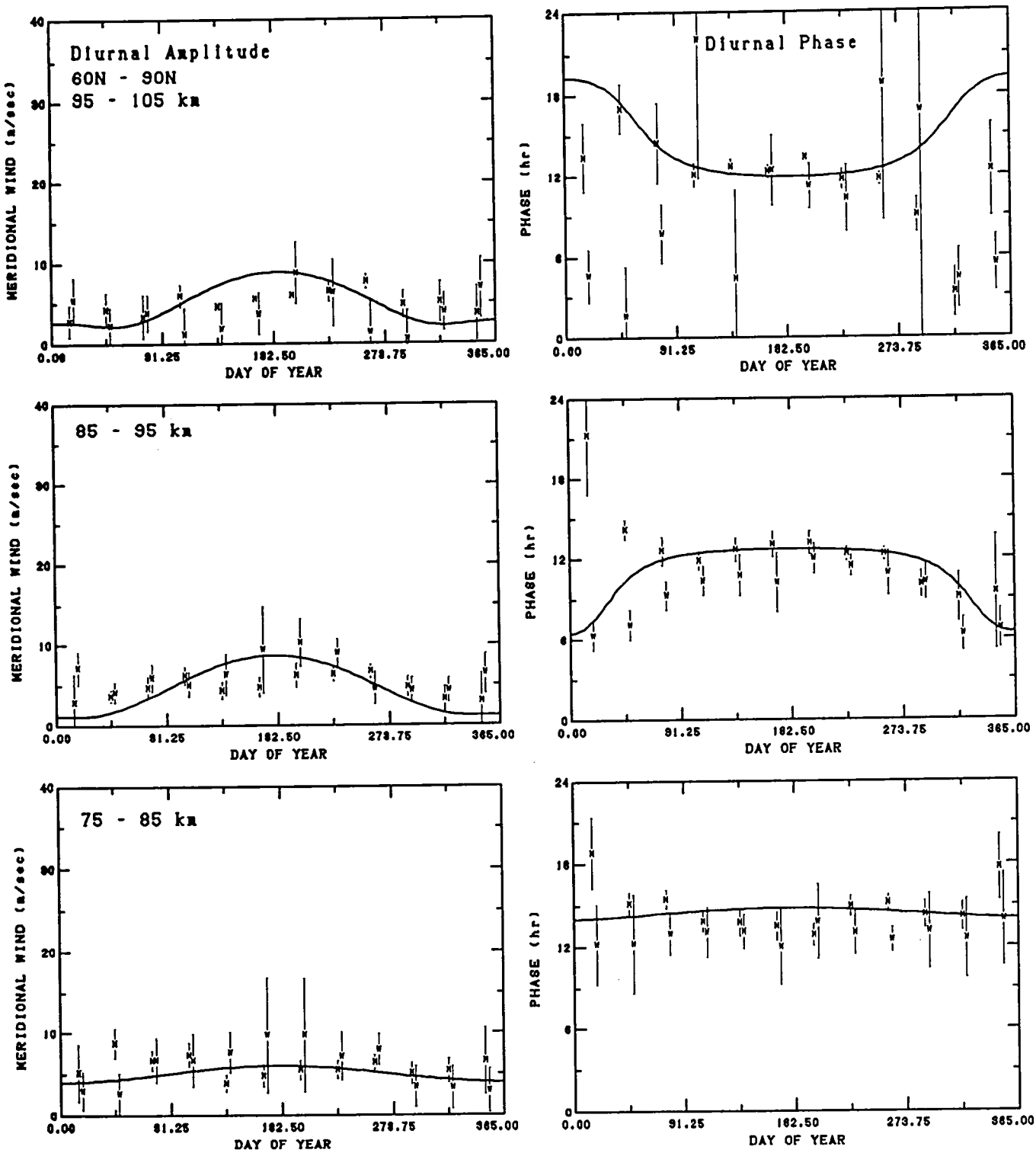

Fig. 13f. Diurnal meridional wind amplitude and phase versus day of year for selected altitudes at northern high latitudes. The HWM93 model (solid line) shown for mid_range conditions. Plot symbols indicate source as given in Table 1.

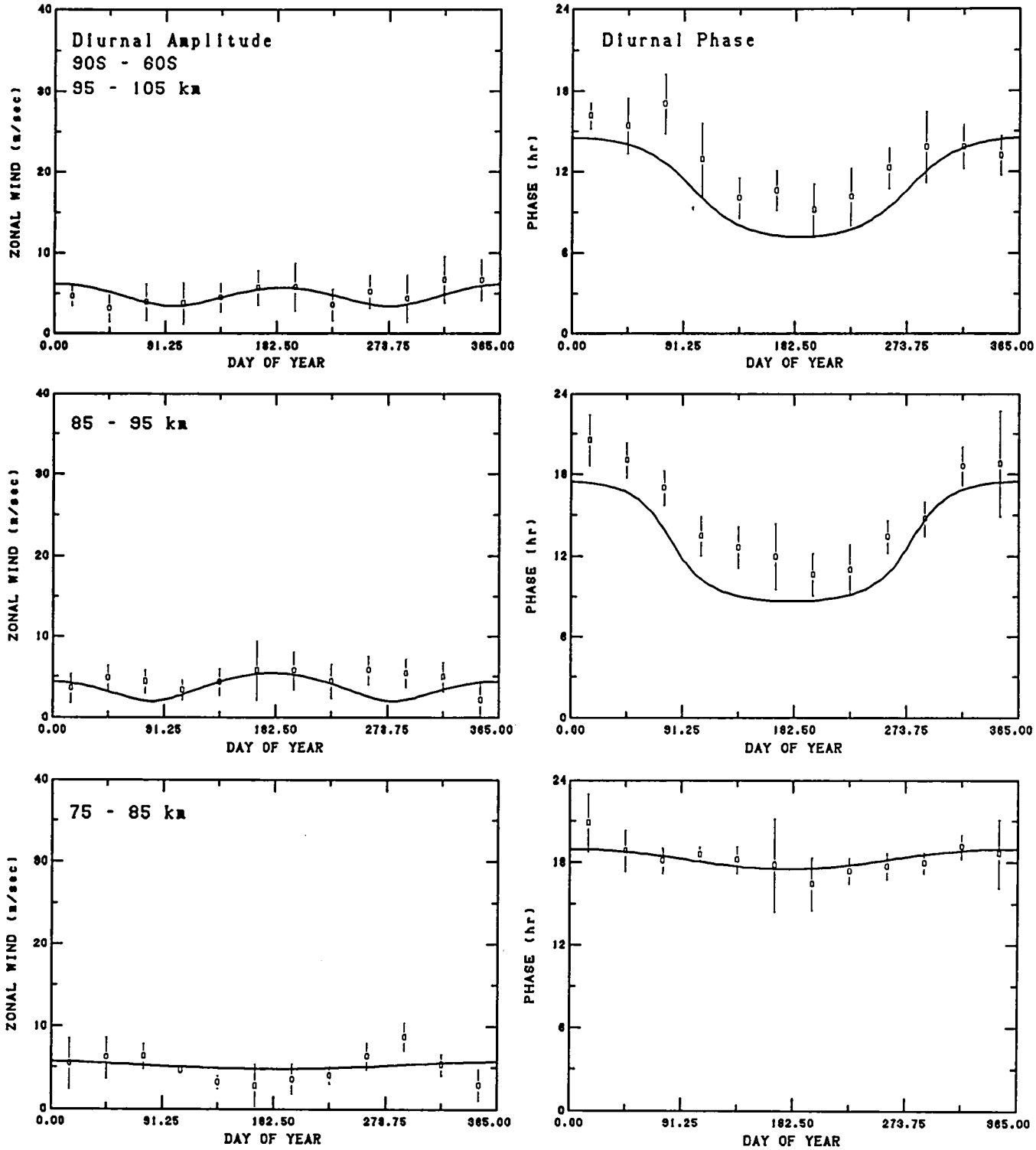

Fig. 14a. Diurnal zonal wind amplitude and phase versus day of year for selected altitudes at southern high latitudes. The HWM93 model (solid line) shown for mid_range conditions. Plot symbols indicate source as given in Table 1.

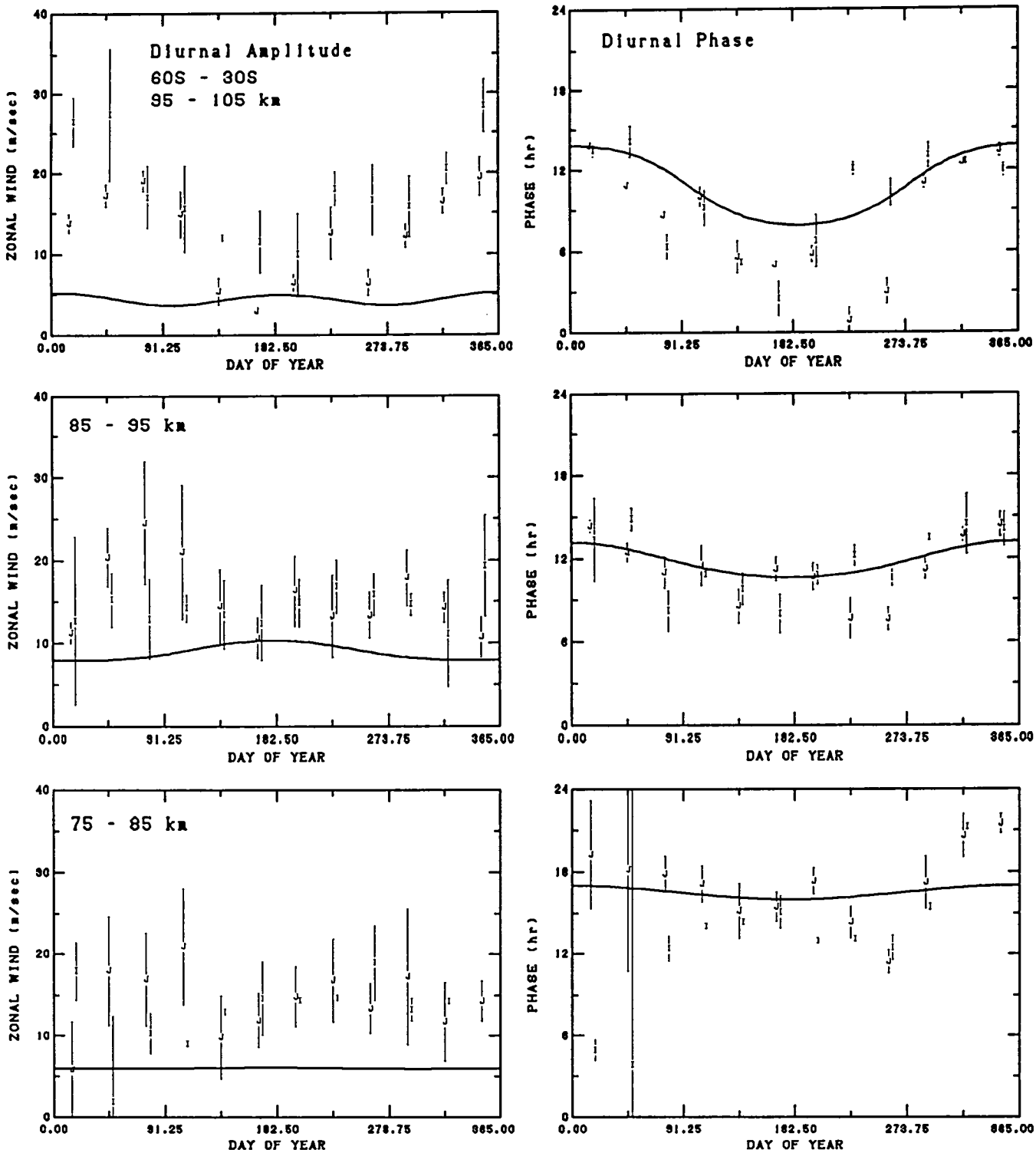

Fig. 14b. Diurnal zonal wind amplitude and phase versus day of year for selected altitudes at southern middle latitudes. The HWM93 model (solid line) shown for mid_range conditions. Plot symbols indicate source as given in Table 1.

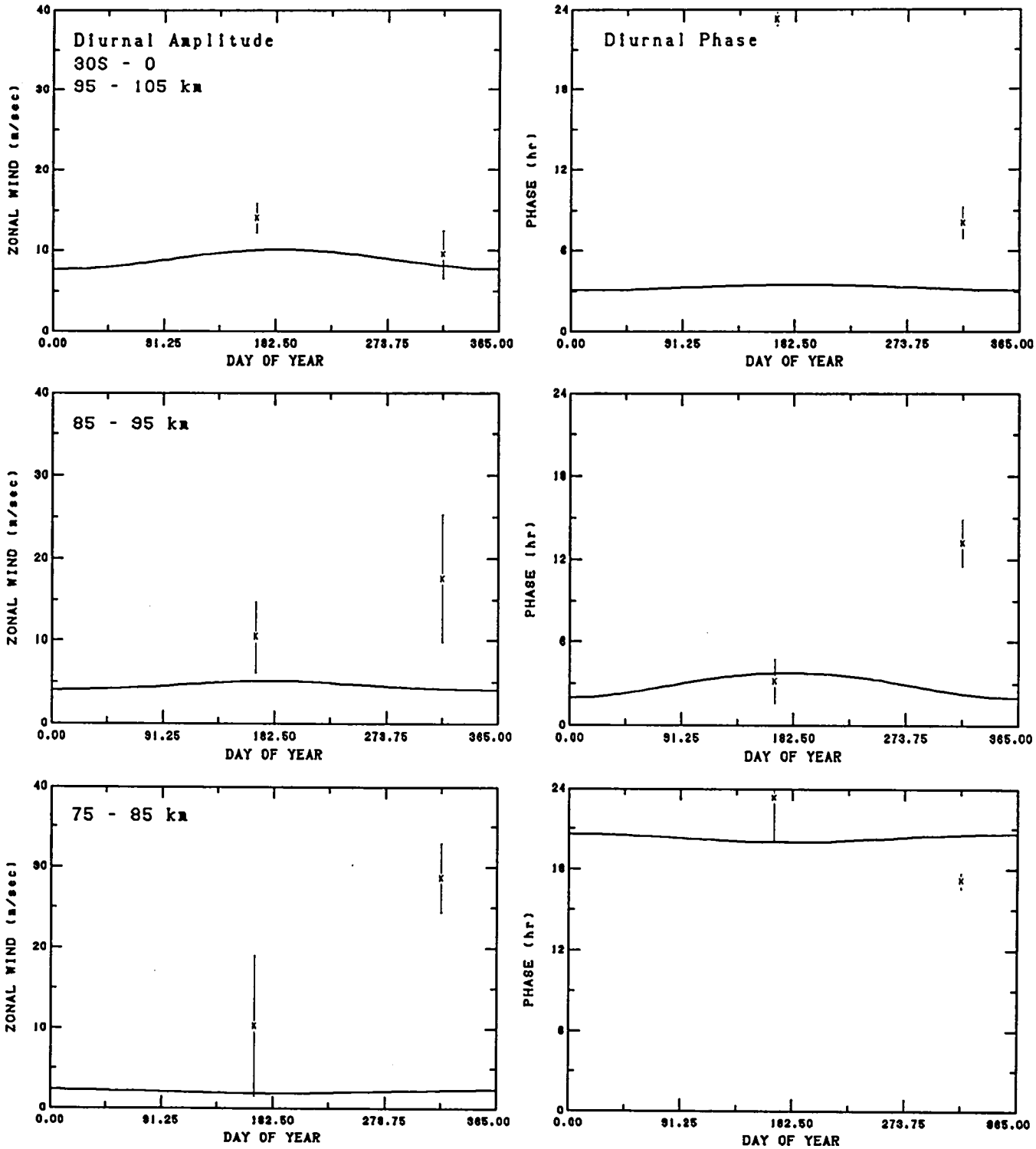

Fig. 14c. Diurnal zonal wind amplitude and phase versus day of year for selected altitudes at southern low latitudes. The HWM93 model (solid line) shown for mid_range conditions. Plot symbols indicate source as given in Table 1.

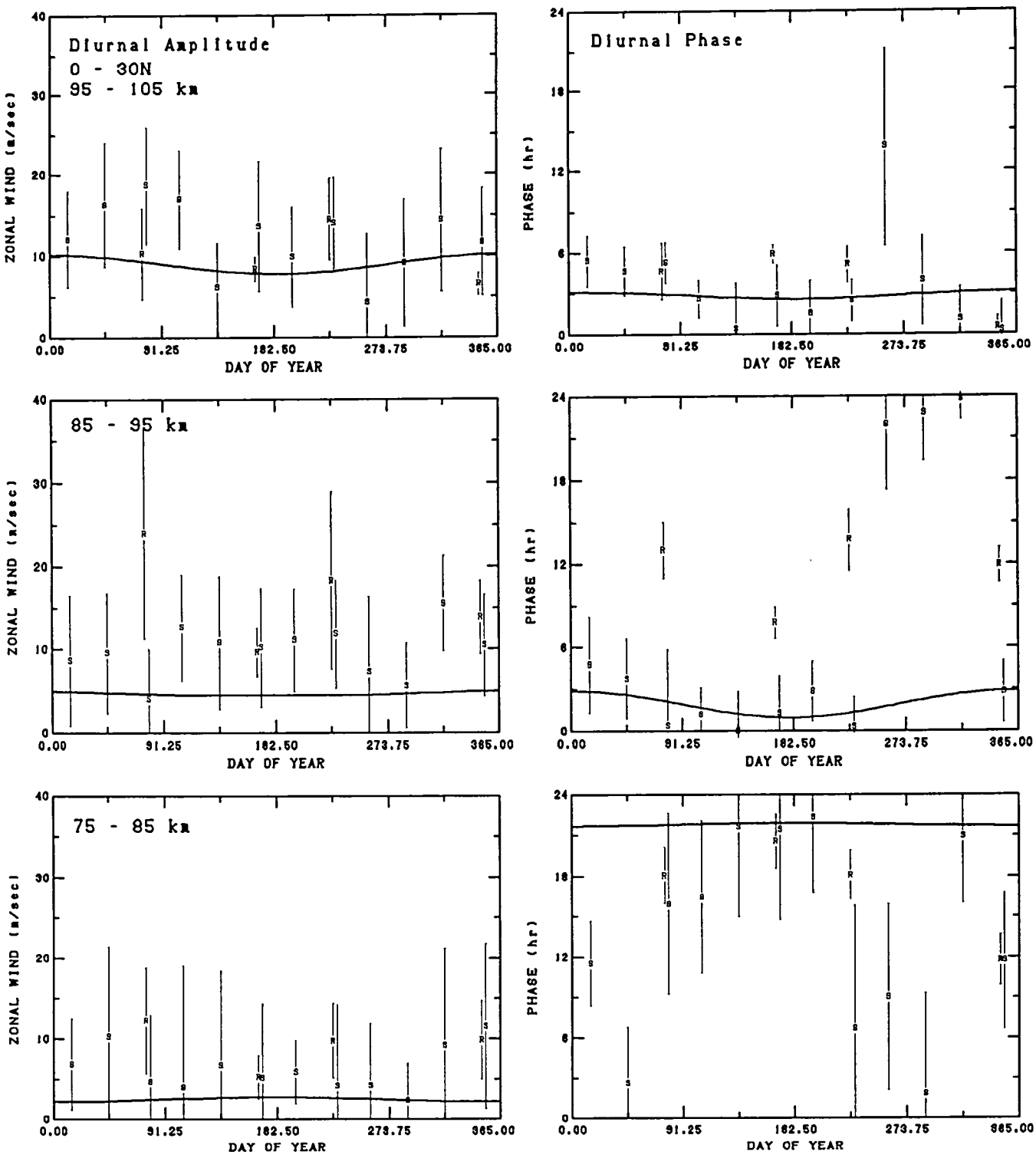

Fig. 14d. Diurnal zonal wind amplitude and phase versus day of year for selected altitudes at northern low latitudes. The HWM93 model (solid line) shown for mid_range conditions. Plot symbols indicate source as given in Table 1.

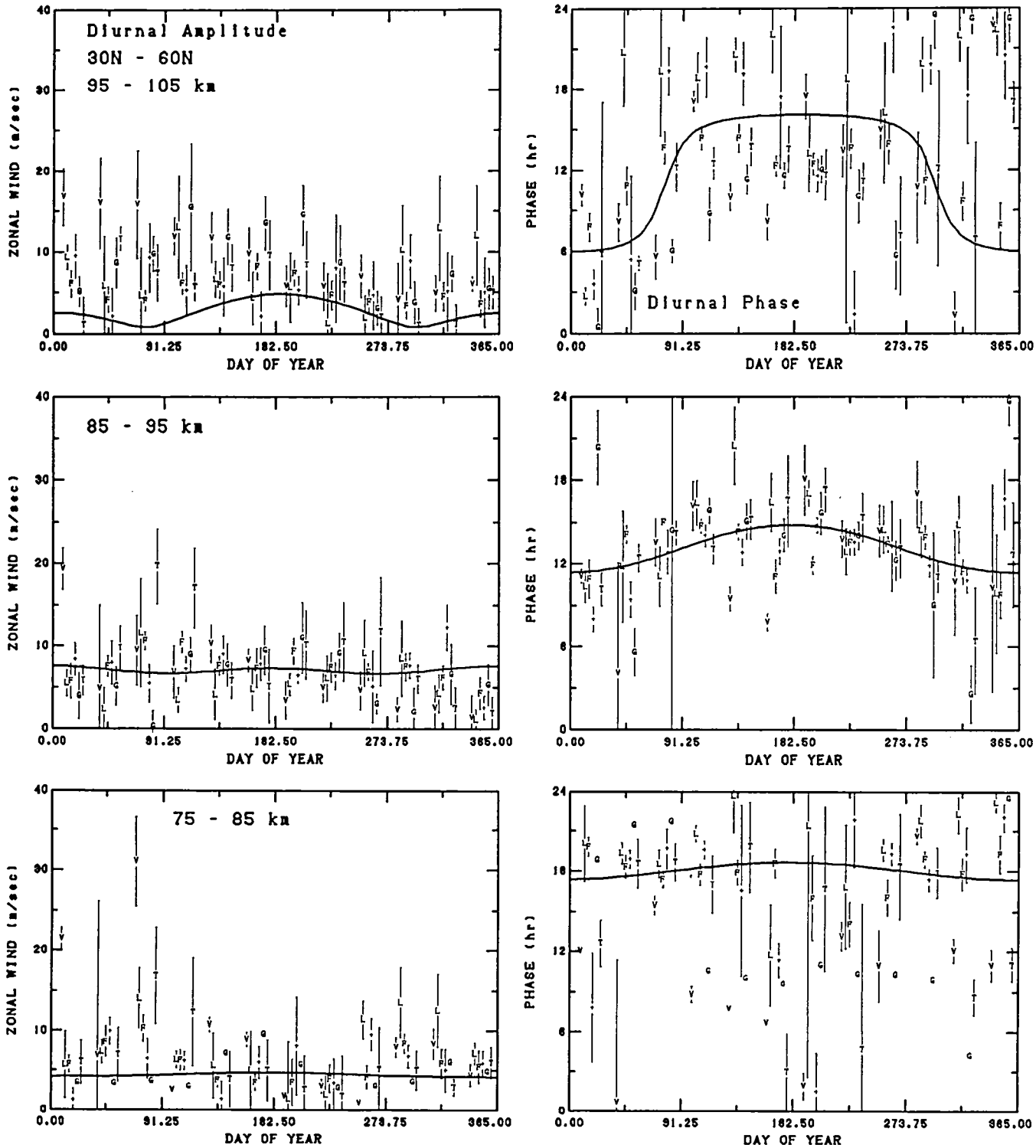

Fig. 14e. Diurnal zonal wind amplitude and phase versus day of year for selected altitudes at northern middle latitudes. The HWM93 model (solid line) shown for mid_range conditions. Plot symbols indicate source as given in Table 1.

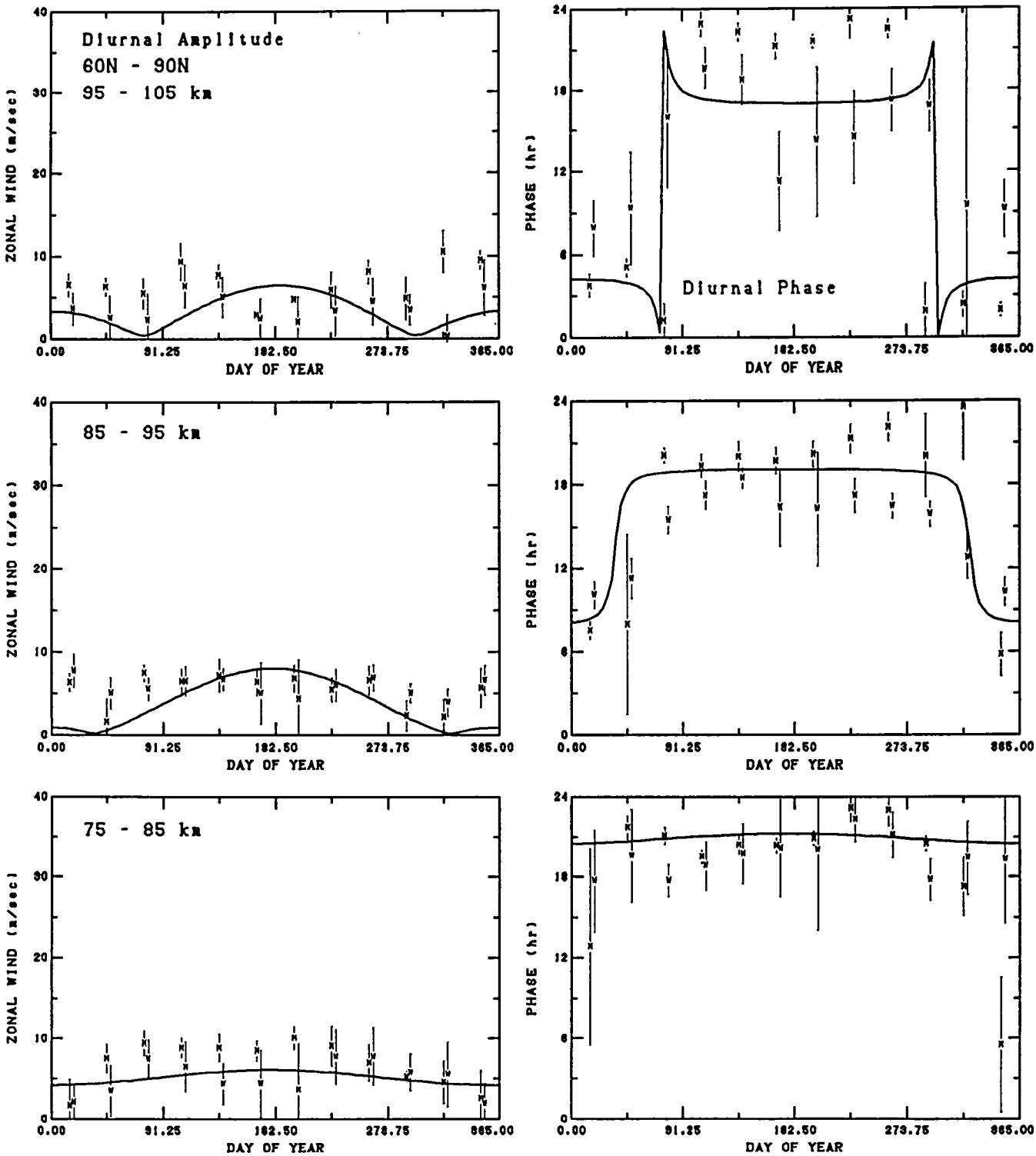

Fig. 14f. Diurnal zonal wind amplitude and phase versus day of year for selected altitudes at northern high latitudes. The HWM93 model (solid line) shown for mid_range conditions. Plot symbols indicate source as given in Table 1.

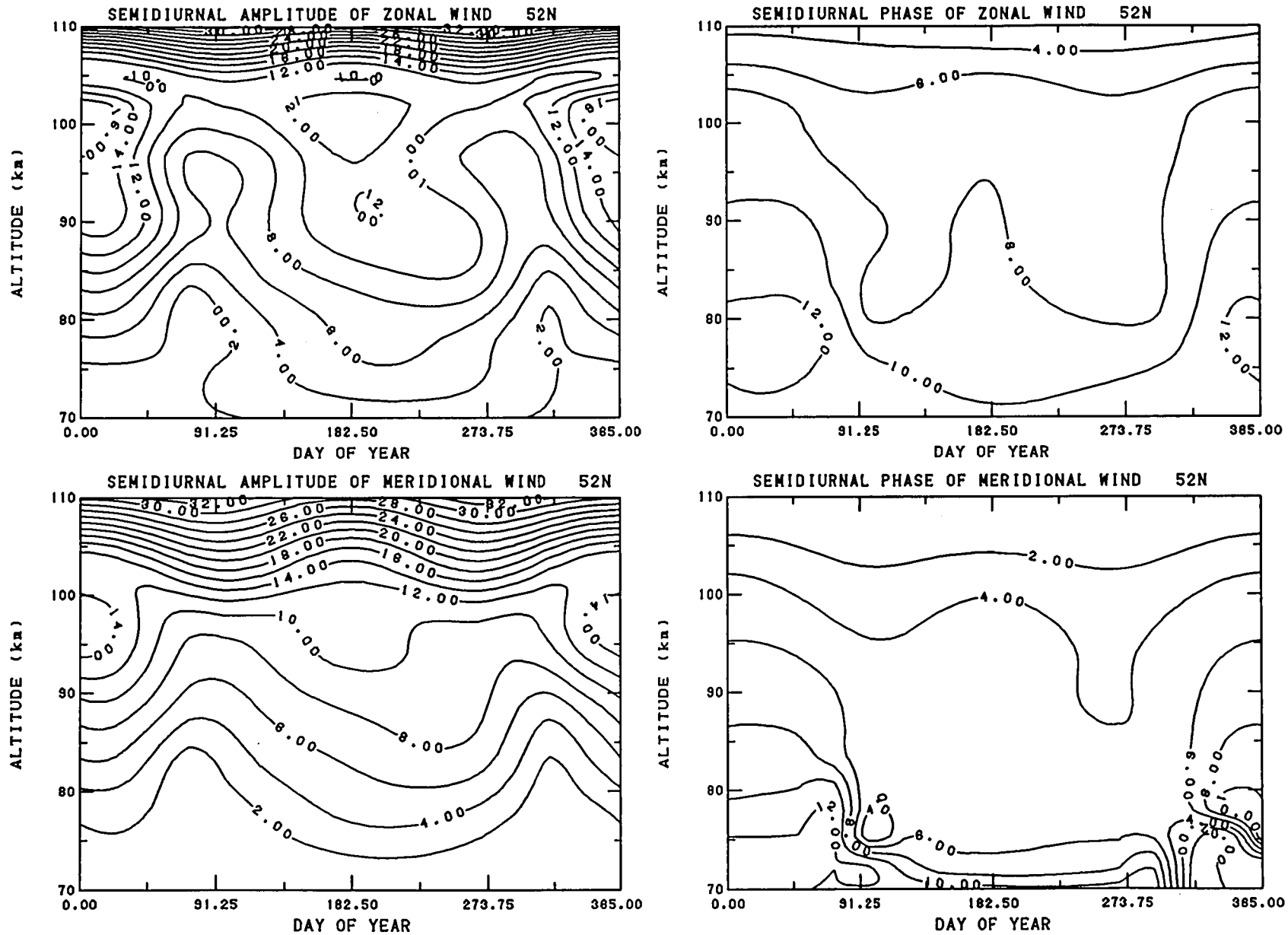

Fig. 15a. Contour plots in altitude versus day of year of the semidiurnal amplitude and phase (dashed negative) of the zonal and meridional wind at 52N latitude.

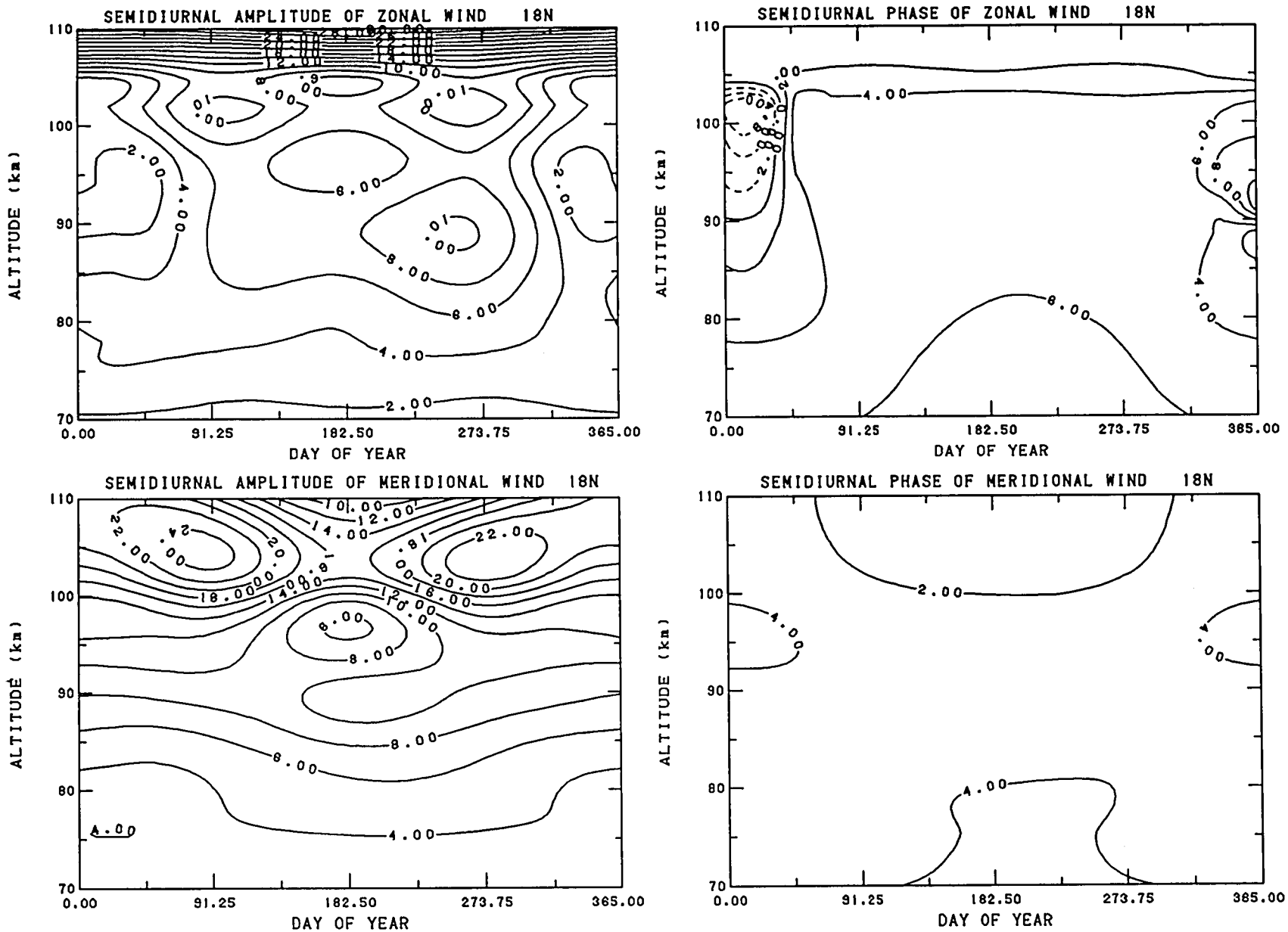

Fig. 15b. Contour plots in altitude versus day of year of the semidiurnal amplitude and phase (dashed negative) of the zonal and meridional wind at 18N latitude.

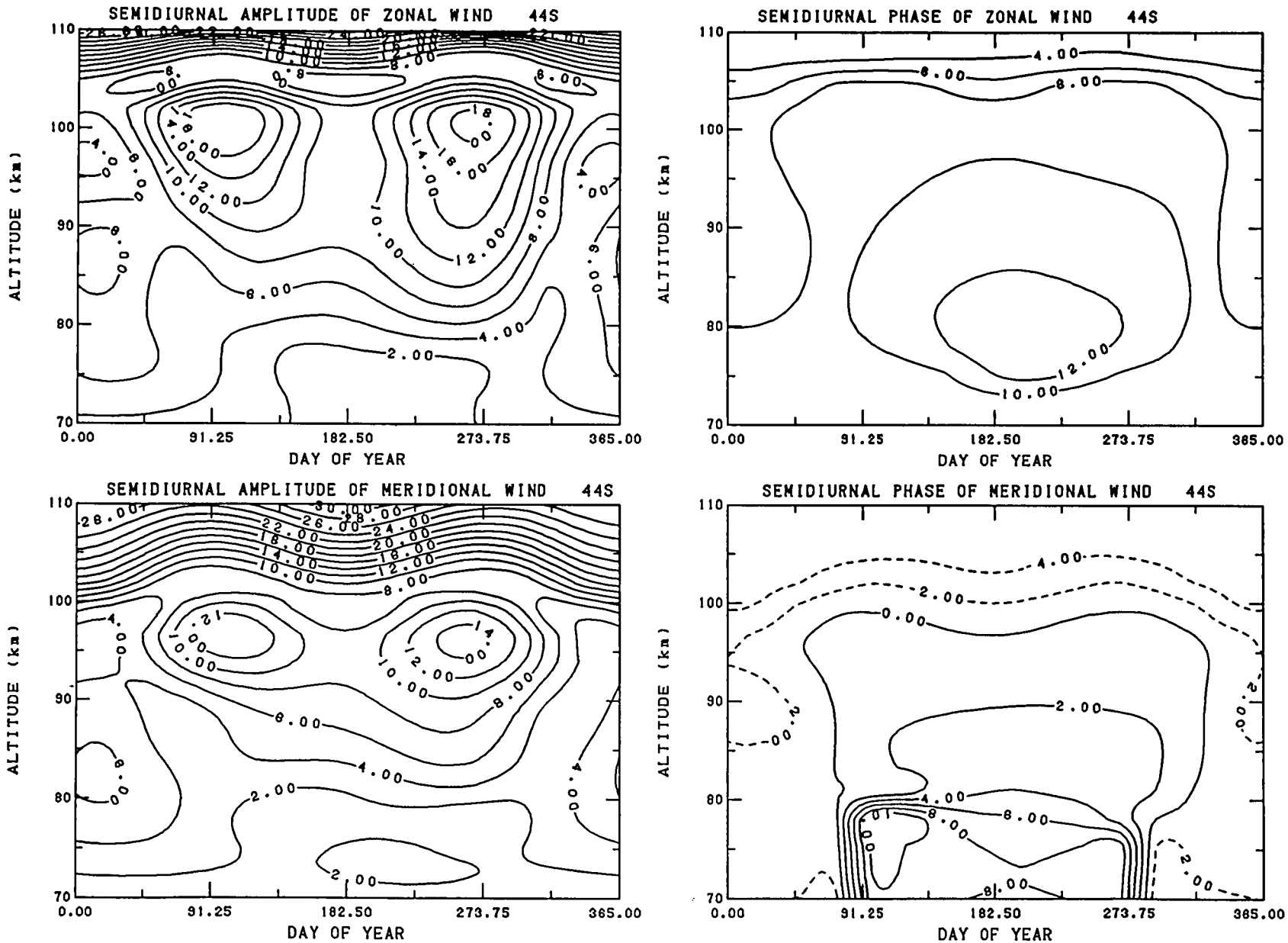

Fig. 15c. Contour plots in altitude versus day of year of the semidiurnal amplitude and phase (dashed negative) of the zonal and meridional wind at 44S latitude.

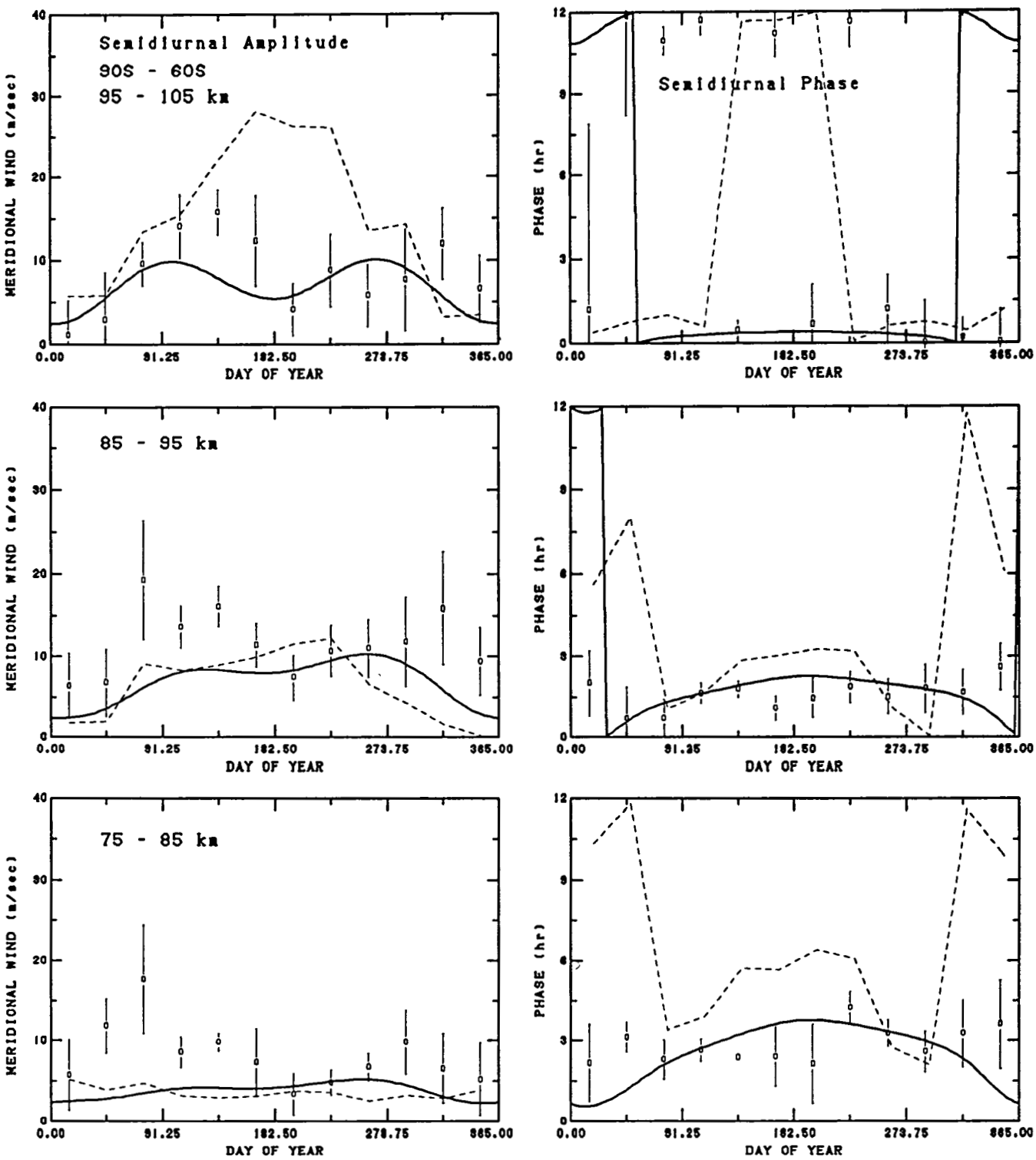

Fig. 16a. Semidiurnal meridional wind amplitude and phase versus day of year for selected altitudes at southern high latitudes. The HWM93 model (solid line) and FV89 (dashed) shown for mid_range conditions. Plot symbols indicate source as given in Table 1.

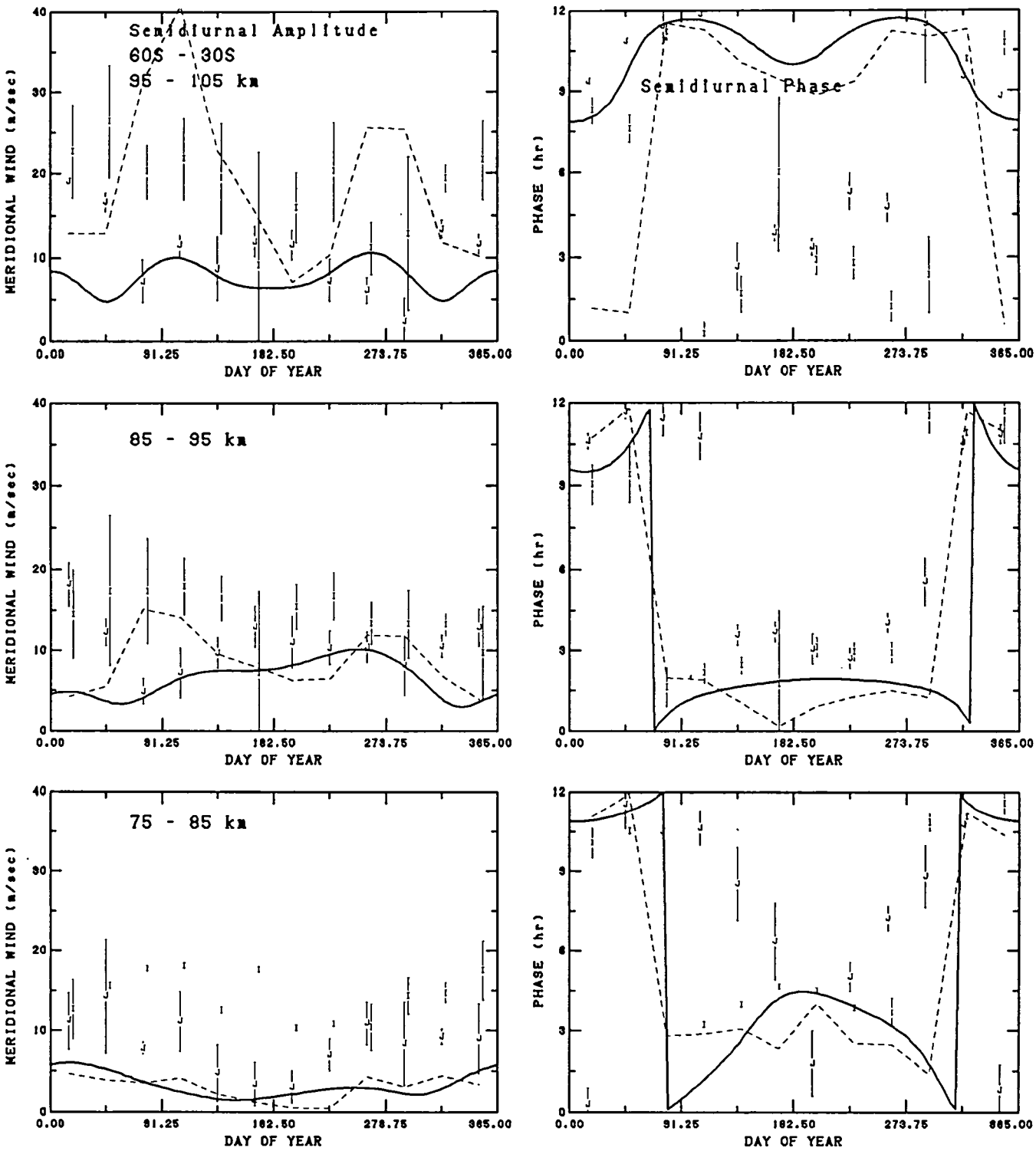

Fig. 16b. Semidiurnal meridional wind amplitude and phase versus day of year for selected altitudes at southern middle latitudes. The HWM93 model (solid line) and FV89 (dashed) shown for mid_range conditions. Plot symbols indicate source as given in Table 1.

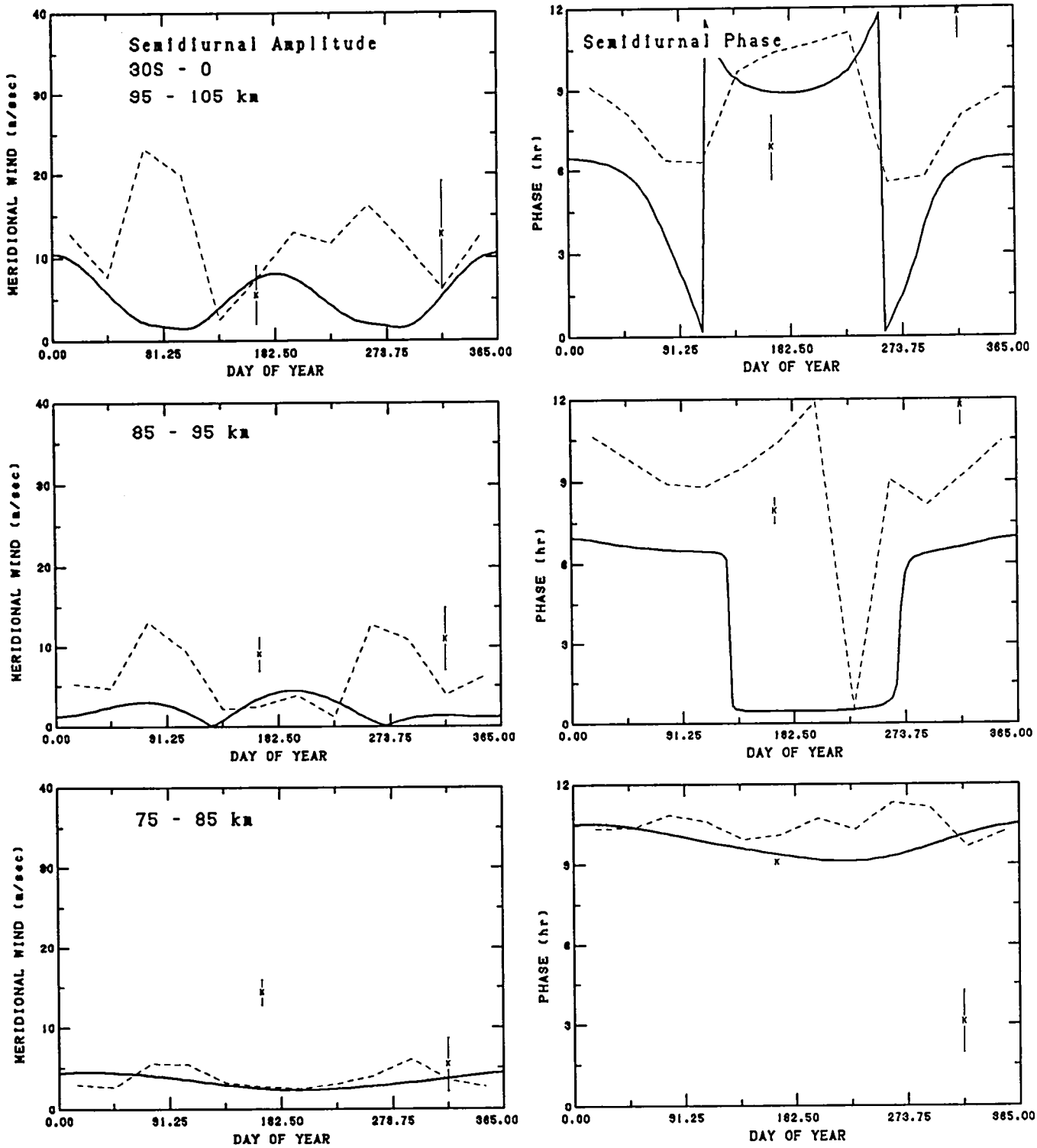

Fig. 16c. Semidiurnal meridional wind amplitude and phase versus day of year for selected altitudes at southern low latitudes. The HWM93 model (solid line) and FV89 (dashed) shown for mid_range conditions. Plot symbols indicate source as given in Table 1.

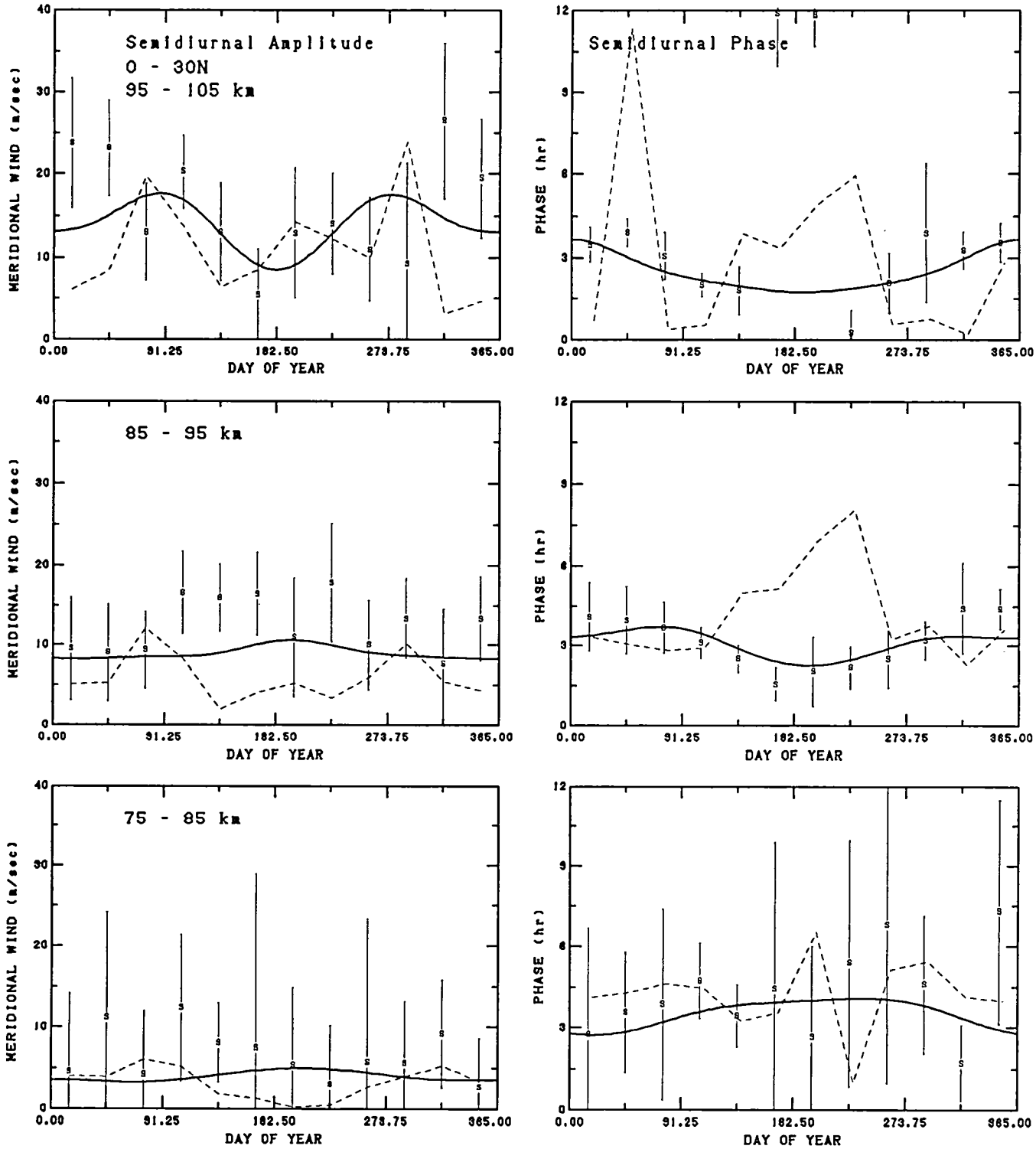

Fig. 16d. Semidiurnal meridional wind amplitude and phase versus day of year for selected altitudes at northern low latitudes. The HWM93 model (solid line) and FV89 (dashed) shown for mid_range conditions. Plot symbols indicate source as given in Table 1.

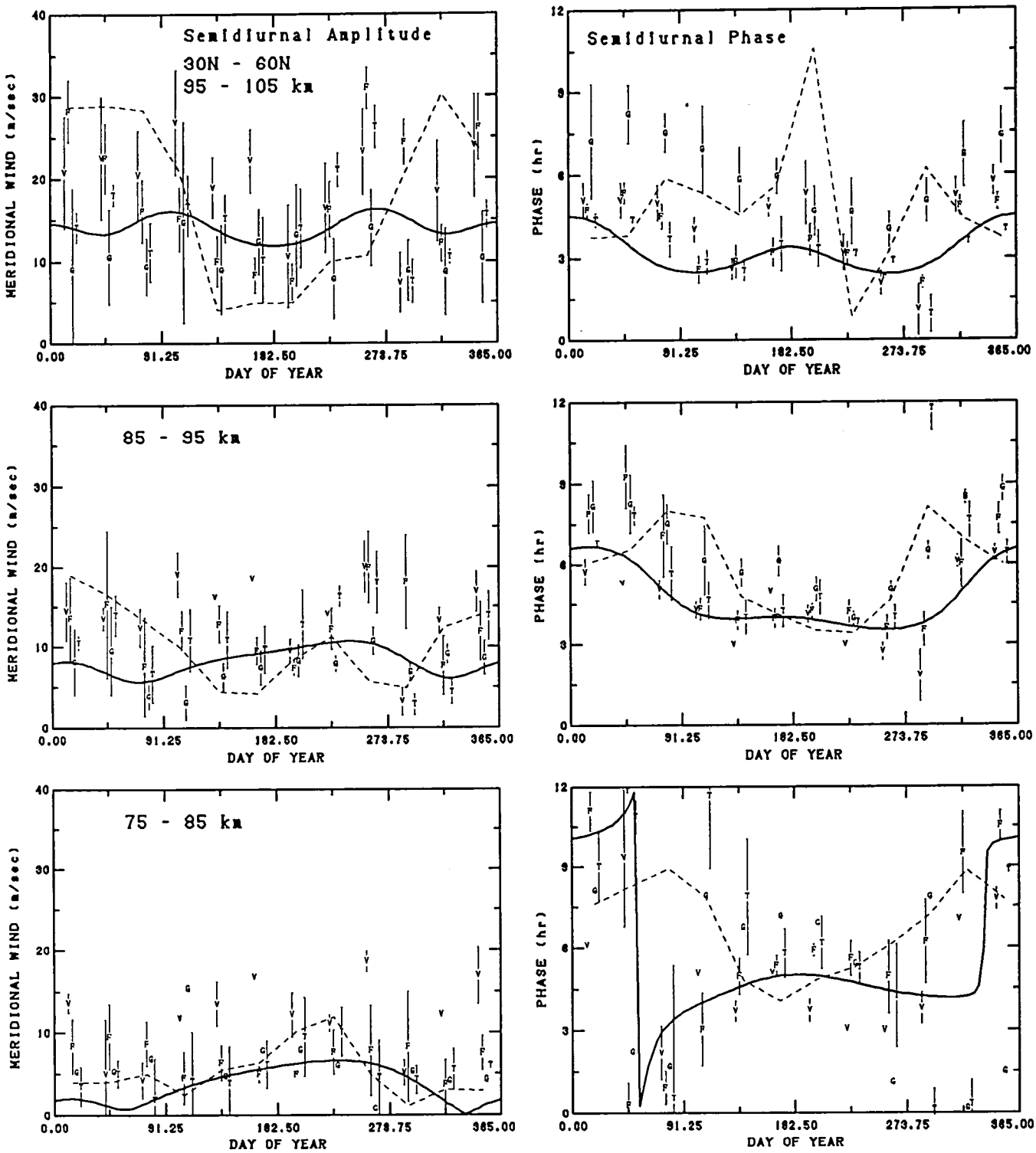

Fig. 16e. Semidiurnal meridional wind amplitude and phase versus day of year for selected altitudes at northern middle latitudes. The HWM93 model (solid line) and FV89 (dashed) shown for mid_range conditions. Plot symbols indicate source as given in Table 1.

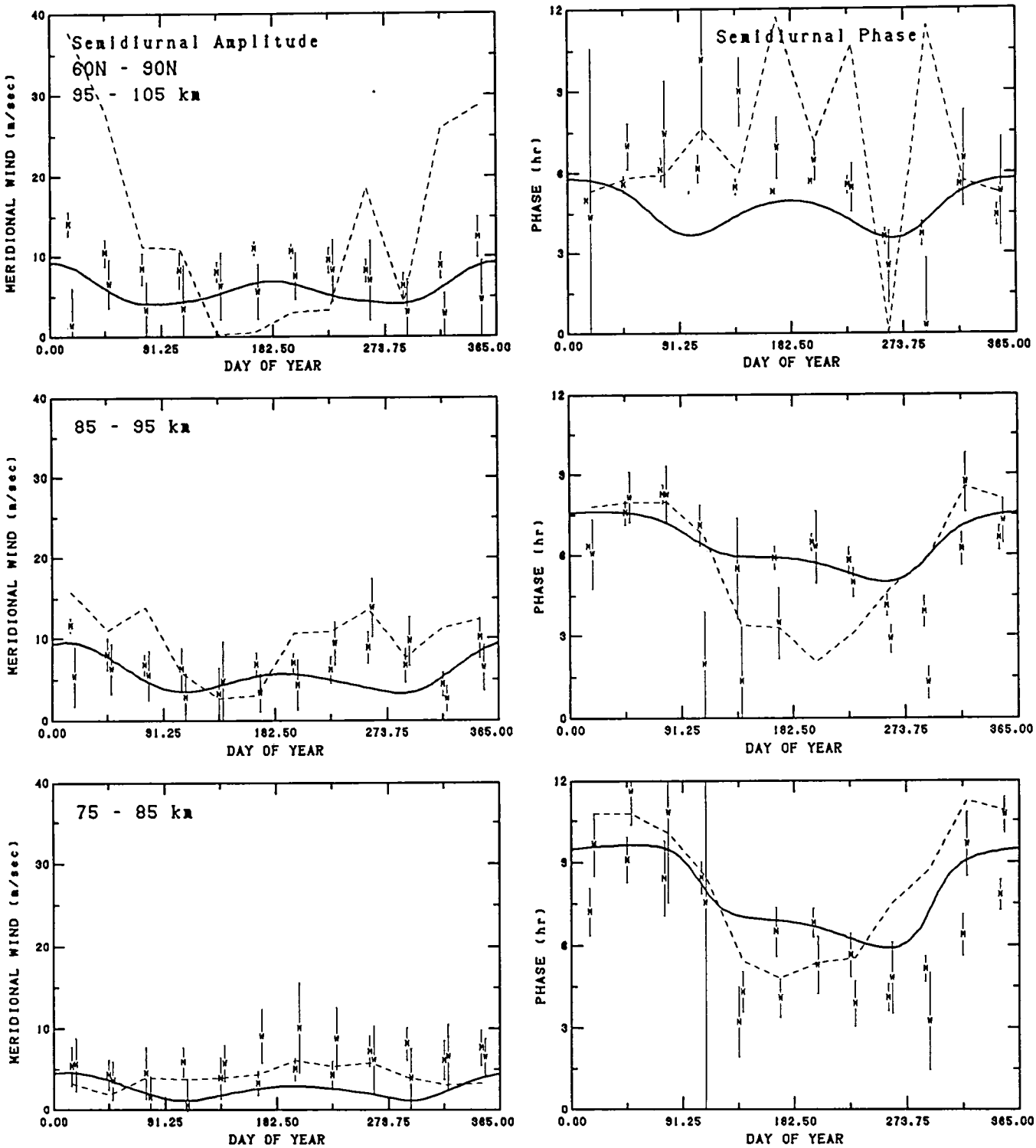

Fig. 16f. Semidiurnal meridional wind amplitude and phase versus day of year for selected altitudes at northern high latitudes. The HWM93 model (solid line) and FV89 (dashed) shown for mid_range conditions. Plot symbols indicate source as given in Table 1.

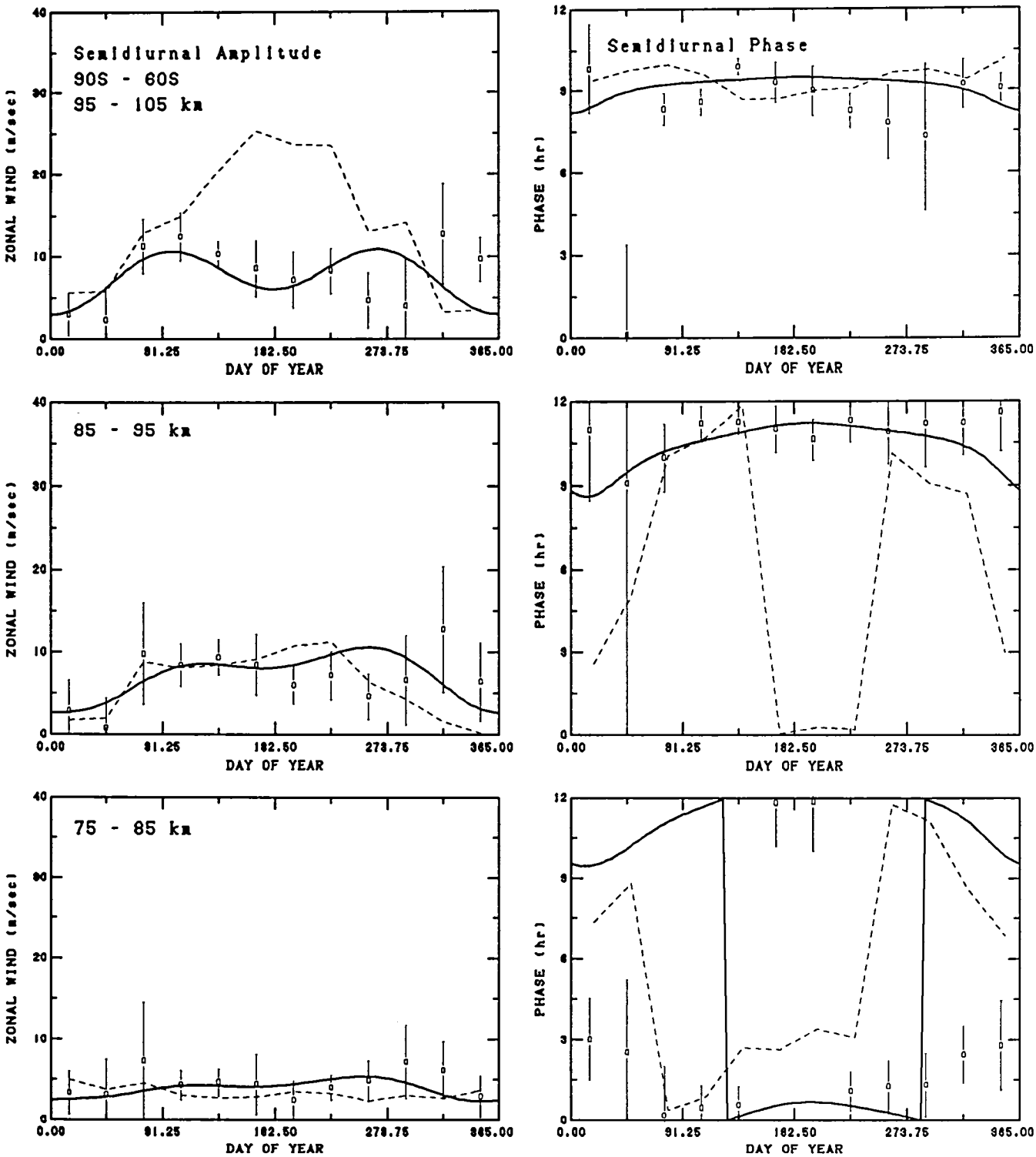

Fig. 17a. Semidiurnal zonal wind amplitude and phase versus day of year for selected altitudes at southern high latitudes. The HWM93 model (solid line) and FV89 (dashed) shown for mid_range conditions. Plot symbols indicate source as given in Table 1.

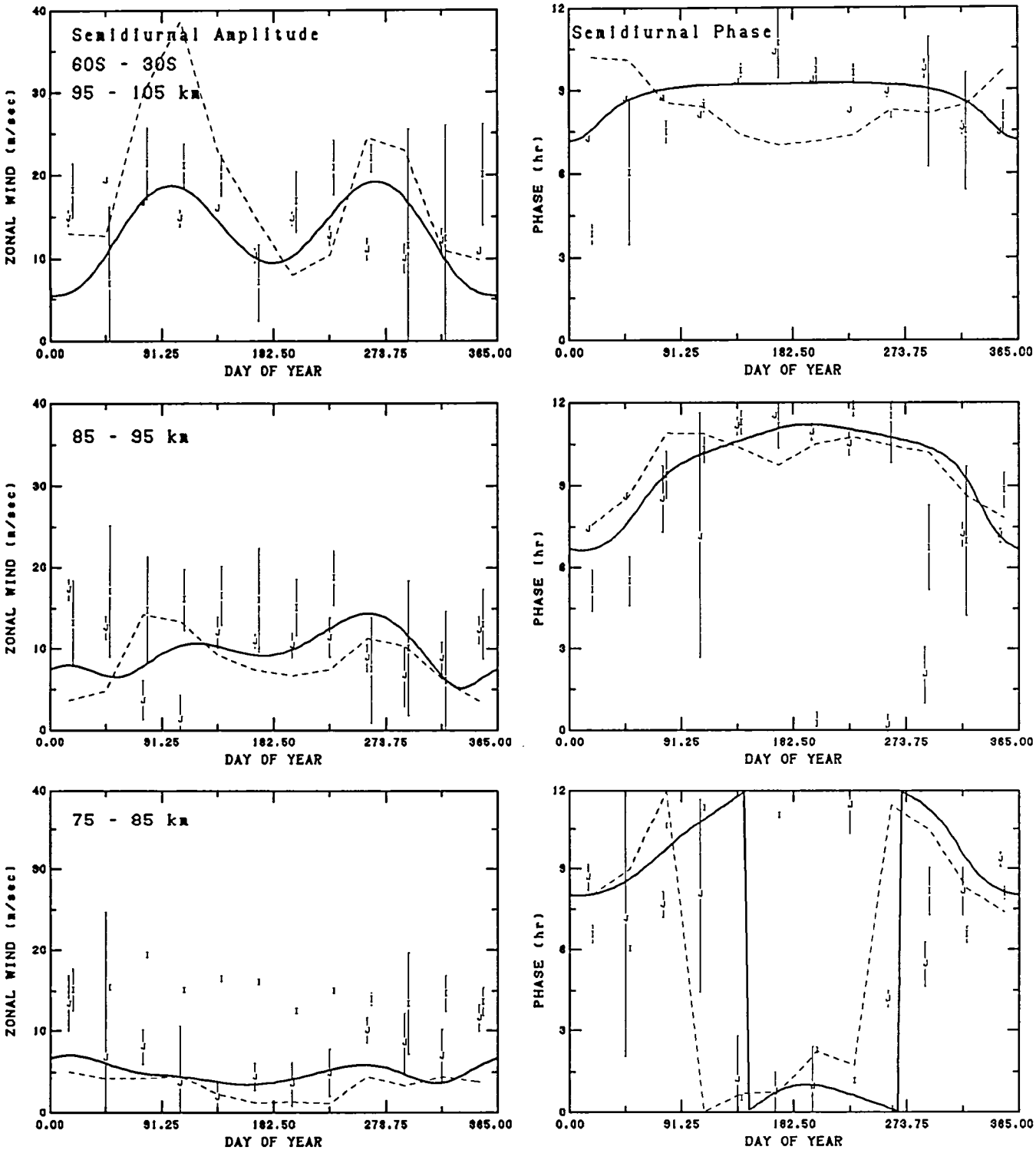

Fig. 17b. Semidiurnal zonal wind amplitude and phase versus day of year for selected altitudes at southern middle latitudes. The HWM93 model (solid line) and FV89 (dashed) shown for mid_range conditions. Plot symbols indicate source as given in Table 1.

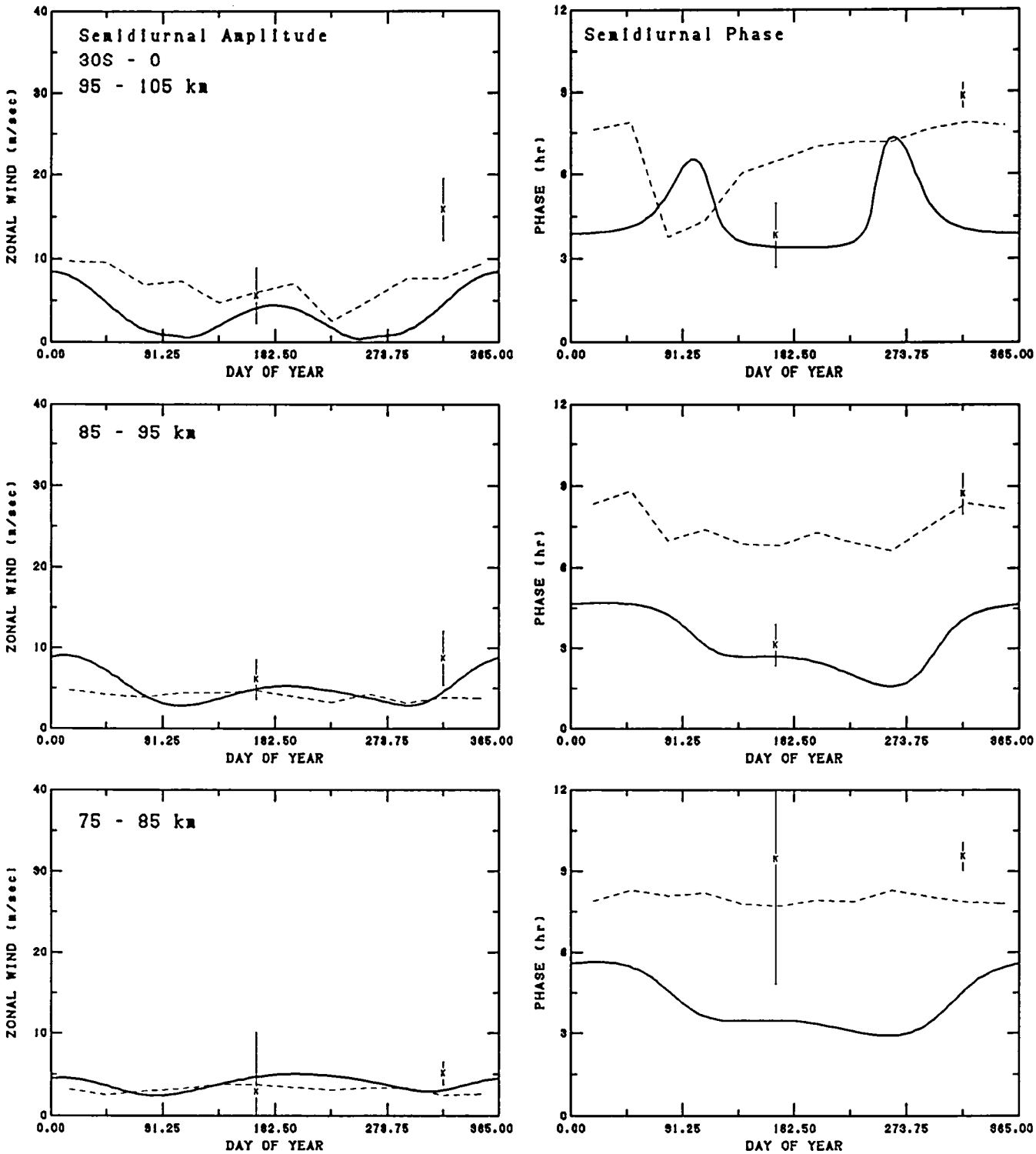

Fig. 17c. Semidiurnal zonal wind amplitude and phase versus day of year for selected altitudes at southern low latitudes. The HWM93 model (solid line) and FV89 (dashed) shown for mid_range conditions. Plot symbols indicate source as given in Table 1.

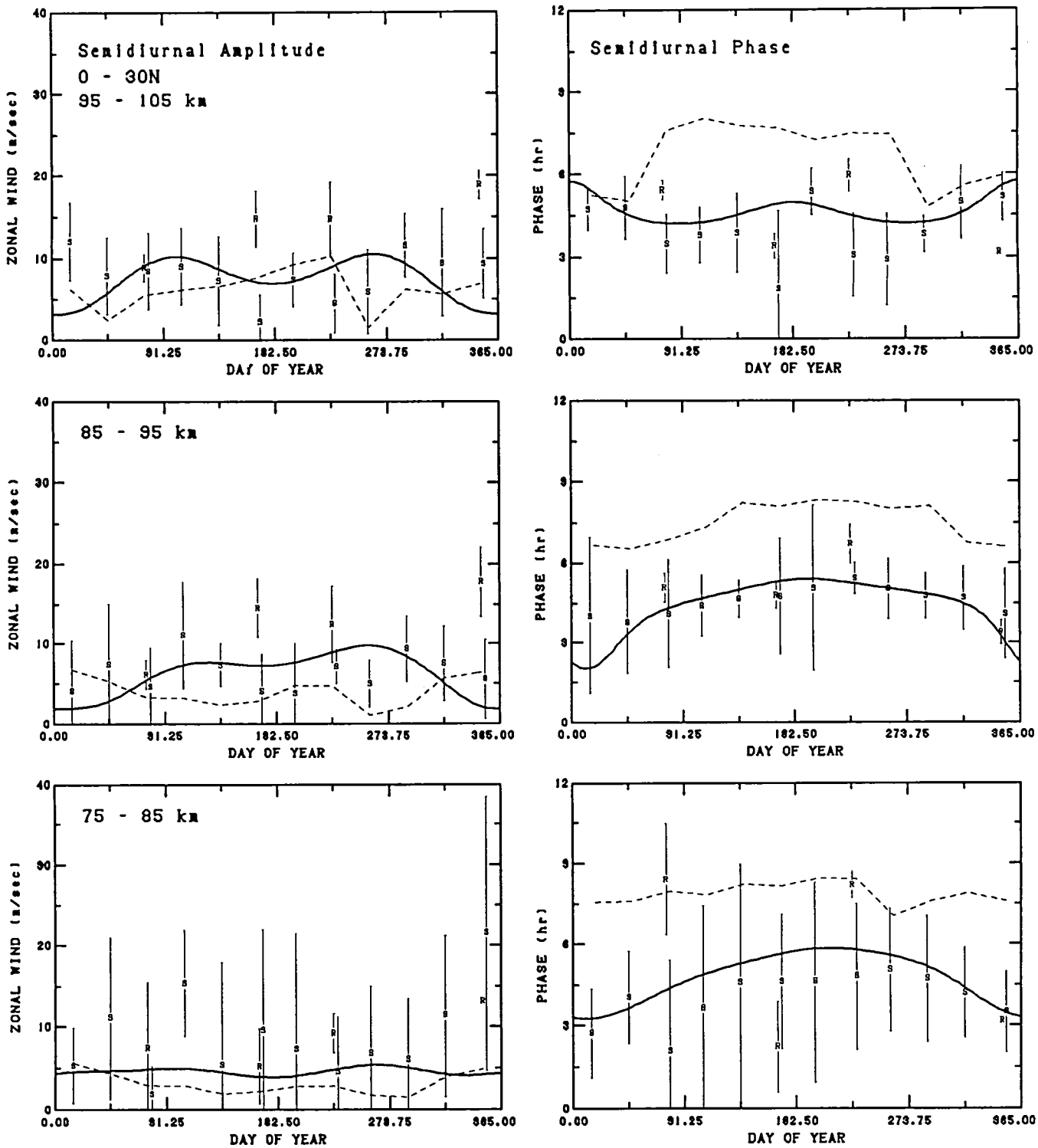

Fig. 17d. Semidiurnal zonal wind amplitude and phase versus day of year for selected altitudes at northern low latitudes. The HWM93 model (solid line) and FV89 (dashed) shown for mid_range conditions. Plot symbols indicate source as given in Table 1.

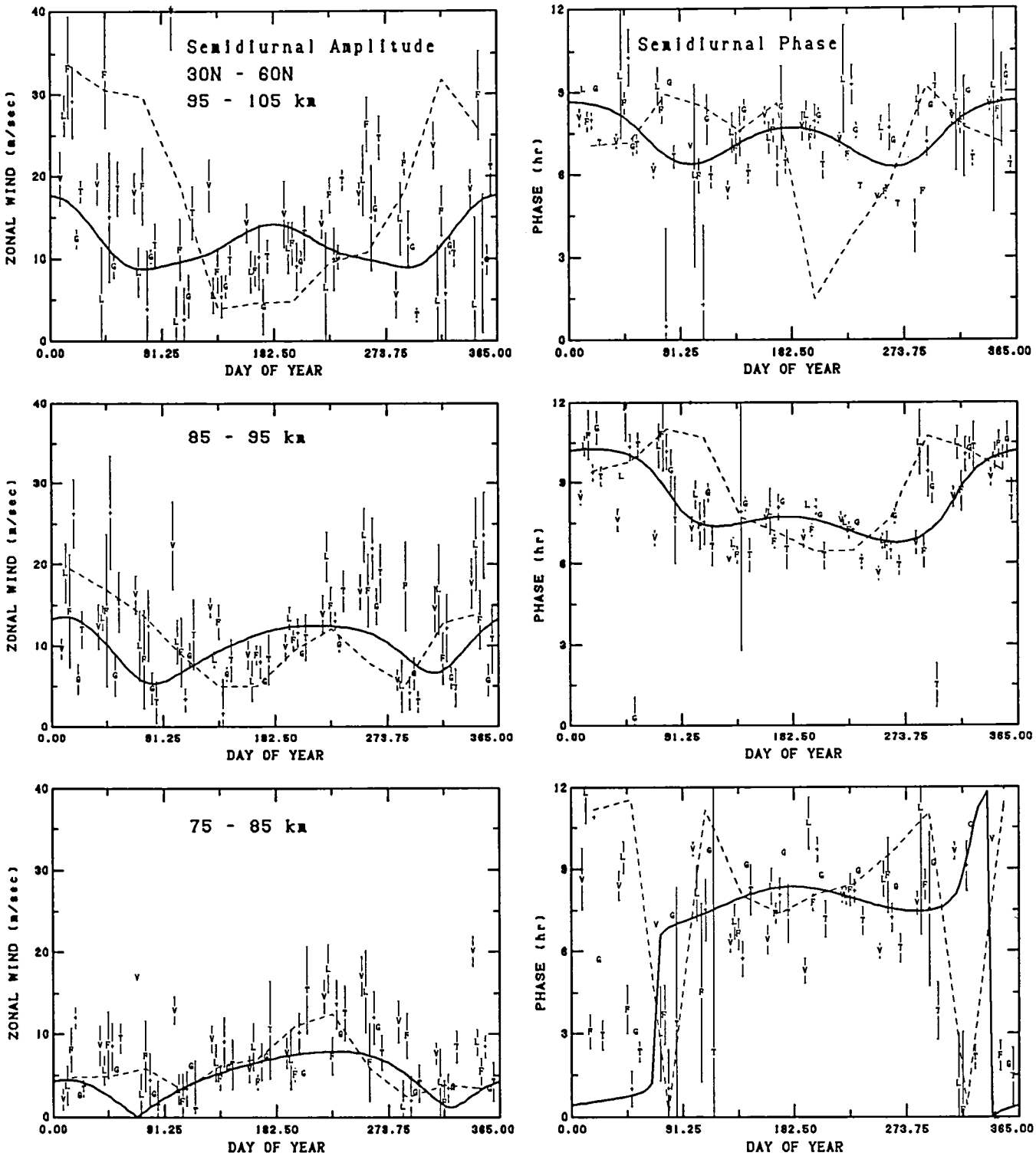

Fig. 17e. Semidiurnal zonal wind amplitude and phase versus day of year for selected altitudes at northern middle latitudes. The HWM93 model (solid line) and FV89 (dashed) shown for mid_range conditions. Plot symbols indicate source as given in Table 1.

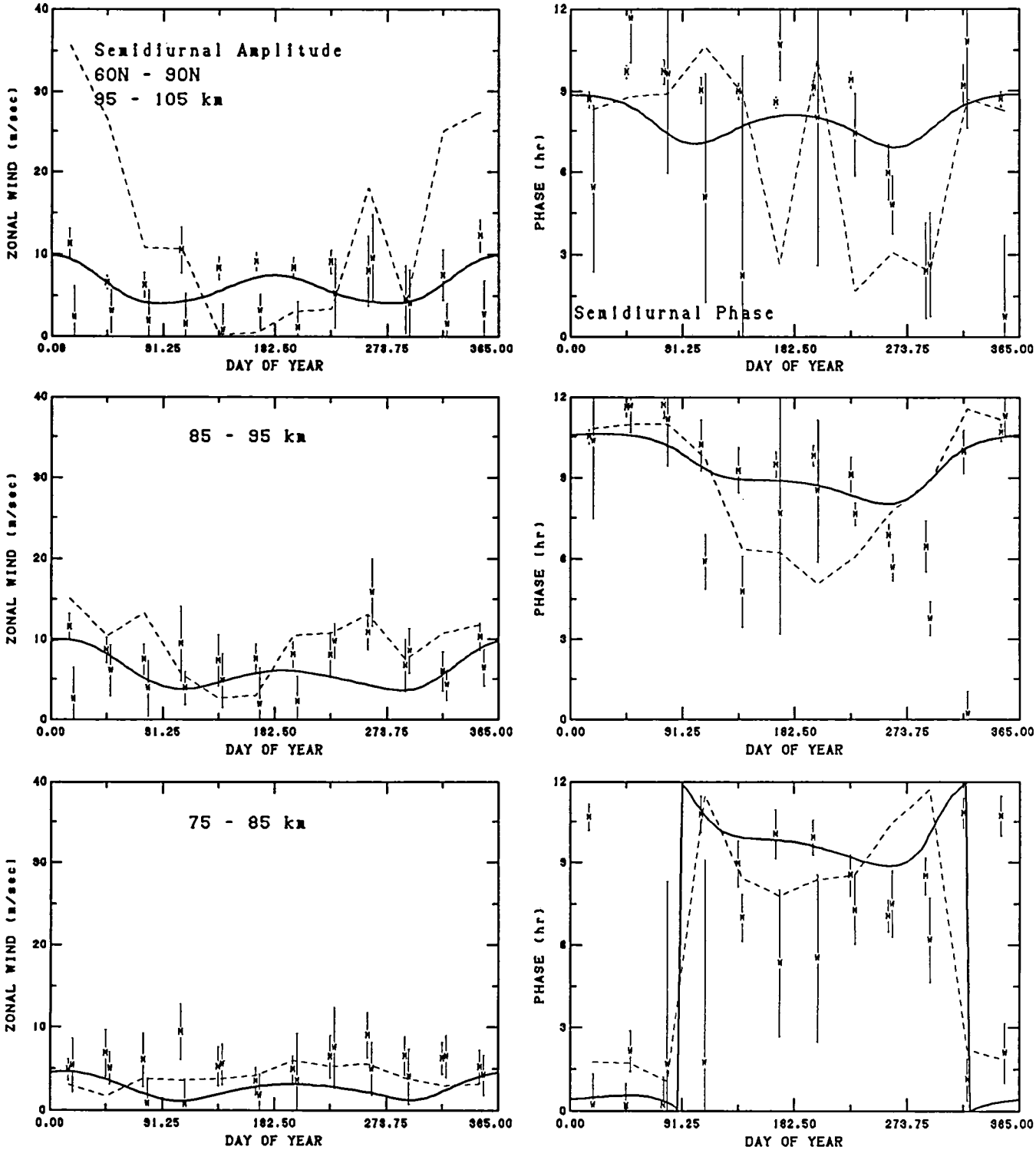

Fig. 17f. Semidiurnal zonal wind amplitude and phase versus day of year for selected altitudes at northern high latitudes. The HWM93 model (solid line) and FV89 (dashed) shown for mid_range conditions. Plot symbols indicate source as given in Table 1.

REPORT DOCUMENTATION PAGE

Form Approved
OMB No. 0704-0188

1. AGENCY USE ONLY *(Leave blank)*	2. REPORT DATE	3. REPORT TYPE AND DATES COVERED
	November 1993	Technical Memorandum

4. TITLE AND SUBTITLE

Empirical Wind Model for the Middle and Lower Atmosphere—
Part 2: Local Time Variations

5. FUNDING NUMBERS

Code 914

6. AUTHOR(S)

A.E. Hedin, E.L. Fleming, A.H. Manson, F.J. Schmidlin, S.K. Avery, R.R. Clark, S.J. Franke, G.J. Fraser, T. Tsuda, F. Vial, and R.A. Vincent

7. PERFORMING ORGANIZATION NAME(S) AND ADDRESS(ES)

Laboratory for Atmospheres
Goddard Space Flight Center
Greenbelt, Maryland 20771

8. PERFORMING ORGANIZATION REPORT NUMBER

94B00005

9. SPONSORING/MONITORING AGENCY NAME(S) AND ADDRESS(ES)

National Aeronautics and Space Administration
Washington, D.C. 20546–0001

10. SPONSORING/MONITORING AGENCY REPORT NUMBER

TM–104592

11. SUPPLEMENTARY NOTES

Hedin: NASA-GSFC, Greenbelt, MD; Fleming: Applied Research Corp., Landover, MD; Manson: Univ. of Saskatchewan, Saskatoon, Saskatchewan, Canada; Schmidlin: NASA-WFF, Wallops Island, VA; Avery: Univ. of Colorado, Boulder, CO; Clark: Univ. of New Hampshire, Durham, NH; Franke: Univ. of Illinois, Urbana, IL; Fraser: Univ. of Canterbury, Christchurch, NZ; Tsuda: Kyoto Univ., Kyoto, Japan; Vial: Ecole Polytechnique, Palaiseau, Cedex, France; Vincent: Univ. of Adelaide, Adelaide, Australia.

12a. DISTRIBUTION/AVAILABILITY STATEMENT

Unclassified–Unlimited
Subject Category 47
Report is available from the National Technical Information Service, U.S. Dept. of Commerce, 5285 Port Royal Road, Springfield, VA 22151; (703) 557–4650.

12b. DISTRIBUTION CODE

13. ABSTRACT *(Maximum 200 words)*

The HWM90 thermospheric wind model has been revised in the lower thermosphere and extended into the mesosphere and lower atmosphere to provide a single analytic model for calculating zonal and meridional wind profiles representative of the climatological average for various geophysical conditions. Local time variations in the mesosphere are derived from rocket soundings, incoherent scatter radar, MF radar, and meteor radar. Low–order spherical harmonics and Fourier series are used to describe these variations as a function of latutude and day of year with cubic spline interpolation in altitude. The model represents a smoothed compromise between the original data sources. Although agreement between various data sources is generally good, some systematic differences are noted. Overall root mean square differences between measured and model tidal components are on the order of 5 to 10 m/s.

14. SUBJECT TERMS

Wind Modeling, Exosphere, Scatter Radar, Zonal Mean, Mesosphere, Lower Thermosphere, Wind Measurements

15. NUMBER OF PAGES

98

16. PRICE CODE

17. SECURITY CLASSIFICATION OF REPORT	18. SECURITY CLASSIFICATION OF THIS PAGE	19. SECURITY CLASSIFICATION OF ABSTRACT	20. LIMITATION OF ABSTRACT
Unclassified	Unclassified	Unclassified	Unlimited

National Aeronautics and
Space Administration
Code JTT
Washington, D.C.
20546-0001

SPECIAL FOURTH-CLASS RATE
POSTAGE & FEES PAID
NASA
PERMIT No. G27

ER: If Undeliverable (Section 158, Postal Manual) Do Not Return